UNIVERSIDADE DE LISBOA
FACULDADE DE CIÊNCIAS
DEPARTAMENTO DE FÍSICA

Correlation of leg impedance and skin deformation during gait

João Manuel Pereira Figueiredo

Mestrado Integrado em Engenharia Biomédica e Biofísica
Perfil de Engenharia Clínica e Instrumentação Médica

Dissertação orientada por:
Professor Doutor Nuno Miguel de Pinto Lobo e Matela
Professor Doutor Jorge Manuel Mateus Martins

2019

Agradecimentos

Aos meus orientadores Prof. Dr. Nuno Matela e Prof. Dr. Jorge Martins, agradeço a infindável ajuda, apoio e orientação que me deram ao longo da criação desta tese.

Ao Prof. Dr. Nuno Matela, pela sua infinita paciência e prontidão nas muitas reuniões que tivemos, impulsionando-me sempre a continuar o trabalho em curso, fornecendo sempre opiniões concisas e construtivas.

Ao Prof. Dr. Jorge Martins, pela sua ajuda e o bom acolhimento que me proporcionou durante o tempo que passei no IST, ajuda e apoio tanto no desenvolvimento da tese como no precioso auxílio no manuseamento de equipamentos utilizados.

Aos meus colegas de laboratório João Gouveia, Mário Torres, Rui Coelho e Paweł Bujalski, pelo ânimo, ajuda e convívio durante a realização da tese.

Aos meus amigos e amigas Ana Viegas, Ana Sofia, Ana Catarina, Beatriz Martins, Cláudia Espadinha, Maria Duarte, Rita Silva e Tiago Silva pela sua enorme ajuda na participação na recolha de dados, sem eles a concretização desta tese não era possível.

A todos os meus amigos, agradeço o apoio, motivação, conselhos e grandes momentos de diversão e camaradagem ao longo destes 5 anos que estivemos juntos.

À Prof. Dra. Dana Solav, por todas as indicações e conselhos fornecidos no início deste trabalho sobre a utilização de ferramentas úteis nesta tese.

Ao meu irmão e aos meus pais, por toda a ajuda e apoio desde o início até ao fim e por poder contar com vocês em qualquer momento.

Resumo

O conhecimento da deformação da pele, juntamente com a cinética e cinemática do corpo humano, são essenciais no planeamento e desenvolvimento de dispositivos médicos em contacto próximo e frequente com a pele humana, fornecendo informações adicionais sobre as características únicas da marcha de cada indivíduo. A forma e intensidade como a pele estica e contrai tem especial atenção nas indústrias têxtil, cosmética e médica que pretendem garantir máxima ergonomia sem sacrificar a eficácia do produto. O planeamento de equipamentos médicos em contacto com o corpo humano (e.g. ortóteses, *soft exoskeletons*) é importante para garantir os sucessos de processos de reabilitação e a melhor adaptação possível ao paciente.

A análise cinética do movimento caracteriza todas as forças que atuam sobre o corpo humano com o objectivo de provocar movimento, sendo as variáveis mais informativas a força de reação (GRF) e a evolução da trajetória do centro de pressão (CoP). Estas duas variáveis apresentam um padrão comum em todos os sujeitos saudáveis, permitindo facilmente a identificação de qualquer problema locomotivo quando os valores apresentam um desvio significativo – marcha patológica. A força de reação vertical apresenta um aspecto característico, com dois picos de intensidade relacionados com especificas etapas do ciclo de marcha: o primeiro pico na fase de apoio de peso, o segundo durante a fase de propulsão. Um pico adicional, por vezes registado no início da fase de apoio, encontra-se diretamente relacionado com o impacto do calcanhar e a forma como o peso é distribuído neste instante – este pico ocorre frequentemente em registos de andar sem calçado, onde não existe amortecimento causado pela sola. Na corrida, geralmente apresenta um pico único, com duração mais curta comparativamente ao andar. O centro de pressão caracteriza-se como a progressão da propagação do vetor da força de reação ao longo do pé, durante o movimento. A trajetória do centro de pressão apresenta uma progressão essencialmente retilínea, com ligeiros desvios quando ocorre a transição de peso do calcanhar para o meio do pé e quando o individuo se propulsiona (localizado nos metatarsos). Na corrida a trajetória é muito menor, devido ao apoio e impulso do sujeito localizado principalmente nos metatarsos. Menos avaliada é a análise da velocidade do centro de pressão (VCoP), que relata a rapidez da transição dos pontos do centro de pressão ao longo do movimento, permitindo observar quanto tempo o sujeito apoia o seu peso numa determinada região do pé. Para o ciclo de marcha comum, costuma apresentar um padrão distinto caracterizado pela presença de 3 picos: estes distinguem a transação rápida do vetor na parte posterior e anterior do pé.

A presente tese continua e complementa trabalho previamente realizado no Instituto Superior Técnico, com principal objectivo a análise da deformação da pele do tornozelo [1] e correlação de variáveis biomecânicas na marcha normal [2], destacando-se por uma análise da deformação da perna inteira e por uma sincronização exata com as restantes variáveis biomecânicas. É apresentada uma análise detalhada dos ciclos de marcha e corrida de 9 indivíduos saudáveis (2 masculinos, 7 femininos), com idades entre 20-28 anos, demonstrando uma sincronização completa da progressão temporal da deformação da pele da perna, força de reação do solo (GRF), centro de pressão (CoP), velocidade do centro de pressão (VCoP) e evolução angular das articulações principais (joelho e tornozelo).

O equipamento de recolha de dados consistiu em duas câmaras de alta velocidade sincronizadas com uma plataforma de força, ambas adquirindo dados durante 3 segundos a uma frequência de 500 imagens (dados) por segundo. De modo a permitir a análise da deformação da pele da perna através de correlação de imagem tridimensional (3D-DIC), foi necessário cumprir os requerimentos necessários de criação e aplicação de um padrão aleatório, anisotrópico e de elevado contraste (i.e. pontos pretos em fundo branco): para tal foram utilizadas tintas acrílicas, atóxicas, para pintar a perna (cor branca), desde

a base do pé até a meio da coxa, cobrindo toda a área lateral, anterior e posterior de forma a poder analisar a deformação nas mesmas vistas. Para aplicar o padrão, foi escolhido o método de estampagem, sendo desenhados e impressos em 3D dois carimbos para "marcar" a perna com cor preta: um maior para rapidamente cobrir a área extensa da perna, um mais pequeno para carimbar as zonas de relevo mais acentuado (i.e. joelho e tornozelo).

Para a calibração do *software* de análise foi necessária a criação de uma grelha de calibração (fornecida pelo programa) adequada á experiência: de forma a capturar a evolução de todo o movimento, o campo de visão foi severamente alargado comparativamente a estudos anteriores, focados no estudo do complexo tornozelo-pé – para ocupar este espaço foi necessária a impressão da grelha em formato A1 (594 x 841 mm). A análise de deformação da pele da perna foi realizada usando a ferramenta VIC-3D da Correlated Solutions para obter a deformação Lagrangiana, extraindo 3 variáveis para análise: *e1*, deformação máxima principal, *e2*, deformação mínima principal e *von Mises*, escalar. Os dados de força e momento registados foram obtidos pelo *software* da placa de forças AMTI e interpretados através de código MATLAB – GRF corresponde diretamente aos valores da componente vertical da força registada, Fz; CoP e VCoP foram obtidos através da aplicação de equações que utilizam os valores de momento e força para extrair o valor destas grandezas. Para a evolução angular das articulações, a sua variação foi medida através da ferramenta Kinovea, ancorando 6 pontos-chave (3 por ângulo medido) nas imagens analisadas e calculando a sua progressão. Para a análise de marcha são apresentadas três vistas: lateral, posterior e anterior. Além do andar e correr, o comportamento de equilíbrio do corpo também foi analisado com o objectivo de identificar um padrão comum na restauração do balanço após os sujeitos serem puxados na direção oposta a meio da fase de apoio.

Com a sincronização de todos os dados, é oferecida uma descrição completa da fase de apoio durante a marcha, fornecendo uma base de dados rica e detalhada das suas características desde o início até ao fim do movimento, validada por resultados presentes na literatura. É possível observar os picos de intensidade de GRF conjuntamente com o pico gerado pelo impacto do calcanhar na totalidade dos testes do ciclo de marcha. Uma comparação das mesmas variáveis entre mais 3 sujeitos permite verificar a existência da repetição do mesmo padrão e notar ligeiras diferenças, como a ausência de pico de impacto de calcanhar em alguns sujeitos e um máximo global em diferentes etapas do ciclo (presente no 1º ou 2º pico). A evolução da trajetória do centro de pressão e da velocidade de centro de pressão também se encontram de acordo com o esperado entre os vários sujeitos. A sincronização destas 3 variáveis permite ao utilizador facilmente observar a sua relação e evolução simultânea ao longo da execução do movimento. Nos resultados dos testes de corrida, à semelhança dos testes do andar, os resultados foram os esperados de acordo com o estudo efetuado, com um pico singular de força registado e uma trajetória de centro de pressão bastante reduzida. Nos testes de análise de equilíbrio após perturbação na direção oposta do movimento, foi identificado um padrão na resposta dos sujeitos, no andar e corrida, caracterizado pela ação da perna em balanço como agente principal de restabelecimento de equilíbrio.

Uma observação aprofundada do evento do impacto do calcanhar permite identificar um período onde o ângulo entre a perna e o pé se mantêm constante, sugerindo uma rotação de corpo rígido, constituído pelo complexo perna-pé, com o bloquear da articulação do tornozelo. Assim, foi possível introduzir uma nova etapa na descrição do ciclo de marcha, ausente na literatura comum, com a identificação do movimento rígido do complexo-tornozelo-pé após contacto com o chão, que decorre entre o impacto do calcanhar e o apoio total do pé no chão.

Palavras-chave: GRF, CoP, VCoP, deformação, 3D-DIC, ciclo de marcha.

Abstract

Knowledge of skin strain, alongside the kinetics and kinematics of the human body are essential for the planning and development of medical devices in close and frequent contact with the human skin and rehabilitation methods, providing further insight into each subject's unique gait characteristics. The present thesis continues and complements previous work performed at Instituto Superior Técnico aimed at skin strain field analysis of the ankle [1] and correlation of multiple biomechanical quantities in normal gait [2]. The following work features a detailed analysis of walking and running gait of 9 healthy subjects (2 male, 7 female), with ages ranging between 20-28 years old, featuring full synchronization of the temporal progression of leg skin strain, ground reaction force (GRF), centre of pressure (CoP), velocity of centre of pressure (VCoP) and principal joint (knee and ankle) angular evolution.

Experimental setup consisted of two high framerate cameras synchronized with a force platform, both acquiring data for 3 seconds at 500 frames (data points) per second. Strain analysis was performed through three-dimensional digital image correlation (3D-DIC) using Correlated Solutions' VIC-3D tool to obtain the Lagrangian strain; GRF, CoP and VCoP data were obtained from the AMTI force plate software, and interpreted using MATLAB code. For the joint angular evolution, their variation was measured with Kinovea. For walking gait, 3 views are presented: lateral, posterior and anterior. Besides normal walking and running gait, the body's balance behaviour was also analysed with the purpose of identification of a common pattern in balance restoring after the subjects were pulled midstance in the opposite direction.

With the synchronization of all data, a complete description of the stance phase during gait is offered, supplying a rich and detailed database of its characteristics from beginning to end. A close up view on the heel strike transient event also introduces a novel stage in stance gait description, with the identification of a rigid body rotation of the ankle-foot complex after heelstrike.

Keywords: GRF, CoP, VCoP, strain, 3D-DIC, gait cycle.

Table of Contents

List of Figures

List of Acronyms

3D – Three dimensional

DIC – Digital Image Correlation

GRF – Ground Reaction Force

CoP – Centre of Pressure

VCoP – Velocity of Centre of Pressure

FOV – Field of View

HFR – High Frame Rate

LoNEs – Lines of Non Extension

ROI – Region of Interest

cm - centimetre

mm - millimetre

s – second

ms – millisecond

1. Introduction

1.1. Motivation and Goals

The study of skin deformation, kinematics and kinetics is an increasingly frequent research topic, mainly due to the information that allows the establishment and development of new medical equipment that involves frequent contact with the dermis and provides assistance to locomotion, like in the motor rehabilitation field. From orthoses to space suits to sportswear, this topic is always present, influencing the success of the created product. Therefore, knowledge of how the skin deforms in movement and the forces that our body is submitted when walking and running is essential to better design these mechanical interfaces and improve their efficiency.

The research performed during this thesis, based on work previously carried out in Instituto Superior Técnico (IST) and Massachusetts Institute of Technology (MIT), aims to correlate skin deformation in the leg and foot with its kinetics during gait, for the purpose of mapping the connection between regions of maximum/minimum deformation with the exerted Ground Reaction Force (GRF), the Centre of Pressure (CoP) and its Velocity (VCoP), establishing a clear and precise representation of the synchronization of these quantities throughout the stance phase of gait.

To achieve these goals, 9 subjects were recruited to perform simple movements, walking and running, where foot strike and skin deformation data were retrieved via force plate feedback and Digital Image Correlation (DIC).

1.2. Human gait Kinetics and Kinematics

To better understand the set of movements and explain the stages that define the gait cycle, it is necessary to learn core biomechanical concepts that are present in both walking and running.

Human locomotion and gait is also an important research topic tied with the development of soft exoskeletons and skin deformation. A clear analysis and description of the various movements that our body performs during walking and running allows for an organized view that can be easily used when designing the aforementioned soft exoskeletons or in the case of this thesis, correlating the various stages of locomotion with the body's kinetics and deformation.

To better understand the description of body motions regarding walking and running, a few anatomic and kinematic terms are outlined [3]. Considering the typical anatomic reference position chart (Figure 1.1) the human body is divided in 3 planes:

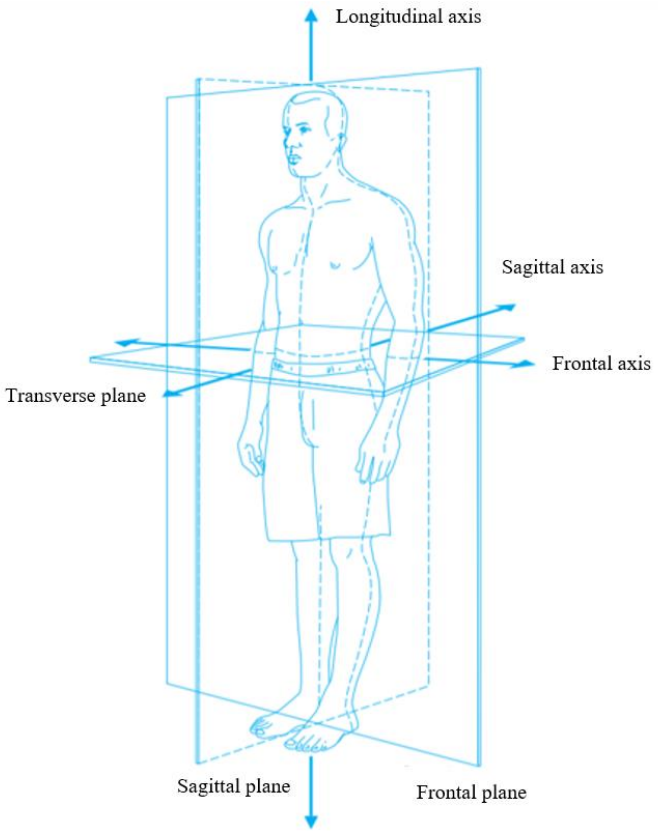

Figure 1.1 – The three anatomical planes, adapted from [3].

- **Sagittal plane** – Divides the body into right and left sides, allows for description of forward and backward movements;

- **Frontal plane** – Divides the body into front and back, allows for description of lateral movements (abduction and adduction);

- **Transverse plane** – Divides the body into superior and inferior parts, allows for description of horizontal movements (medial and lateral rotations);

Regarding the sagittal plane, for the description of leg movements, when walking the limb performs **flexion** – bending movement of the lower leg, posteriorly directed. **Extension** is classified as the movement that rests the limb to its anatomical reference position. Regarding the frontal plane, the limbs can perform **abduction**, when the subject moves the body segment away from the body's midline, or **adduction**, when the segment closes the gap towards the midline of the body. The leg can also rotate outwards (**lateral rotation**) or inwards (**medial rotation**) in relation to the body's midline.

The movement of our feet can be described in two terms: **dorsiflexion** and **plantar flexion**. **Dorsiflexion** consists of moving the foot closer (towards to) the lower leg whilst **plantar flexion** consists of the opposite. The rotation of the foot can also be described: **eversion** is an outwards rotation of the foot and **inversion** is an inwards rotation.

Overall foot motion during gait can be described with **pronation** and **supination**: the former is a combination of dorsiflexion, eversion and abduction while the latter consists mainly of plantar flexion, inversion and adduction.

The gait cycle is a repetitive event, with a cycle being entirely defined by the time interval elapsed between two occurrences of the same phase during locomotion. By rule, the beginning of the cycle is considered when one of the feet (usually the right foot) makes contact with the ground, and ends with the start of a new cycle (i.e. when the same foot contacts the ground again). To simplify further explanations, and in concordance with the tests performed in this thesis, the analysed movements will be in regards to the right lower limb.

Gait in general can be explained by three main stages: the observed cycle begins the moment the heel makes contact with the ground (heel strike), following all movement of the foot until the touch of the toes (toe strike) and finalizing with toe lift off (toe off). These definitions can be both applied to walking and running gait, although with slight changes applied (Figure 1.2).

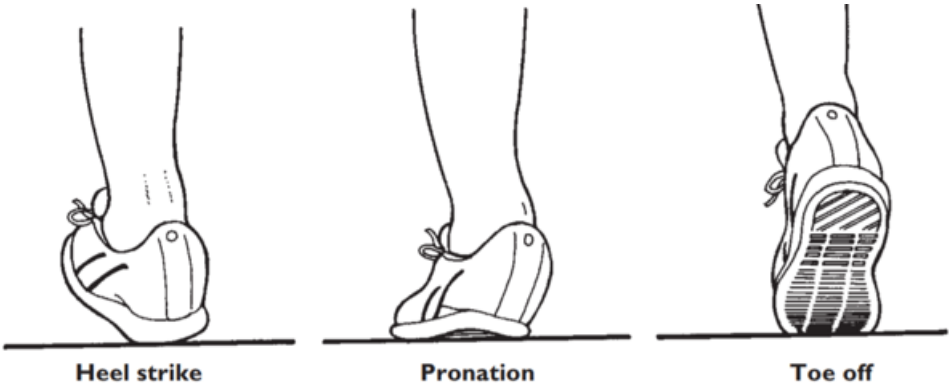

Figure 1.2 – Posterior view of foot stance during 3 stages of gait [3].

However, the description of the cycle can be more detailed when one divides the cycles into phases, introducing more stages that better characterize it. As such, previous work ([1], [4]) and literature ([5], [6]) describe 2 major phases in the gait cycle: **Stance** and **Swing**.

- During **stance phase** the foot is in contact with the floor, starting from heel strike and ending on toe off. The stance phase can be further divided into 3 stages in regards to foot contact:

    - **First double support** – both feet are in contact with the floor;
    - **Single limb stance** – left foot is in swinging motion and right foot is still in contact with the floor;
    - **Second double support** – both feet are in contact with the floor once more;

    Stance phase can also be further decomposed into several events like:
    - **Foot strike** – beginning of the cycle;
    - **Foot-flat** – plantar surface of the foot is in full contact with floor;
    - **Midstance** – swinging foot passes stance foot, leg is fully stretched;
    - **Heel-off** – heel rises and push off is initiated;
    - **Toe-off** – End of stance phase;

- During **swing phase**, the foot is in the air and swinging forward towards the next footstrike. It begins as soon as the foot is no longer in contact with the floor (i.e. toe off) and finishes where the stance phase begins. It can also be decomposed in 3 events regarding foot/leg motion:
    - **Acceleration** – Muscles accelerate the leg forward;
    - **Midswing** – Identical to midstance;
    - **Deceleration** – The leg slows in anticipation of foot contact;

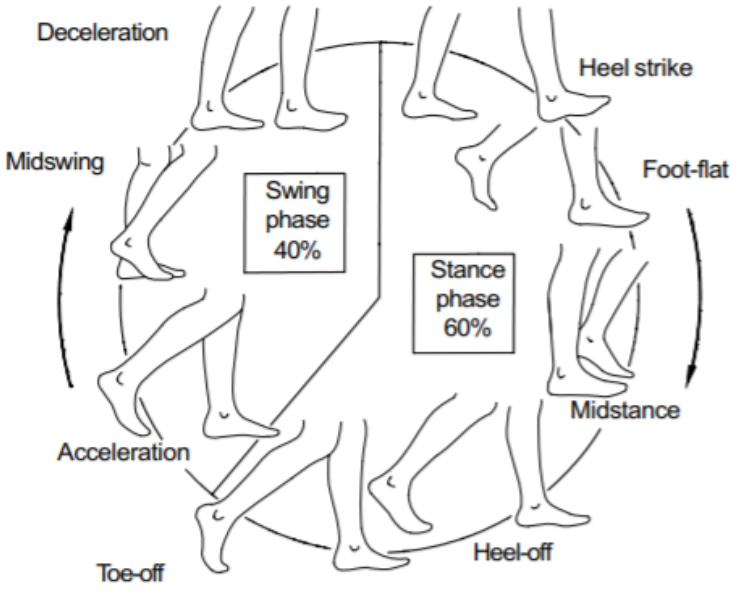

Figure 1.3 – Gait cycle [5].

The duration for each phase varies from subject to subject due to different gait speeds, however, for standard walking gait, around 40% of the cycle time is occupied by the swing phase and the remaining 60% by the stance phase (Figure 1.3).

The way that we walk and run has also changed throughout the times: for centuries people walked barefoot or with minimal footwear (e.g., sandals), a stark contrast to what we see in today's society where a wide variety of protective footwear is available[3], [7]. The style of used footwear is also a big influence when it comes to quality of running – runners consist of a group that are frequently subject to bone and muscle injury, of which some are believed to be due to an incorrect technique of running. One of the appointed reasons is the difference in gait that the human body performs when running barefoot versus shod, more specifically, the way that the feet strike the floor:

- When running in cushioned shoes, the inexperienced runner tends to land on their heels, as one typically does when walking. This means that the full impact of the running body is placed on the heel and then spreads throughout the leg;

- When running barefoot, due to the uncomfortable pain the user would experience when landing on their heels (due to the higher forces and momentum involved), the runner tends to midfoot or forefoot strike and then landing the rest of the foot. This striking technique dissipates the initial impact peak, eventually diminishing the probability of stress-related injuries.

Regarding human kinetics during gait, their time evolution during movement can be measured using a force plate. By registering the response to the downwards and sideways force that our body exerts on the plate (known as **ground reaction force**, or **GRF**), the impact and impulse forces can be plotted over time. These plots allow for an easy view of the forces at play in different types of movement (e.g., running vs. walking) and foot strike (e.g., heel strike vs. forefoot strike).

Analysing the plots registered by Tongen. A. and Wunderlich, E. [8] , it is easy to correlate the different stages of GRF with gait phases. In Figure 1.4 (a), 2 notable peaks are displayed in regards to **walking** – the first corresponds to the moment immediately after heel strike, when the centre of gravity is directed downwards (towards the force plate). The second peak corresponds to the impulse of the foot to propel the body forwards, where the forefoot and fingers "push" the floor away. The depression in the middle is mainly due to the change of direction of the body's centre of gravity – after contact of the entire foot with the floor and beginning of impulse, the centre of gravity rises away from the ground, decreasing the applied force (i.e., meaning less reaction force).

Looking at the **running** GRF, one can notice a single peak: higher in comparison to walking GRF (more velocity involved, higher impact) and overall shorter time (faster movement, around 0.3 seconds in duration). The existence of only one peak is due to the downwards centre of gravity only changing once after foot-floor contact, to quickly propel the body forwards.

The last plot, **speed-walk**, validates the difference of GRF in a softer foot contact in contrast to heel strike in running gait. The overall "M-shape" of the plot is similar to the walking plot, but features and additional peak near the first one, called an impact peak .This peak is also observable in the running plot, and can be mitigated with a better running technique, performing forefoot strike. The difference in GRF is easily observable in the research conducted by Lieberman, D. [et al], where forefoot strike and heel strike approaches are compared (Figure 1.4, (b) and (c)).

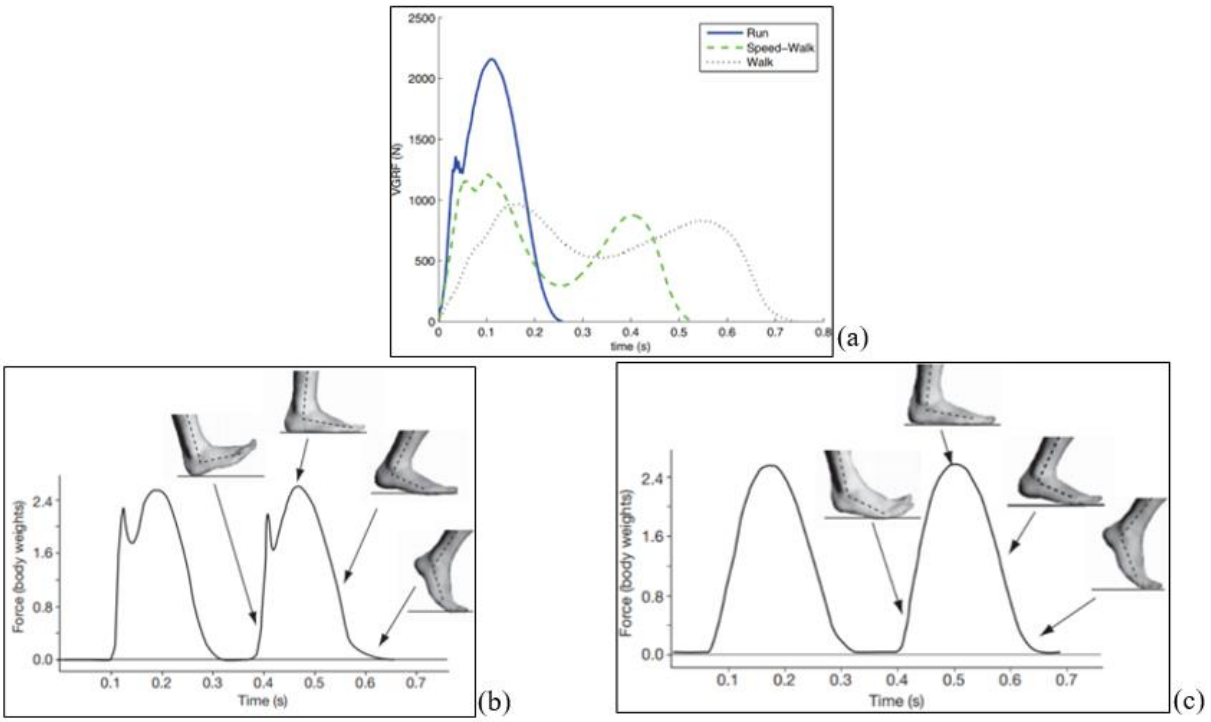

Figure 1.4 – Differences of Vertical Ground Reaction Force (VGRF) registered in different types of gait (a) [8], difference of impact peak registered in heel strike (b) and forefoot strike (c) [7].

Another very important measurable quantity in biomechanics, knowledge of the Centre of Pressure (CoP) trajectory when walking or running offers valuable information regarding possible gait pathologies the subject might have, being also helpful for the creation of orthoses, footwear or any other medical device related to gait correction [9]. CoP, by definition, is where the GRF vector propagates for the duration of the stance phase. It is the centroid of all existing forces acting on the foot, which usually start in the rearfoot, due to heelstrike, transition towards the midfoot, as the foot comes down in contact with the floor and end in the forefoot, when the subject propels himself forward [10], [11].

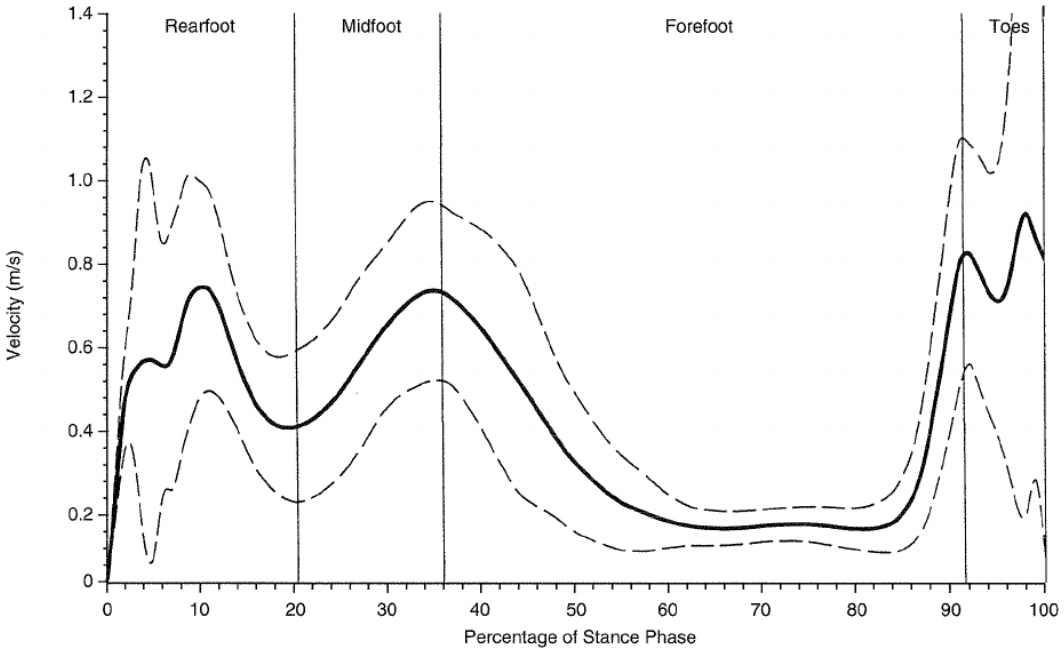

Figure 1.5 – Mean Velocity of Centre of Pressure during walking. Dashed lines represent +- 1 standard deviation [11].

CoP velocity (VCoP)[11] is also an important indicator of gait quality, with atypical changes in VCoP being closely related to some sort of muscle deficiency that affect either foot contact or limb motion. Although varying from subject to subject, it usually features a common triple peak pattern as seen in Figure 1.5.

Much alike the GRF measurement method, CoP data is also gathered from the force plate: depending on the type of force plate, the sensors quantity and location may vary. Since the plate used in this thesis' experiments featured a six component transducer, an output of six variables was offered - *Fx*, *Fy*, *Fz*, *Mx*, *My* and *Mz* – with the following equations illustrating the calculation of the CoP trajectory and VCoP throughout gait. The centre of pressure coordinates are obtained through [9],[10]:

$$CoP_x = -\frac{M_y + F_x d_z}{F_z} \tag{1.1}$$

$$CoP_y = \frac{M_y - F_y d_z}{F_z} \tag{1.2}$$

Where *CoPi*, *Mi*, and *Fi* are the CoP coordinates, moment and force values in the *i* direction, respectively. *dz* is the platform thickness (*dz* = 42 mm). CoP velocity is calculated as the distance between consecutive points (each point defined by *n*), dividing by the capture frequency *f* (500 points/second, in this case *f* = 1/500):

$$VCoP_x = \frac{CoP_x(n-1) - CoP_x(n)}{f} \tag{1.3}$$

$$VCoP_y = \frac{CoP_y(n-1) - CoP_y(n)}{f} \tag{1.4}$$

$$VCoP = \sqrt{{VCoP_x}^2 + {VCoP_y}^2} \tag{1.5}$$

1.3. Lower limb gait actuators

A small introduction to the muscles and joints responsible for leg and feet movement, allowing for a clearer understanding of the musculoskeletal function.

Gait is achieved by continuous mutual interaction of various muscles and joints throughout our body, with the lower limbs performing most of the movements in gait and the upper limbs having an important role in equilibrium maintenance. To better understand the mechanisms behind lower limb movement (analysed in this thesis), it is essential to comprehend the behaviour of the two main joints, knee and ankle [3], [9].

The knee is where the femur and tibia join and where the positon of the foot is determined in walking/running gait. The knee allows for multi oriented movements, ranging from flexion and extension (lateral view), rotation (top down view) and abduction/adduction (posterior/anterior view) - flexion and extension will be the ones mainly visible in the footage of this thesis. It plays a major role in stability and load bearing during movement due to the action of 14 muscles, with the quadriceps playing a major role in knee extension and the rest in flexion [3], [6]:

- During knee **extension**, the vastus lateralis, vastus medialis, vastus intermedius and rectus femoris (forming the quadriceps) are activated, with muscle intensity peaking between heel strike and mid stance, where flexion starts (Figure 1.6 (b)).
- The 3 hamstring muscles (posterior thigh muscles), semitendinosus, semimembranosus and biceps femoris are the main actuating **flexors**, together with the assistance of the gracilis, sartorius, popliteus and gastrocnemius muscles (Figure 1.6 (a)).

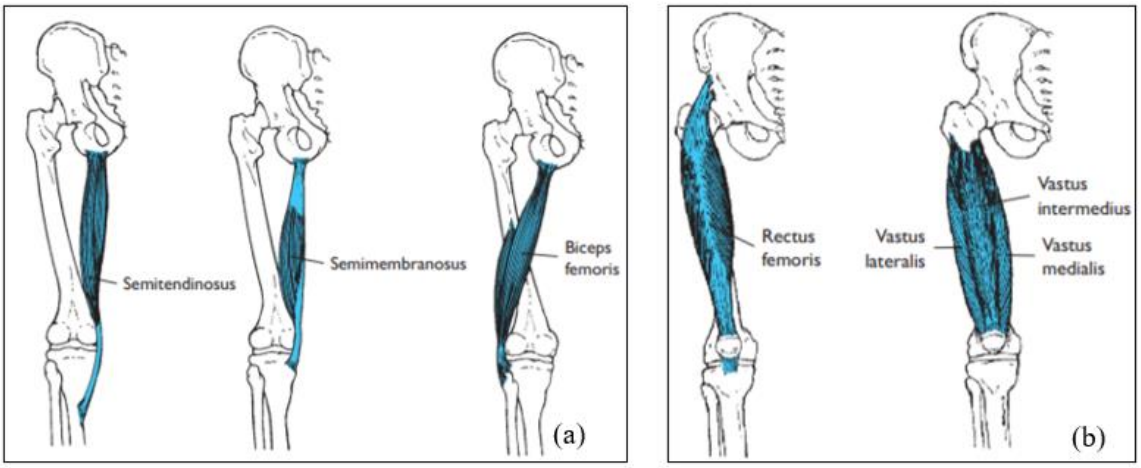

Figure 1.6 – Posterior view (a) of the hamstrings and anterior view (b) of the quadriceps muscles [3].

The ankle – or ankle-foot complex – is a much more elaborate region, where 3 joints can be found: distal tibiofibular, tibiotalar (where the majority of motion occurs) and fibulotalar joints. Here, all of the muscles participate in both phases of gait, ensuring dorsiflexion and plantarflexion when necessary, however, the major muscles responsible for these movements are present on the leg:

- Major **dorsiflexors** consist of tibialis anterior, extensor digitorum longus and peroneus tertius, with assistance of the extensor halluces longus (Figure 1.7 (a)).
- Major **plantar flexors** consist of gastrocnemius and soleus muscles, with the assist of other local muscles like the tibialis posterior, peroneus longus, peroneus brevis, plantaris, flexor hallucis longus and flexor digitorum longus (Figure 1.7 (b)).

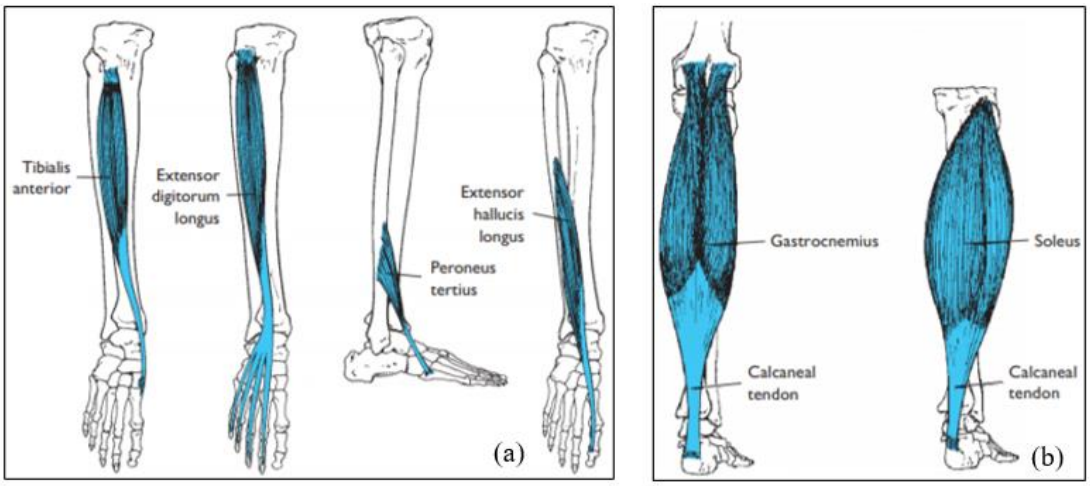

Figure 1.7 – Dorsiflexors (a) and plantar flexors (b) of the ankle [3].

.

1.4. Skin deformation

A small introduction to the skin, its properties and the development of devices that frequently interact with it is made to further clear the purpose of this thesis.

As the largest organ in the human body, the skin acts as a barrier against harmful interactions. It is subjected to various deformations (e.g., stretching, pinching) during daily activities, but unless major damage occurs, the skin returns to its original state due to its viscoelastic properties[12],[13]. This ability to stretch and distort under loading conditions while maintaining full performance of its functions (physical protection, regulation of the human body's temperature, vitamin synthesis, among many others) demonstrates its unique mechanical properties, mainly due to the presence of elastin and collagen fibres in its constitution.

Typically represented in a stress-strain curve (Figure 1.8), its behaviour is considered non-linear due to its heterogeneous nature: when submitted to lower stress (i.e. strain levels below 40-50%) elastin fibres assume a major role in load bearing; as stress levels rise, the skin stiffens and collagen fibres straighten, supporting the rising load levels. When the load rises to extreme values, all of the fibres align to support until defibrillation occurs[14], [15].

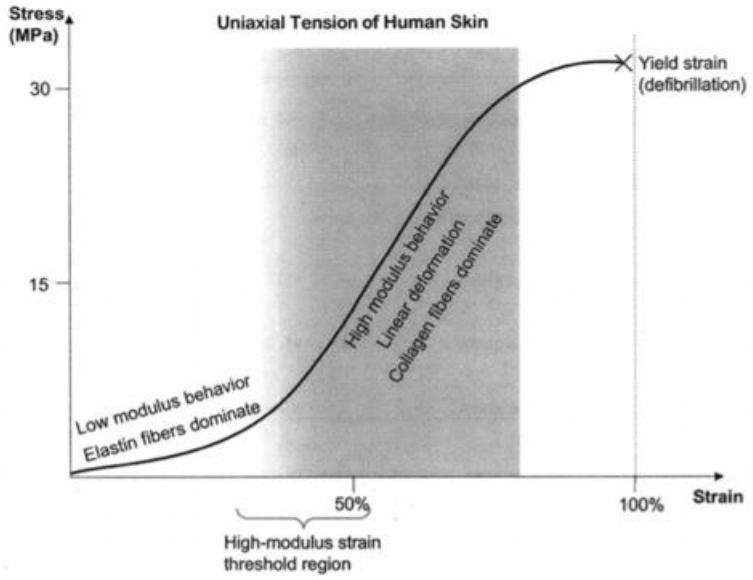

Figure 1.8 – Skin stress-strain curve evolution [15].

Under the skin lies our musculoskeletal system, responsible for allowing the movement of our body. When performing any kind of movement, muscle activity and the interaction of the body with the ground can be "seen" through their manifestation along the skin, with the activation of our muscles resulting in extension of the skin, and the floor's reaction to our leg impact slightly deforming the skin. To gather information for the creation of garments, medical devices (e.g. orthosis) and more, the study of skin behaviour, of the regions that suffer most deformation and the lines that show very little to none deformation at all, is essential to ensure their quality.

A concept that benefits from the study of skin behaviour is the soft exoskeleton. A soft exoskeleton (also known as soft exosuits) is built using innovative textiles that allow for an easy interaction with the human body[16]. Due to their light nature, they present some unique advantages when compared to more mechanical-based, bulky exoskeletons: easier articulation mobility (lack of rigid structures), lightweight rig and good ergonomics[16], [17]. One such exoskeleton (Figure 1.9) was developed in the Massachusetts Institute of Technology (MIT) with the purpose of being used in outer space, replacing the bulky typical spacesuit with a skin tight version [18]. The created garment features coils distributed along specific lines all over the body, that contract whenever a certain threshold of heat is present.

Figure 1.9 – Second skin suit developed at MIT [18].

The distribution of these coils follow the concept of Line(s) Of Non-Extension (LoNEs), that can be defined as the lines along the human skin that suffer neither contraction nor extension during movement – in terms of skin strain magnitude analysis, LoNEs correspond to directions with zero strain magnitude. The purpose of their study is to implement, along these lines, specialized strands that help with supporting loads, without hampering body motion.

First studied by Arthur Iberall[19] in 1951, this research was aimed at assisting the development of space suits, to allow for an easier locomotion, without interfering with established components – through observation of the lack of mechanical stress along certain lines of the human skin, it was concluded that the suit should be constrained along those lines in order to minimize energy expense.

Although it didn't find much success in the military and space exploration areas, the research of soft exoskeletons benefitted with the concept of LoNE, finding interest in the biomedical field, where the results can help or even improve existing projects related to muscular augmentation or physical therapy.

1.5. Strain analysis

A quick explanation of the basics of deformation and strain, the most commonly used tensors in this type of analyses, including the ones used and presented in this thesis.

As mentioned before, due to the skin's viscoelastic and anisotropic properties and the importance of their behaviour to the medical/textile/cosmetic field, choosing the correct method to analyse retrieved data is essential to guarantee the quality of the end results. Therefore it is necessary to have a complete understanding of the two major definitions in play when studying skin mechanical behaviour (i.e. kinematics) - deformation and strain ([20], [21]).

- Deformation is the modification of the body shape from an undeformed state (usually at time t_0) to a deformed state (at current time t), due to the action of a deforming agent (e.g. external loads, temperature, etc.). Two approaches or descriptions can be followed, Lagrangian or Eulerian. These differ in the perspective of what to analyse: Lagrangian approach follows material points on the target object and registers the changes in its properties; Eulerian approach focuses on a given point in space and registers all of the changes of the elements that pass through the chosen location.

- Strain is the quantification of deformation. It is a dimensionless quantity, that demonstrates, at time t, how much the target has deformed from its original shape in t_0 . There are several strain tensors that are capable of interpreting deformation, such as the Cauchy-Green, Lagrangian (aka Green-Lagrangian) and Eulerian (aka Euler-Almansi) strain tensors, for example. By norm, positive strain values represent an extension and negative values represent a compression of the object.

  Out of the chosen tensors, one can extract multiple variables important to the analysis, notably:

- e_{xx}, strain on the X-direction of the chosen axis;
- e_{yy}, strain in the Y-direction;
- e_{xy}, shear strain;
- e_1, major principal strain;
- e_2, minor principal strain;
- *von Mises*, von Mises strain;

von Mises strain is a scalar quantification of the strain state of an object, measuring all extensions exerted on it. As a scalar, it always features positive values. It represents an essential way of measuring the maximum yield strength for any isotropic material.

The principal strain is the largest registered strain, calculated by taking a derivative to e_{xx} and/or e_{yy}. Following VIC-3D manual definition, it is "the strain for a reference frame that is rotated such that shear has become zero, leaving only two strain components at 90º angles"[22].

1.6. Digital Image Correlation (DIC)

Digital Image Correlation is the main concept behind every evaluation during this entire thesis, allowing for the analysis of the deformation, rigidity and strain of the skin during gait in both walking and running manoeuvres – a definition of the core procedures is presented.

Digital Image Correlation, in sum, is a non-contact, optical method that registers the changes in small areas (subsets) in a contrasting pattern, present in the target specimen. These changes are compiled and their spatial and temporal evolution characterize the deformation of the object when submitted to stress[23].

For every evaluation, two sets of images of the specimen are required: when static or undeformed (reference image) and deformed. When obtained, it is necessary to run through a calibration process that allows for spatial correlation between the images: these images are divided in "smaller sub-images (facets)", and subsequently an algorithm matches the differences of these facets between reference and deformed images[24].

Although some differences may arise when analysing different specimens, the experimental methodology to gather the images necessary for digital image correlation usually follows these steps:

- **Surface pattern preparation** – For the software to recognize and calculate the deformation of the target over time, its surface needs to feature a randomized pattern. This pattern, either naturally present or created by artificial means (e.g. painting, spray), should follow a random distribution, present a high contrast (e.g. black dots over a white background) and an adequate speckle dot size. A random distribution ensures low levels of noise and quality speckle tracking, avoiding false matching. An adequate speckle size avoids the presence of small sized dots, which can cause aliased results.

- **Positioning and calibration of camera system** – The user has to ensure that the camera system is adequately put in an ideal position, with a clear view of the target. Calibration of the system consists of finding out the cameras' extrinsic parameters (i.e. the ones that "connect" both cameras such as distance and angles) and intrinsic parameters (i.e. parameters unique for each camera, like focal length, aspect ratio and skew coefficient). There is also a need to calibrate the analysis software, and although the process may differ in different types of software, it usually consists of multiple pictures of a calibration grid in various positions. This calibration grid typically consists of pattern of dots or squares arranged in rows and columns that are required to fill the field of view of both cameras and be recognized by the DIC calibration software.

- **Data acquisition** – In this phase, the desired test should occur: the system should capture the target in an undeformed state and then all of the physical changes that it is subjected to.

- **Image correlation** – The final output of this process is heavily influenced by the chosen correlation algorithm parameters. With the sequence of images in hand, the user has to: select a region of interest (ROI) adequate to the speckled target; choose a balanced facet size (M*N pixels of the sub-images), larger than the speckle dots but small enough to ensure good resolution; choose grid spacing – "distance between two consecutive facets". Other parameters like validity quote and application of filters can also be adjusted to better improve analysis.

Overall, when comparing with other full-field, optical measurement techniques like holographic interferometry, speckle interferometry and others, DIC offers many advantages in regards to the wide range of sizes and materials it can analyse, the intensity of deformation (i.e. from small to large values of strain), the ability to use in *in vivo* studies and its minimally invasive procedures (i.e. surface preparation)[24].

1.7. Thesis objectives and structure

In the present section, all of the thesis' established objectives and overall presentation structure are outlined in order to simplify and facilitate the reader's comprehension of what is to come. After a

comprehensive literature review and examination of existing equipment useful for performing the experiments, objectives were established:

- Study of the skin strain, GRF, CoP and VCoP synchronized temporal progression during stance phase of:
    - Walking gait;
    - Running gait;

- Identification of an equilibrium recovery pattern in "pull" tests for both gaits, consisting of pulling the subjects in the opposite direction of movement in mid stance;

- Identification of rigid body rotation of the ankle in walking gait;

The present work is organized in five chapters, established as follows:

In Chapter 1, the main focus is to explain the motives guiding this work and the basics of the three essential topics approached in this thesis: human gait kinematics/kinetics and skin strain analysis, both analysed in the results, and digital image correlation, the tool utilized to map skin strain.

Chapter 2, State-of the-Art, features the same three topic oriented structure, with correlation of gait kinetics and kinematics section presenting work that correlates biomechanic quantities (similarly to this thesis purpose); skin strain analysis studies focusing on the evolution of skin deformation analysis methods and results; and numerical image correlation tools focusing on highlighting the purpose and validity of the tools used in frame analysis.

Chapter 3, Experimental Methodology, focuses in detail the experiments and their procedure, to allow for an easier future reproduction. The preparation for the tests and chosen analysis parameters are also both approached here.

Chapter 4, Results, demonstrates the achieved output of the analytic processes developed in Chapter 3 and test data interpretation.

Chapter 5, Conclusions, presents a review of the experienced positive and negative results from the experiments, ending the chapter with hints and suggestions useful for future work.

2. State-of-the-art

2.1. Correlation of gait kinetics and kinematics

The following state of the art details the work done to better describe the relation between human gait and the kinetics involved in movement.

In 2006, Verdini *et al.* [25] studied the impact peak present in GRF readings, defined as the heel strike transient HST, and its correlation to muscle activation in the lower limb. The presence of this transient can be associated to gait related pathologies (e.g. osteoarthritis).

A total of 25 healthy subjects performed the experiment, following a simple protocol consisting of walking barefoot and foot striking the force plate. A six-channel surface electromyographic system was used to measure muscle activity whilst the force plate registered gait related forces.

Results showed that a majority of trials had the presence of a sharp HST (around 76%), whilst a minority had no presence at all (10.7% of trials), leading to the necessity of more trials in order to define a tresholod that separetes a healthy subject from an unhealthy one, based on HST presence and intensity (Figure 2.1).

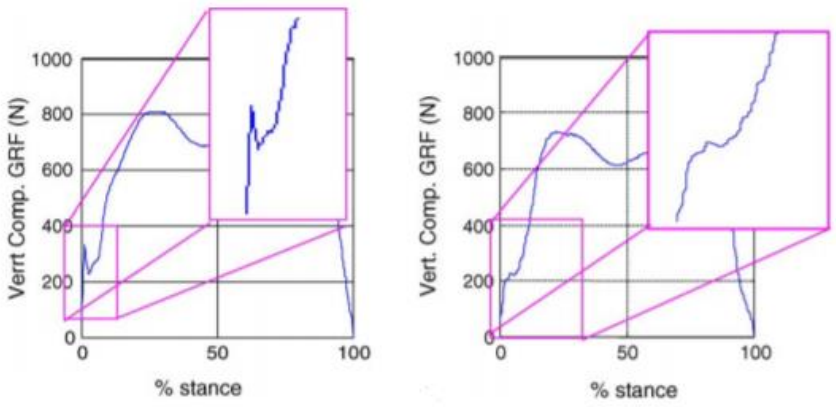

Figure 2.1 – Difference between sharp (left) and smooth (right) HST [25].

Fuchioka *et al.* [26] focused on the study of the CoP trajectory and its relationship with kinematic changes in gait of older adults. Using an insole pressure sensor both CoP and the anterior-posterior displacements were quantified, compared and used for the calculation of CoP velocity for the three foot regions – rearfoot, midfoot and forefoot.

Sixty-eight subjects participated in the tests, consisting of performing walking gait over a 10 meter distance at a natural pace. Foot pressure was recorded at 50 Hz along 960 sensing locations. Results revealed a high correlation between gait speed and velocities of the rear and midfoot, indicating the importance of VCoP as predictor of gait speed.

Joana Capacete[2], in 2016, focused on the correlation and analysis of GRF, CoP, VCoP and dorsal skin deformation of the ankle foot-complex, based on previous work performed by Ricardo Ferreira [1]. Using the same set-up (camera and force plate), with the FOV focused on the ankle, the subjects performed walking gait under normal conditions. Overall data was according to literature, however perfect synchronization wasn't achieved (Figure 2.2). The same hypothesis analysed in this thesis was evaluated here, where it was stated that at around 10% of stance the ankle and leg move as a rigid body.

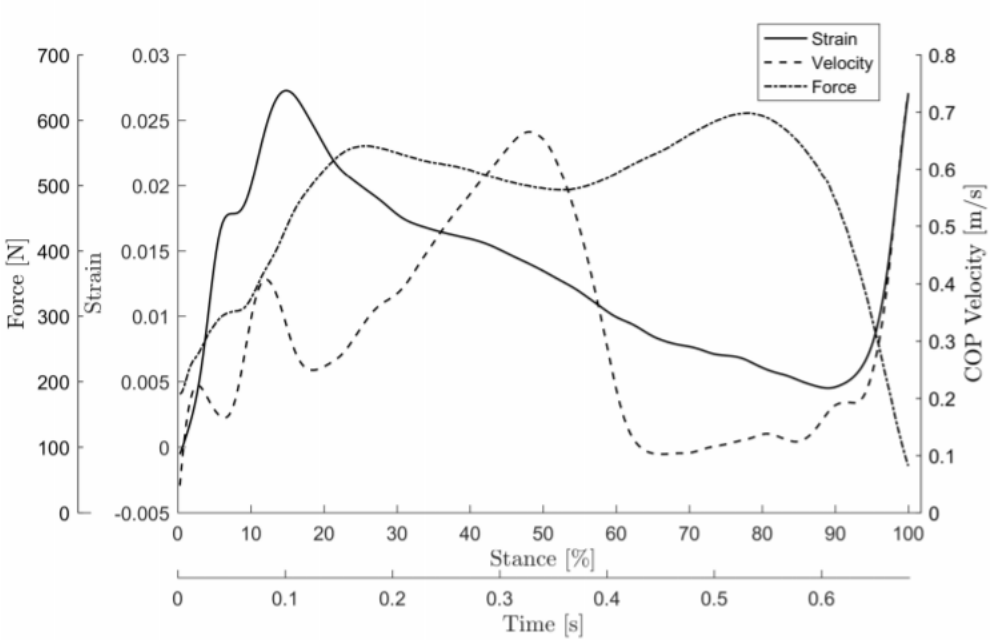

Figure 2.2 – Gait velocity, force and skin strain correlated data [2].

2.2. Skin strain analysis

The following state of the art was the result of a narrowed search for studies that either focused on the study of the lower limb's skin properties or the mapping of its LONE's.

The first study of LoNEs by Iberall[19] used ink circles stamped on the skin as a method for mapping the lines along the body - when the subject performed the requested movement, the deformation of the marked skin meant the deformation of the circle into an ellipse. To check for directions in which the skin had not deformed, the two unstretched diameters of the figures were marked, a process that was done multiple times, in multiple areas of the body (Figure 2.3). There were three evaluated subjects in total, and the resulting LoNE positioning was overall the same for all bodies.

A simple prototype net suit was woven and used by one of the subjects together with another rubber suit, a layer that would make possible the pressurization tests: several movements were performed (e.g. jumps, squats, writing) whilst under pressure to test the effectiveness of the suit, yielding overall positive results.

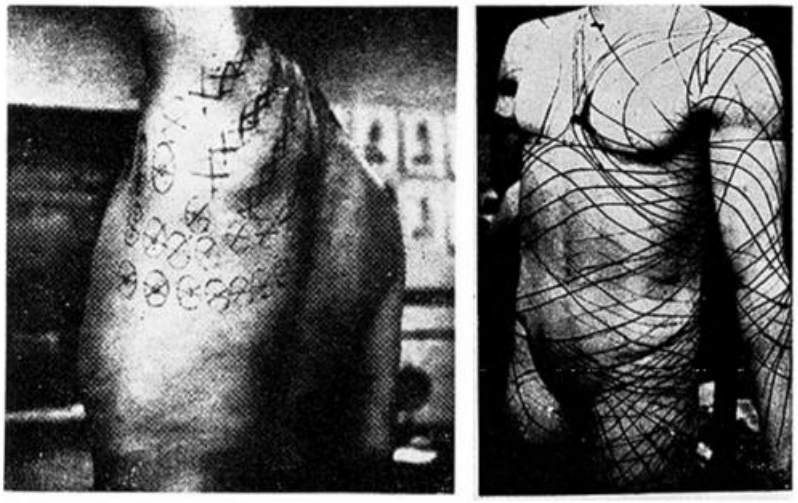

Figure 2.3 - Arthur Iberall's method for discovery of the direction of LoNEs (left) and LoNE mapping of the body (right) [19].

New technologies were eventually developed that allowed for an easier evaluation of the stress behaviour of materials (in this case, the skin), such as the aforementioned Digital Image Correlation (DIC), used in many biomechanical oriented studies due to its advantages.

In 2005, Kristen Bethke[15] studied the effect of human skin deformation caused by knee flexion, mapping the respective strain affected areas. To further existing research in the theory of advanced locomotion mechanical counter pressure (MCP) spacesuits, two experiments were performed – an analysis of the variation of surface area and volume of the leg and the strain field developed during knee gait.

The chosen method to record skin behaviour was through a 3D laser scan, in which over 156 position trackers were placed on the subject's leg. The dots were approximately 4 millimetres in diameter, and separated from each other by 3 centimetres (Figure 2.4). The calculated values were evaluated by the displacement of each trio of dots.

Movement was recorded from an initial state (0 degrees – extended leg) upwards to a 90 degree flexion state. The retrieved data was then given as input to several MATLAB functions, to perform adequate strain and directional analysis. End results were able to show the directions of minimum stretch and also allowed to root out errors in the chosen method, making it possible to draw some guidelines for future work.

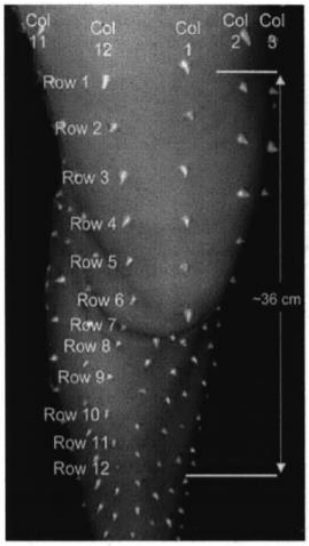

Figure 2.4 – Marker disposition on the leg [15]

Sara Marreiros' Masters thesis[27] also focused on LoNE mapping, with the goal of observing the skin deformation surrounding the ankle and foot, when dorsiflexion and plantarflexion was performed. All data from this research served the purpose of designing a second-skin orthosis that would help with drop-foot pathology correction.

The acquisition system was comprised of four infrared cameras and retro-reflective markers, responsible for detailing the spatial variation on the skin (Figure 2.5). These markers were approximately 4 millimetres wide and spread 2 centimetres apart from each other, organized in rows and columns. The retrieved data was analysed by the Qualisys Track Manager Software (supplied the trajectories of the present markers), MATLAB code (evaluated skin strains, magnitudes and LoNE's) and ABAQUS software (calculated deformation and strain tensor).

Figure 2.5 - Marker disposition on the foot-ankle complex (left) and capture system (right)[27].

Some setbacks were noted, namely the low number of cameras and the 2 cm spatial resolution. A higher number of cameras would allow to observe all regions as a whole, instead of being divided into multiple views; a smaller grid would allow for better definition on the analysis of skin deformation. Main conclusions showed higher values of deformation in anterior and posterior regions of the ankle: anterior region suffered largest extension during plantar flexion and largest compression during dorsiflexion; for the posterior region, opposite values were observed. Various sets of direction of LoNEs

were also identified, despite the irregularities caused by noise generated by the markers spatial acquisition process.

In an effort to boost the precision of strain measurements of the skin to improve the quality of mechanical interfaces with the body, Andrew T. Marecki presented a strain analysis toolbox that allows for the reconstruction of 3D model of the body from input photographs[28]. To prove the effectiveness of the tool, reconstruction and strain analysis of an amputated lower limb was performed (Figure 2.6).

The toolbox uses several photographs of the target in various deformed positions to reconstruct the model, and then proceeds to analyse the strain variation, all in an automated process. For this purpose, it uses Autodesk's 123D Catch program and MeshLab to create the model and divide it into meshes, respectively, whilst the strain analysis is performed via MATLAB scripts. User controlled parameters consist of adjustable dot resolution and area of analysis, allowing for focused study of specific, desired areas.

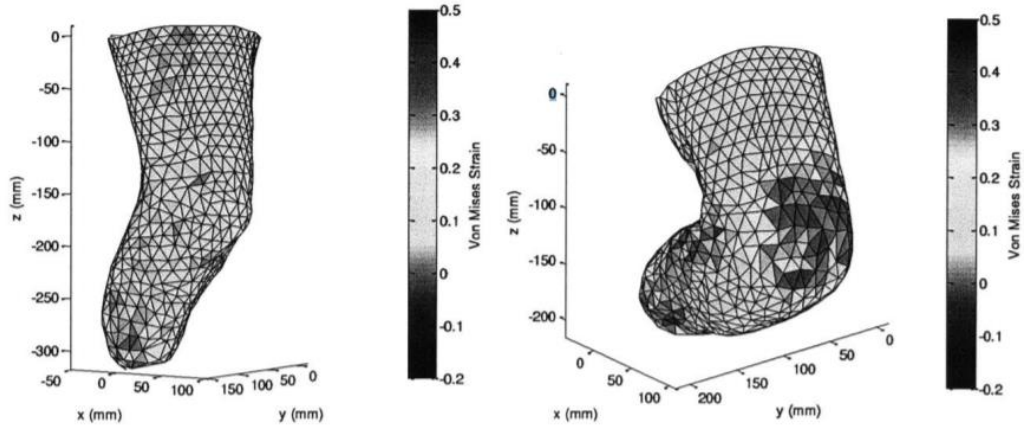

Figure 2.6 - 3-D representation of the strain map of the knee when extended (left) and folded (right) [28].

Published in 2012, Wessendorf work [29] presented a novel method to analyse the strain fluctuation in the knee region when its natural movements are performed (i.e., flexion and extension). A motion capture system consisting of eight infrared cameras was used to acquire the position of several markers in a subject's leg when performing a squatting movement – a total of 144 4mm and 6mm spherical reflective markers, spaced approximately 2-3cm between each other, were used.

Data registry consisted of two stages, stationary and dynamic: for the static stage, data was captured when the subject had her leg fully extended and fully contracted (squatting); for the dynamic stage, a squatting cycle was recorded, starting in an extended position, then a complete flexion of the knee and ending again in a fully extended position.

All of this data was processed by MATLAB code that outputted strain data, directions of LoNE's and lines of minimum compression/extension (Figure 2.7). The highest value of strain registered for all directions was 0.446, conforming to expectancies from previous studies. Other important registered values were the ranges of minimum and maximum longitudinal strain (-0.303 to 0.446), circumferential strain (-0.832 to 0.116) and shear strain (-0.113 to 0.105). Coupled with plots of LoNE's and strain maps, this method supplied accurate and precise information.

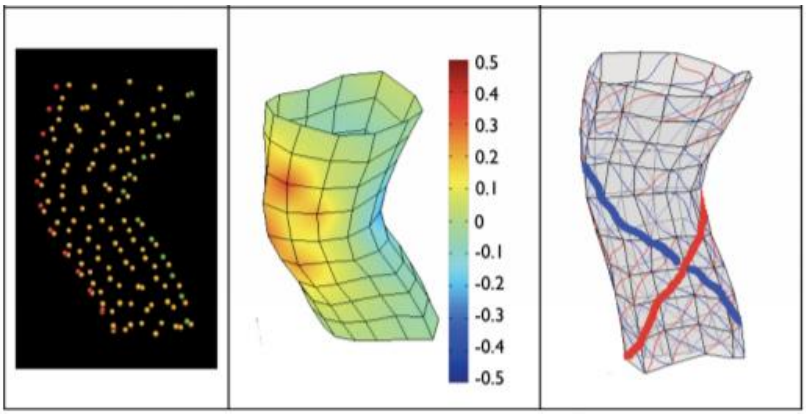

Figure 2.7 - 3D cloud point distribution of the leg (left), longitudinal skin strain of the knee (middle) and posterior view of calculated LoNEs on the knee (right) [29].

For her PhD thesis during 2014, Domingues [4] focused on the study of the dynamics of the skin surrounding the ankle and its activity during movement (plantarflexion and dorsiflexion). The proposed concept was the implementation of actuators along the LoNEs, with the lines of maximum extension guiding their distribution and alignment to better adapt the orthosis to the human body.

Overall, 2 methods were used (Figure 2.8), contrasting each other in the different resolution of the markers:

- Use of *Qualisys Motion Capture System* (8 infra-red cameras), using 85 markers spaced 2 cm between each other;

- Use of *Polaris Spectra*, with 410 points acquired along the leg, featuring a spatial resolution of 1 cm.

After data acquisition, MATLAB code analysed skin strain around the ankle-foot complex, providing strain fields, LoNE direction and a comparison between both used methods.

Results regarding areas of deformation were in concordance with previous studies [27], with values of longitudinal strain ranging between -0.34 to 0.40 (first method) and -0.32 to 0.40 (second method).

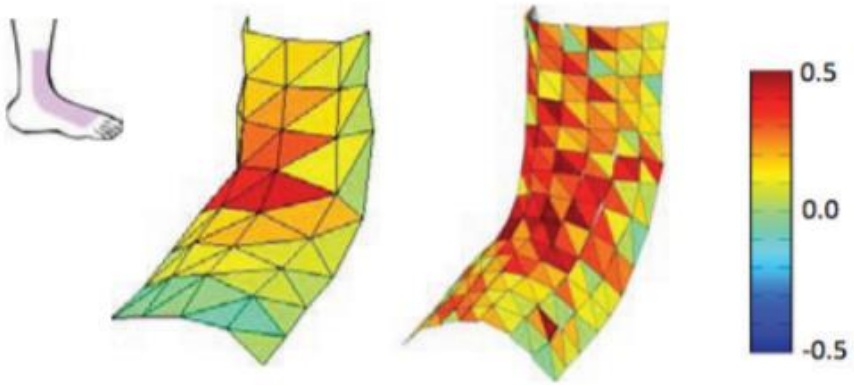

Figure 2.8 - Comparison of longitudinal strain maps obtained between both methods (1st on left, 2nd on right) [4].

In his Masters' thesis, Ricardo Ferreira[1] further developed the studies of skin strain on the ankle-foot complex, using VIC-3D (digital image correlation tool) to analyse eighteen subjects. One of the major improvements over previous work was the marker resolution: a higher resolution was achieved due to an approximate 2 mm spacing between each marker (in this case, a speckle marked on the skin).

Using two cameras (Mikrotron EoSens MC-1363) with overlapping fields of view, 3 seconds of footage were recorded using a high frame rate for maximum information during movement of the foot – 500 frames per second. During the 3 seconds of recording, a set of movements were performed, totalling in 3 analysed movements: plantarflexion and dorsiflexion, inversion and eversion, pronation and supination.

The obtained data was then fed to MATLAB programs that computed strain magnitudes, principal directions of deformation and LoNEs (Figure 2.9). Overall, obtained results matched expectancies and results from other studies[27].

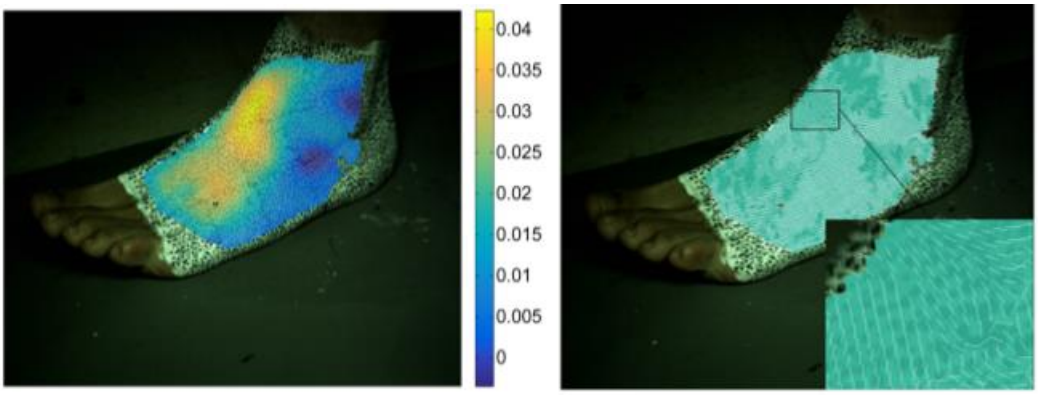

Figure 2.9 - Anterior views of major strain components (left) and LoNE representation (right)[1].

2.3. Numerical image correlation tools

This section details the two tools to be used in this thesis: VIC-3D has been used in a wide variety of skin studies and Kinovea is an open source developed tool, aimed for biomechanical studies.

Developed by Correlated Solutions, VIC-3D is a commercially available tool that features non-contact (i.e. optical) measurement of full-field displacements and strains through the application of digital image correlation[22]. This method allows for the measurement of the deformation on the surface of an object, through the measure of grayscale changes (i.e. pixel displacement) in a small neighbourhood (denominated subset).

As a 3D-DIC analysis tool, it requires the acquisition of the following essential sets of images:

- Stereo calibration images – Necessary to perform system calibration and distortion correction for correct analysis;

- Speckle images – Necessary to evaluate the deformation of the speckled object (in this case, the entirety of the leg) in different positions;

Distortion correction consists of finding the best parameters that correct the distortion effect present on both calibration and speckled object images. These parameters are obtained with the application of specific algorithms on the images retrieved with help of a flat checkerboard.

The correction process consists of taking several flat checkerboard images by slightly varying the pitch, yaw and roll axis of the board, without exceeding the camera frame, allowing the algorithm to check for the dots (or squares) in the board in multiple angles.

This step only needs to be performed once for each camera – unless its intrinsic parameters (focal lengths, principal point, field of view) and/or lens focus are changed. The cameras can also be moved from their place, although this is not advised as it easily changes the cameras intrinsic parameters.

Stereo calibration uses the DLT algorithm to obtain the mapping between 2D image points and 3D world points, calculating reprojection errors (i.e., the error between a projected point and a calculated one).

VIC-3D is a well-known strain analysis tool widely used in the scientific community with a wide range of applications - more relevant to this thesis, it is frequently used to analyse skin stretch behaviour ([30]–[34]). However, most of these studies focus on what is established as a stationary test – the target is fixed in place and stretched in one or multiple directions, whilst the experiments performed in this thesis feature a large rotation of the target region of interest (plus than 40 degrees) from start to finish, introducing correlation error in the analysis.

Kinovea is a free, open source video analysis software usefull for observation and measurement of human body motion. After video recording, the resulting footage can be edited to the user's purpose, featuring plenty of tools that range from standard video manipulation (e.g. image transformations, zoom, aspect ratio change) to marker tracking, measuring trajectories, angular motion, displacements and velocities, all performed with subpixel accuracy. The accuracy and reliability of this tool for angle mesurement has been tested multiple times ([35]–[39]), proving this tool's efficiency and precision in the biomechanic's field.

3. Materials and Methods

This chapter provides a detailed insight on the data acquisition method, explaining the camera setup and force plate trigger connections, the applied speckle pattern and its properties, the performed movements and both GRF / Digital Image Correlation processing.

The work performed during this thesis was carried out in Instituto Superior Técnico (IST), where the necessary conditions for data collection and analysis were gathered. For data collection, it was used in tandem the force plate and camera setup present in the laboratory – these are adequately placed in the workplace, with the camera setup pointed towards the force plate, and the force plate in a wide and clear area that allows for the subjects to run and walk along the plate. Also present in the laboratory are the brushes and paints used to create a speckled on the subject's leg, needed for the experiment. For data analysis, an activation key is required to work with VIC-3D software, installed on the laboratory's computer.

3.1. Stereo acquisition system

In order to acquire images of running and walking gait, a setup consisting of two Mikrotron EoSens MC-1363 cameras and two LED bundles (RAYLUX 300 Long-Range White Light Illuminator) was used (Figure 3.1).

The HFR (High Frame Rate) cameras were synchronized with each other and the Force Plate to guarantee the simultaneous trigger and subsequent data capture over a duration of 3 seconds. The cameras were oriented in a way that their FOV would overlap the Force Plate and cover a wide enough area so that the entirety of the movement and leg were visible during gait execution. To present a "cleaner" and uniform image, a white tarp was used to cover the background. A total of 3 seconds of footage were recorded per test, with the cameras prepared to acquire 500 frames per second. To ensure video quality during footage gathering, especially during the running procedure, the cameras standard shutter speed was adjusted to avoid blurring of the subject's leg – shutter speed was decreased by lowering the shutter time value of 1970 to 850 milliseconds. To elevate the amount of light captured by the camera, their aperture was opened to the max.

Figure 3.1 – Video acquisition setup.

Each LED bundle consisted of three grouped lighting sets, pointing towards the Force Plate. Their purpose is to help with DIC measurements, ensuring a high contrast present in the speckled leg, facilitating the identification and differentiation of the pattern. Their diagonal positioning assured a wide illuminated area and a somewhat vertical focused lighting, allowing for better contrast along the leg.

3.2. GRF acquisition system

To register the impact and kinetics of the subjects when performing the desired gait, a Force Plate (AMTI BP400600 Biomechanics Force Platform) was used. Present in the laboratory, the plate occupies a central location in an unimpeded area, large enough to accommodate the subject while he/she performed the desired movements (Figure 3.2). It was also set up to gather data at a rate of 500 points per second, synchronous to both cameras. Midway through data collection, the plate was fitted with a white paper sheet to ensure better contrast between the floor and the feet, in order to facilitate the identification of the heel strike correspondent frame for better analysis.

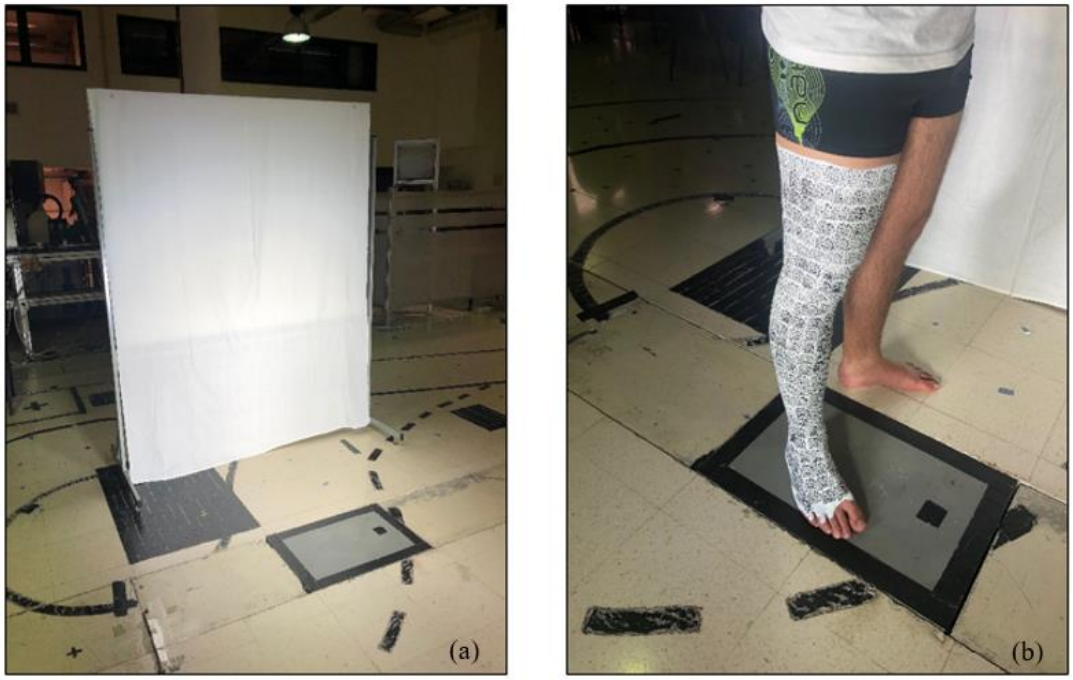

Figure 3.2 – Experiment space background (a) and example of force plate – subject interaction (b).

3.3. Calibration process

Depending on the task at hand, to guarantee the maximum possible quality of footage, the user has to adjust the cameras existing parameters to their ideal values. These parameters are especially important during camera calibration (very useful in Digital Image Correlation), where one estimates the best values to correct lens distortion, calculation of 3D coordinates of the camera and even estimation of depth/length in non-pixel units (i.e. millimetres or centimetres).

These parameters are divided into **extrinsic** and **intrinsic**: **extrinsic** parameters define the relation between camera and world 3D coordinates – the camera's location and direction can be found

in regards to the world's coordinate system; **intrinsic** parameters are inherent to the camera (i.e. focal length, aspect ratio) and manipulated by the user; they relate camera coordinates to the pixel coordinates of a given image coordinate system[23], [40].

Focusing on the manipulation of the camera to provide the best quality (i.e. intrinsic parameters management), the user has to ensure the correct location and direction of the cameras: the target shouldn't be too far as to prevent loss of spatial resolution, nor to close to avoid field of view interference. After positioning, two major factors must be managed – **focus** and **brightness** – each one complementing the other [40]:

- A correct **focus** of the target's surface avoids blurring and therefore results in optimal image quality. The focus is manually controlled by the user via adjustment of the focus ring, present on the camera. For a correct focus adjustment procedure, one should first open the lens' aperture to the maximum, to reduce depth of field and highlight focus quality; then the user should scroll the ring enough to see the image before and after passing the perfect focus region, allowing for an optimal setting.

- The **brightness** is controlled by aperture and exposure settings: the aperture ring (also present in the camera) can be manually adjusted to allow more or less light through the hole of the lens; exposure is the amount of time a camera shutter is open to gather light before a new image is taken.

Increasing aperture size makes the image brighter whilst decreasing the depth of field and vice-versa; in regards of calibration, a poor depth of field may also make it difficult to gather calibration target photos in various angles. For exposure, a higher value (i.e. longer time) makes the image brighter but can also create blur if high speed motion is registered – lowering exposure time minimizes blur. Regarding camera calibration, exposure time can be altered after performing calibration since it does not affect the quality of it.

In contrast to previous work, the calibration grid used for these experiment needed to adapt to the wider FOV of the cameras. Previous work featured an A4 sized calibration grid (210 x 297 mm), this one featured an A1 sized grid (594 x 841 mm), consisting of 13 rows and 18 columns, equally spaced by 55 mm. A0 size (841 x 1189 mm) was also tested, but due to its size, when performing the calibration procedure, the glare issues contributed to a worse calibration score, leading to the use of the A1 sized grid (Figure 3.3). Per VIC-3D instructions, the printed grid was glued to a flat, wooden board to guarantee a fully straight grid, minimizing calibration errors.

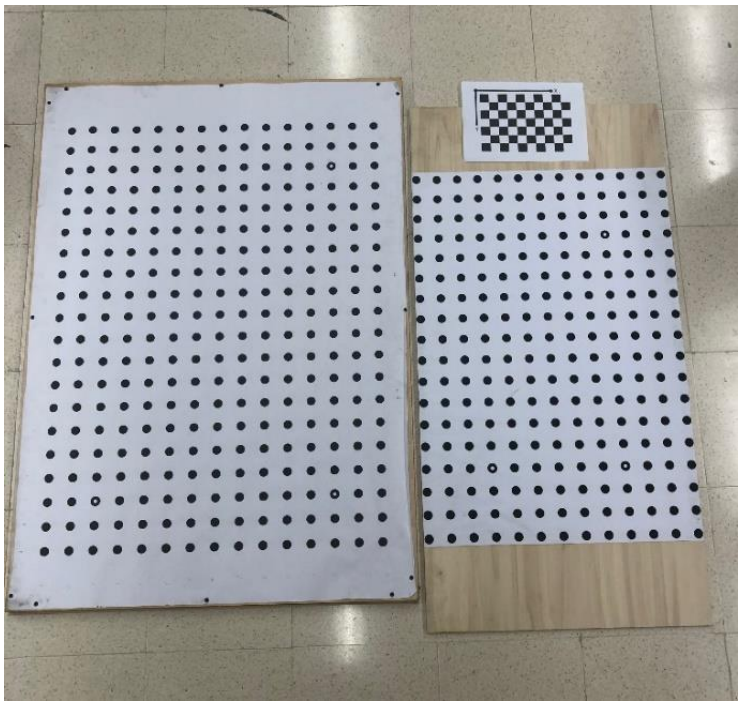

Figure 3.3 – Calibration grids used in experiments, A0 (left) and A1/A4 (right).

3.4. Speckle pattern

As mentioned before, the quality of the speckle pattern has a very high impact in the quality of the end results. Following previous studies, the utilized application method was stamping: from a randomly created pattern it was generated a 3D printed stamp, which would then be used on the entirety of the leg.

The pattern itself consists of several equal-diameter circles, randomly distributed on a surface. It was generated using VIC-3D's recommended programme, Speckle Generator – it allows the user to manage the diameter, density and randomness of the pattern and then export it to a .pdf file. This file was then exported to SolidWorks 3D CAD (SolidWorks Corporation), where the model of the stamp was created to then be 3D printed. The pattern used in the experiments consists in a random distribution of 3 mm diameter speckles, present in two stamps. These stamps differ only in their area of application, one smaller (3 x 3 cm) and a larger one (7.5 x 4 cm) (Figure 3.4).

Their purpose was to shorten the time of the stamping process, covering the area of the leg as quickly as possible - the majority of the leg was stamped using the larger one, while the smaller stamp was used mainly for the more rugged, steep areas of the ankle-foot complex and knee.

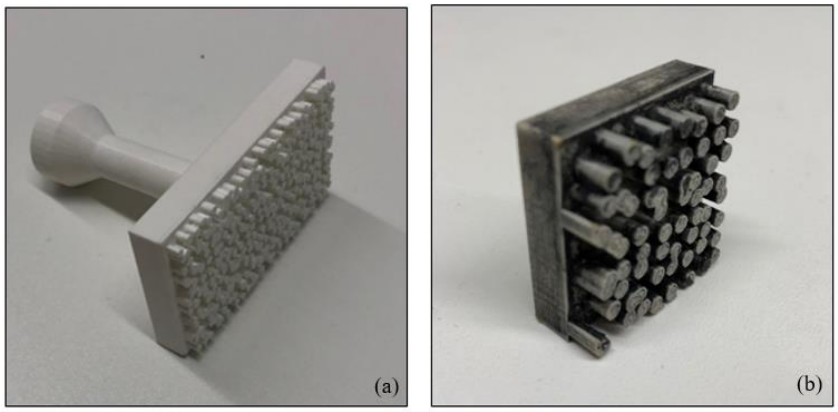

Figure 3.4 – Large (a) and small (b) stamps used in the experiment.

The leg was painted with a white, non-toxic, acrylic paint (Amsterdam All Acrylics) from mid-thigh to the base of the foot, covering its entire outer surface so that it was possible to analyse the deformation in a lateral, semi-posterior and semi-anterior view (Figure 3.5). After the surface was dried, the dots were marked using a water-based black paint (Giotto Tempera).

Application of the speckle pattern is a somewhat difficult task that the user has to deal with: a right amount of paint has to be stamped, since a small quantity (of paint) means imperfect dots (not fully coloured, or with white spots) and a large quantity means larger, bloated dots. There is also the matter of when to stamp: after applying the white paint to the leg, one has to wait for it to dry, however, the paint should not be fully dried when stamping due to the quick formation of cracks and tearing that occurs on the surface (mainly on the joint regions, around the knee and ankle), degrading its overall quality. The entire process is quite lengthy (equipment preparation – leg painting and stamping – data gathering – paint removal), taking up to 2 hours per subject.

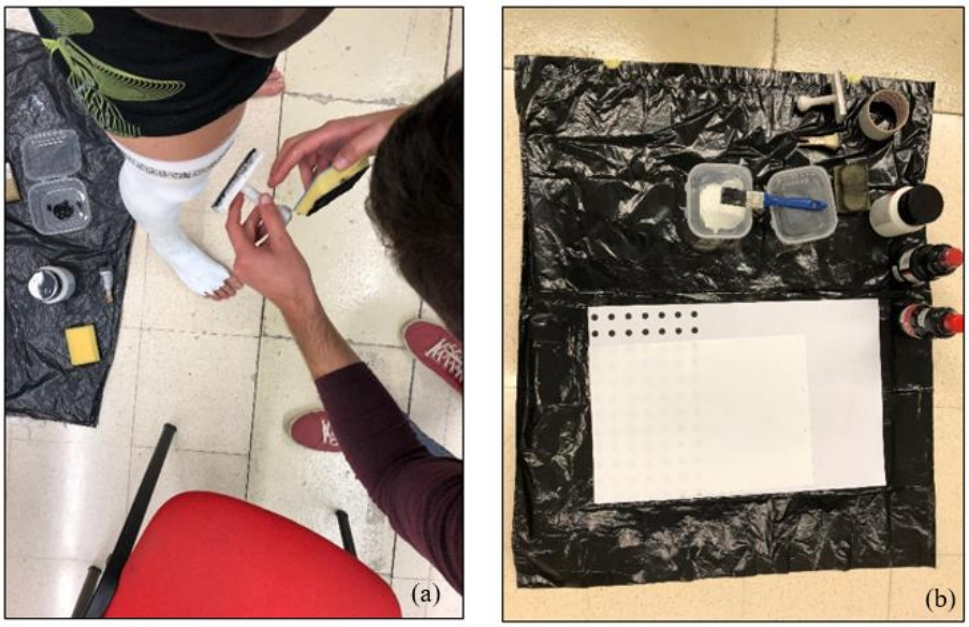

Figure 3.5 – Speckle pattern stamping (a) and painting/stamping equipment (b).

3.5. Experiment protocol

After the subjects were prepared (i.e. leg painted and stamped) and the acquisition system was readied, the recording of the tests was initialized. The main objective was to analyse the evolution of the deformation of the skin, Ground Reaction Force (GRF) and Centre of Pressure (CoP) of the subject during gait, in this case walking and running.

The walking procedure consisted of three tests, each one having the subject strike the platform in a different view: one allowed for a lateral view of the movement, another for a posterior view and another for an anterior view (Figure 3.6). Each test was performed twice to have a backup in case of data corruption – no more than two tests were performed for each view to minimize the destruction of the speckle pattern.

An extra test was performed, only in lateral view, in which the subject had a rope wrapped around the hip – when walking, after striking the plate (around the midstance phase), this rope would pull the subject in an opposite direction, upsetting his/her balance. The purpose of this test was to measure and analyse the GRF forces and CoP behaviour involved in the reestablishment of the body's equilibrium, as well as identification of a kinematic behaviour pattern.

The running procedure consisted of one test, performed in a lateral view. Anterior and posterior views were not possible due to space restrictions not allowing the subject to reach sprinting speed when striking the plate. Again, using the rope to provide a destabilizing pull during the foot strike, another test was performed to measure the body's response. To more easily identify these tests, they will be mentioned with "walking-pull" and "running-pull" terms.

To aid the subjects to perform the required movements, their initial starting position was marked: it is important to guarantee that the lower limb will strike exactly on the force plate and not out of it to ensure a correct GRF reading. This initial marking is unique to each subject - since each one has a unique stride length, it is imperative to match this length with the force plate location.

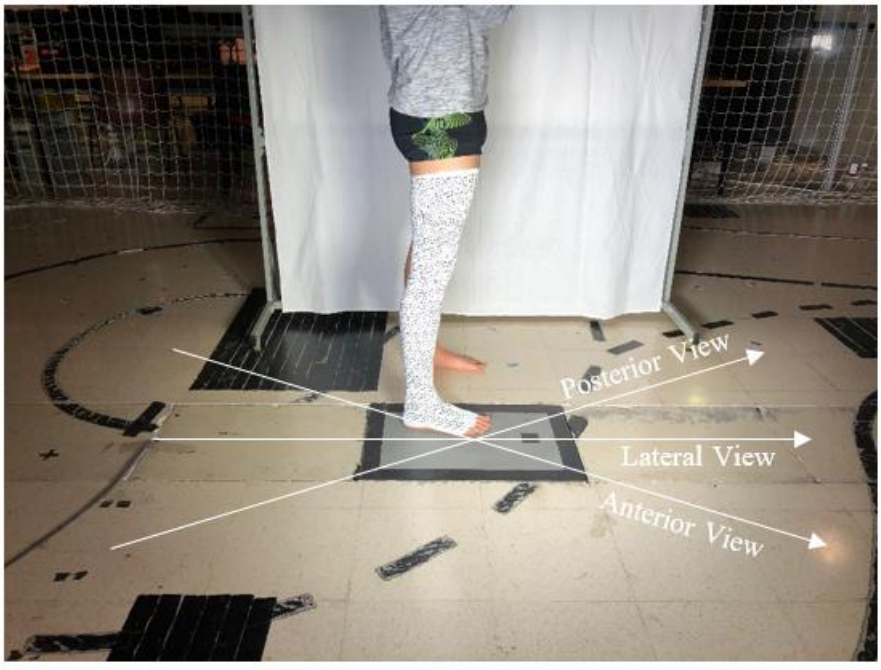

Figure 3.6 – Trajectories followed by the subjects for each view.

After performing all of the required movements, and without altering the lighting conditions nor camera settings, a set of three calibration videos were made, featuring the calibration grid in several positions, varying in roll, pitch and yaw (three videos were sufficient to gather quality footage from the calibration grid in several angles). When handling the board, one has to be cautious to not perform the movements out of the field of view and avoid tilting the board at extreme angles, where part of the board falls out of focus (consequentially, its dots) and suffers from light glare issues (which interfere with the software's recognition of the dots). Therefore, to ensure proper calibration, the grid has to be clearly visible in both camera's FOV, with all of the dots visible and no cast shadows or over illuminated areas.

The calibration software presented by VIC-3D features a score system that evaluates the quality of the calibration images – a threshold score of 0.1 separates a good calibration score (below 0.1) from a bad one (0.1 or higher). Recommended by its creators, when performing a calibration, one should aim for an ideal score of 0.05 or less, to ensure the best calibration and results possible – this recommendation was followed during the realization of the experiments.

With the calibration done and all of the gait frames extracted, a project for each test was created in VIC-3D. To minimize file size and perfect the presentation of results, both image and GRF data was filtered, showing only the frames (and force data) correspondent to the movements between heel strike and toe off. Out of the 1500 frames gathered, only around 400 to 500 were used, due to the quick nature of the experiments (a duration of about 0.5 seconds out of the 3 seconds recorded showed the subject touching the plate).

3.6. Subjects

A total of nine healthy subjects were analysed, two male and seven female, with ages ranging between 20-28 and weight ranging between 52-74 kilograms. The chosen subjects showed no hints of pathological gait. All subjects consented to the performance of the experiments. The following figure illustrates the total subject's gender distribution, their attributed number (in chronological order of test performance) and weight, respectively. Only subjects' 1, 4, 5, 7, 8 and 9 results are presented in the current work; subjects' 2, 3 and 6 data featured high correlation error and therefore couldn´t be used with acceptable levels of precision.

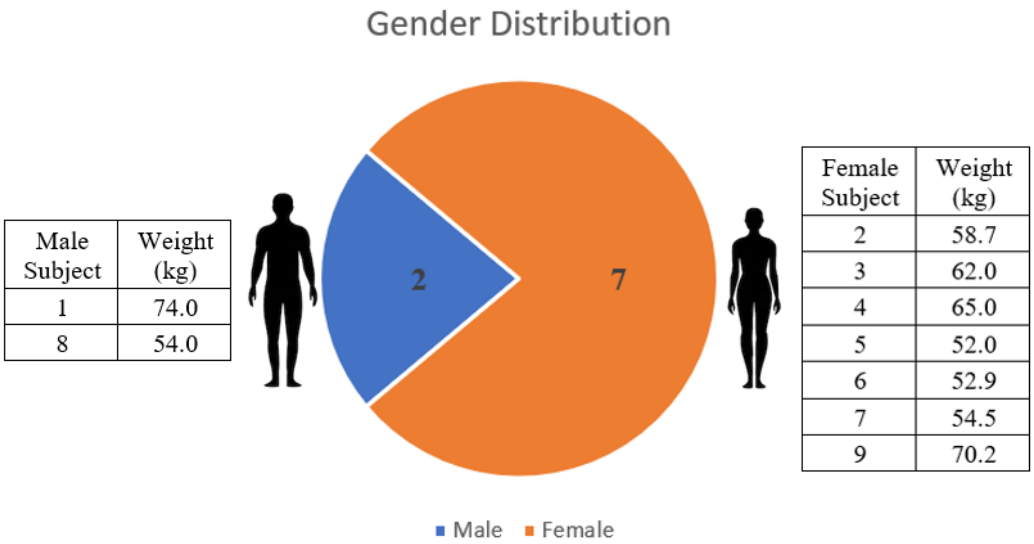

Male Subject	Weight (kg)
1	74.0
8	54.0

Female Subject	Weight (kg)
2	58.7
3	62.0
4	65.0
5	52.0
6	52.9
7	54.5
9	70.2

Figure 3.7 – Gender, number identification and weight of test subjects.

3.7. VIC-3D analysis parameters

Inside each project, VIC-3D supplies the user with tools and parameters to better fit the experiment at hand: these were set individually for each subject in each test, but some parameter values were equal among all tests to guarantee an identical, and therefore comparable, analysis.

To explain the parameters adjusted during analysis, three figures of each parameter tab are presented (Figure 3.8, Figure 3.9 and Figure 3.10). For a full description of all parameters, the reader is directed to the VIC-3D manual [22], where their definition and impact on analysis are explained. The individually set parameters are described as follows:

Region Of Interest (ROI)

- Applied in the reference image (selected by the user), it is a user-set tool that allows for the selection of the speckled area, avoiding unwanted regions (i.e. background) and suboptimal areas (i.e. edges of the leg, blurred spots, uneven lighting areas).

Subset size

- After selecting the ROI, a grid is established inside the selected area, consisting of several squares - the size of these squares is controlled by this parameter, subset size. Therefore, it is responsible for the size of the data that is tracked between two images. The size has to be big enough to fit a distinct speckle pattern inside of it. VIC-3D also features an automatic subset size suggestion "which is calculated to give an optimal match confidence of 0.01 pixel for a given assumed noise level". Values ranged from 19 to 28.

Step size

- Step size is defined as the value of spacing between the points that are analysed during the correlation, thus establishing how many data points are tracked overall (smaller step size – more data points). Values ranged from 8 to 15.

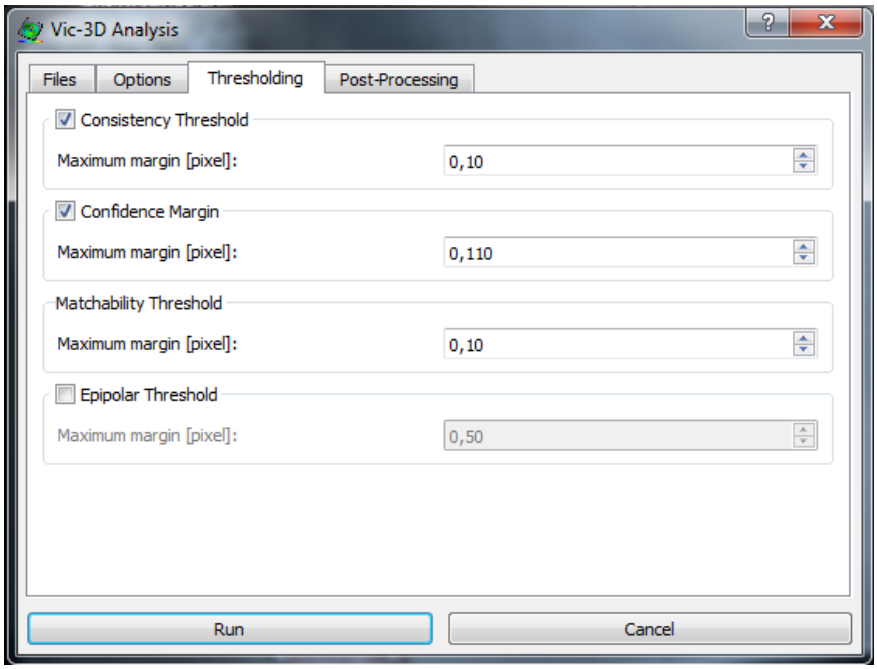

Figure 3.8 – VIC-3D Thresholding tab.

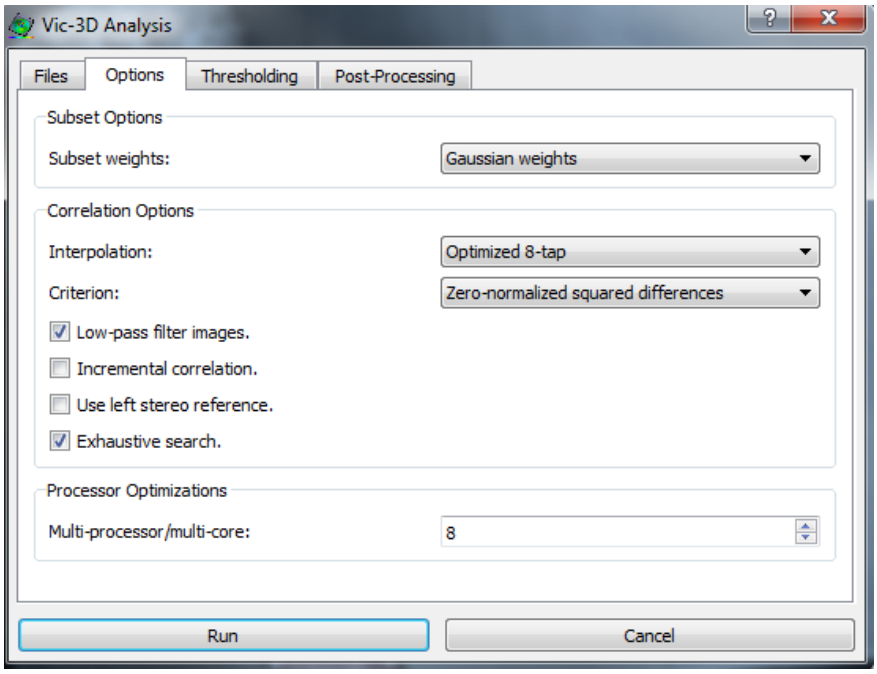

Figure 3.9 – VIC-3D Options tab.

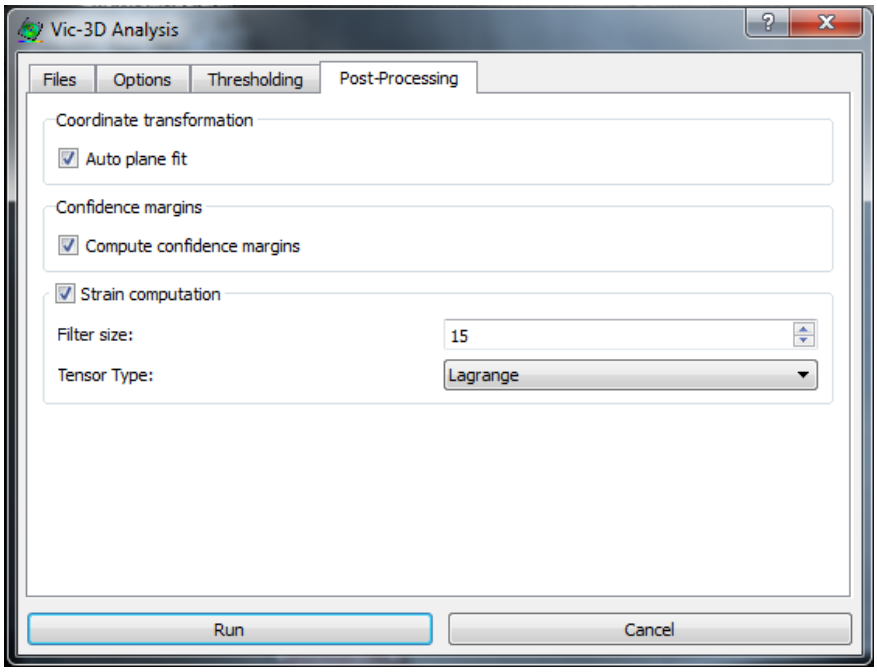

Figure 3.10 – VIC-3D Post-Processing tab.

3.8. MATLAB Processing

After exporting the analysed images, the .txt files (containing information of Fx, Fy, Fz, Mx, My and Mz) exported by the AMTI software needed to be analysed and interpreted; this was done via MATLAB, a helpful tool for creating and displaying all graphical information.

Template code was created for this thesis and can be used for future work, requiring only the input of the subject's .txt file and outputting graphical representation of the evolution of GRF, CoP and VCoP over time:

- **GRF_Creator** – Represents the evolution of GRF (i.e. Fz) over time. Highlights the peaks in GRF, supplying the user with the datapoint index for frame synchronization.
- **CoP_Creator** – Represents the evolution of CoP trajectory over the plate. Highlights the same points supplied from GRF_Creator for full synchronization.
- **VCoP_Creator** – Represents the evolution of VCoP over time. Highlights the same points supplied from GRF_Creator for full synchronization.

For each of these scripts, a .gif version was created to join all of the information in a video format, useful for simplifying the presentation of data, and observing the continuous evolution of all variables.

3.9. Kinovea analysis

Kinovea was used as an angle measurement tool of the knee and ankle joints of the subjects throughout the entire stance phase. A key image was selected – heel strike – and the anchor points of the angles were selected: for the knee, the central point was on the middle of the ROI, with the other points anchored on the upper thigh and the ankle. For the ankle, the two extremities were anchored on the knee and the foot's chest.

The following flowchart (Figure 3.11) summarizes the entire experimental procedure from data collection to full synchronization of analysed results:

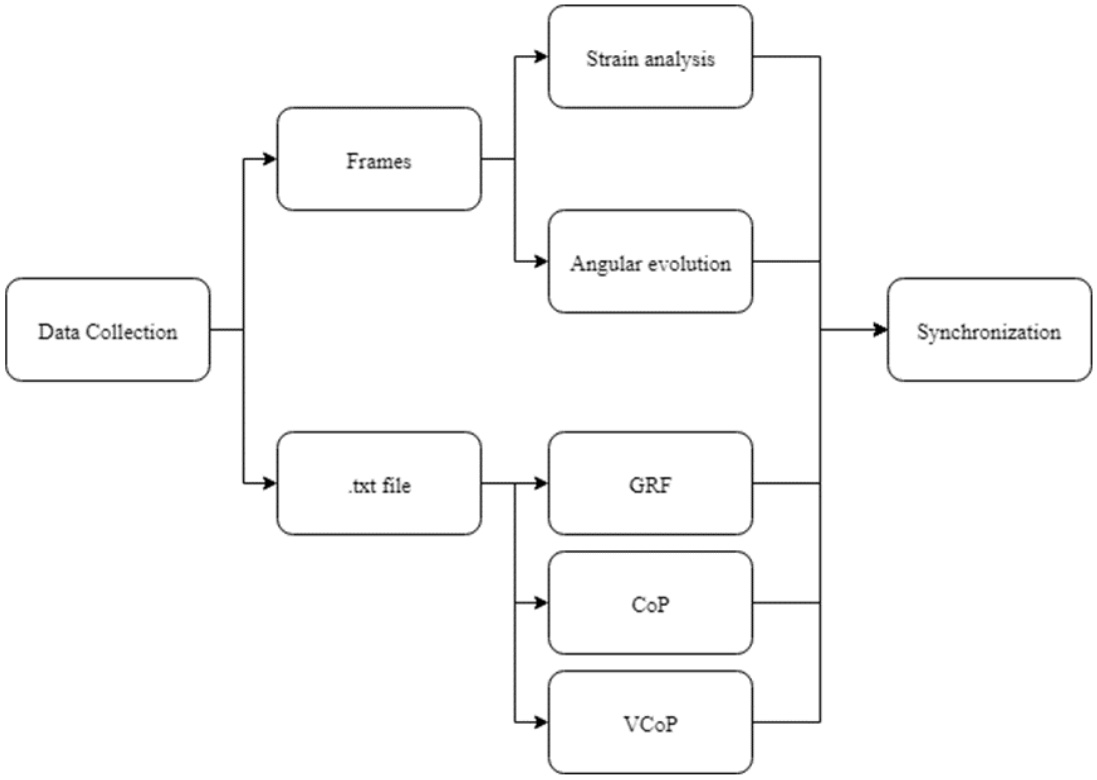

Figure 3.11 – Flowchart of data analysis procedure.

4. Results

The results from skin strain analysis, GRF, CoP, VCoP and joint angles are presented in this chapter. To present an in depth explanation of the results, one subject was chosen and all of the matching information is presented (Different views, stages, full graphs). For inter-subject analysis, 3 other subjects' data was compared to the chosen subject, highlighting differences and similarities. Since demonstration of continuous temporal evolution of the frames and graphs is impossible on paper, several key stages were identified and all of the data of that instant is presented.

4.1. General Information

All of the performed movements were saved, except for subject nº9's running gait, with a total of 780 Gb of data saved for all subjects. Also worth mentioning is the reason behind the lack of running-pull tests present in some subjects: it was noted midway through their realization that the subjects were already conditioned when performing this test, visible by their sudden deceleration when nearing the plate (in anticipation of the pull in opposite direction). This of course meant the inviability of their results and thus, to shorten time and prevent further speckle pattern destruction, these tests were no longer performed.

- For **skin strain analysis**, multiple views are presented (lateral, posterior and anterior) alongside with the values of major principal strain (*e1*), minor principal strain (*e2*) and von Mises strain (*von Mises*).
- For **GRF**, the graphs display the entire data points between heel strike and toe off. For a general understanding of the forces applied on the subject, instead of raw values (i.e. presenting values in Newtons), it is used the percentage of body weight of the subject: above the Body Weight line – 100% – applied forces exceed the subject's weight, and vice-versa.
- For **CoP**, two views are presented, the "plate" view and an adjusted view. The "plate" view is an unzoomed view featuring the length and width of the plate, allowing for the viewer to check the different areas where the footstrike of multiple subjects happened. Adjusted view is a zoomed, more adequate visualization of the CoP evolution. All views of the CoP trajectory are top down views, with each trajectory changing its direction depending on the test.
- For **VCoP**, the graphs present the filtered values (lowpass, 15 Hz) calculated by the equations previously described in Chapter 1.2.
- For the **heel strike analysis**, the frames are identical to the ones showed in skin strain analysis. They show the profile evolution of markers on the ankle, knee and mid-thigh, mapping their trajectory during the stance phase. Their main purpose is to help explain the rigid body motion associated to the heel strike transient present in the acquired footage.

For all of the walking views, the main analysed subject is the same – subject 5 – allowing for an easy comparison of gait and strain behaviour between different views. Although separated and described individually, a comparison of all 3 views' full information is presented (Figure 4.20). For the running test, due to high correlation error values in strain analysis of subject 5, subject 8 was chosen for presentation (featured the lowest correlation error). Subject 1 performed the pull tests at full gait speed, showing no signs of deceleration due to the imminent cord pull, therefore chosen to present pull test results.

4.2. Walking Gait – Lateral view

Starting with the lateral view of walking gait, overall results did not present major discrepancies with known literature. The amount of presented data was regulated by the amount of GRF data points since these constrict the beginning and end of stance phase, meaning that same quantity of data points are present in the CoP and VCoP graphs, leading to perfect synchronization. The analysed frames were also in sync with GRF data retrieval from the beginning of heel strike and ended shortly after the second peak, leaving only a couple of non-analysed frames in sync with the rest of the data (~30 frames).

The chosen reference frame (Figure 4.3 (a)) is the one portraying the beginning of the stance phase – heel strike – where the GRF values start to increase from their baseline and the leg is stretched. The chosen ROI gathers data from mid-thigh to the ankle, featuring a fixed scale (varies between variables) and principal strain directions (only in *e1* and *e2* analysis). Maximum and minimum registered values are shown, however, these often are the result of correlation error: the edges of the ROI, where both cameras FOV overlap boundaries are established, are where the majority of errors occur, leading to higher than usual values present.

Starting with GRF (Figure 4.1), the common M-shape is present, featuring a double peak and an impact peak transient – with the marked points corresponding to highest (and lowest) registered values of GRF: Point **A** corresponds to the heel impact transient, point **C** to the highest value of the first peak, point **D** to the lowest value between peaks and point **E** to the highest value of the second peak. Point **B** is an intermediate point useful for the description of the evolution of kinematics between impact peak and first peak.

The CoP (Figure 4.3 (b)) and VCoP (Figure 4.2) graphs feature the same key points as the GRF graph, to easily compare values. The CoP graph demonstrates the evolution of foot centre of pressure throughout gait, showing its contact from heel to toe. The VCoP graph demonstrates how quickly the points of CoP change from one another, featuring a triple peak-pattern also present in literature.

To simplify the description of events, these will be characterized point by point:

- **Point A** – Located around 5% of stance, corresponds to the impact peak of the heel strike. The GRF values surrounding the peak are widespread (i.e. consecutive datapoints are widely spaced), demonstrating the short period of the heel transient (~ 4ms). Analysing CoP data, point A is located on the rear foot region as expected. In the VCoP graph, point A is amidst a steep decrease of velocity, where the following points' values will reach a minimum.
- **Point B** – Located midway through points A and C (around 10% of stance), represents a phase of transition: while in the GRF graph it is the peak of a small change in values, in the CoP graph this point is located right before a sudden change in direction of the CoP (a slight deviation to the right). This change in trajectory is due to the rotation of the tibia to accompany the evolving gait, accompanied by the continuous increase of contact area of the foot. In VCoP graph it is near maximum of a small bump, right before a small decrease and a following sudden increase – as the gait continues, there is a shift of the CoP from the rear foot to the mid foot.
- **Point C** – Located around 20% of stance, it is the peak value of the first peak. Here, GRF is around 20% higher than the subjects' body weight. This rise of GRF is due to the body's changing center of mass direction, from downwards to upwards. In the CoP graph, this point is located at the end of the rear foot/ beginning of mid foot. In terms of VCoP positioning, it shares a somewhat similar positioning to point B, near the minimum value between the second and third peaks. The following datapoints rise in value which is consistent with the fast alteration of

the CoP as the body goes through the midstance phase, with the heel rising (decreasing the applied force on it) and the forefoot bearing more of the weight.

- **Point D** – Located in the valley between the two peaks, around 40% of stance, is when the subject is in late midstance. There is a decrease in GRF due to the rise of center of gravity as the body propels forward of the stance foot, accompanied by the forward swinging motion of the opposite foot. A drastic change of CoP position is observable, the force vector is now positioned on the forefoot of the subject. In the VCoP graph, the change on CoP is justified: between points C and D the velocity reaches its highest peak, describing a rapid changing CoP position.
- **Point E** – Located around 70/80 % of the stance phase, it is the second peak in GRF value. Once more, the subject is exposed to over 20% more of his own bodyweight. This increase in force value is due to the forefoot push off, where the body propels itself upwards and forward to finish the cycle, where the values drop off to baseline values (~ 0 N). The CoP trajectory aligns itself to the left due to the rotation (i.e. eversion) of the foot. The following points indicate that CoP rapidly shifts towards the front of the forefoot, reaching the toes and ending as these lift from the floor – this quick shift of CoP trajectory can be observed in the VCoP graph, where after point E it is observable the occurrence of a peak in velocity (also observable by the spacing of data points after point E in CoP graph).

This pointwise description is the same for other views, since the only changing parameters are the subject's gait speed (produces small changes in graphs) and kinematic view; as such, this detailed description will not be repeated to avoid saturation of information, only the registered differences will be commented. For strain analysis, the description will focus more on the kinematics and strain values present in each frame (Figure 4.4, Figure 4.5 and Figure 4.6).

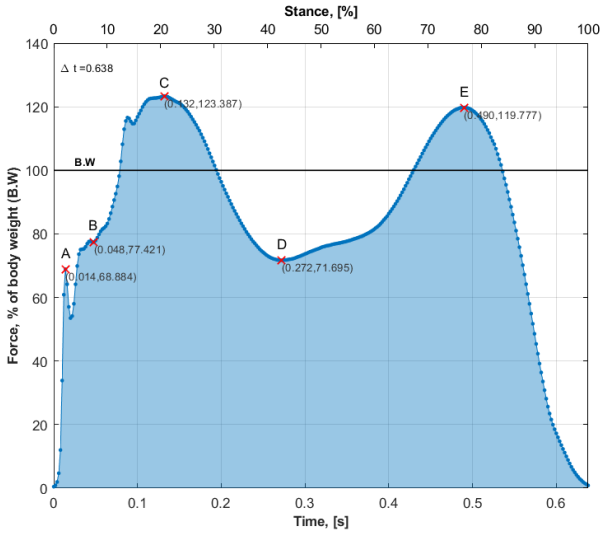

Figure 4.1 – GRF evolution of the walking lateral view test of subject 5. Points A, B, C, D and E correspond to the peaks of GRF data.

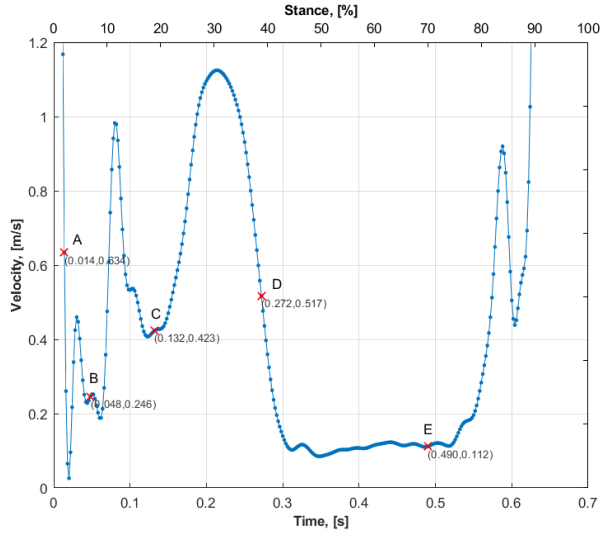

Figure 4.2 - VCoP evolution of the walking lateral view test of subject 5. Points A, B, C, D and E correspond to the peaks of GRF data.

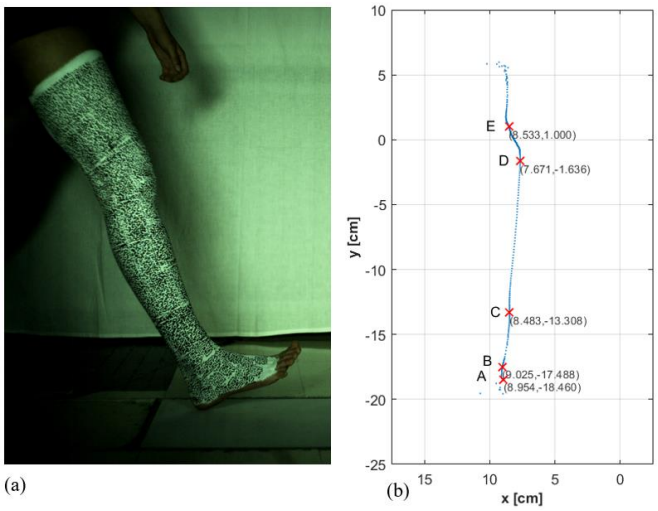

Figure 4.3 – Strain analysis reference frame (a) and CoP evolution (b) of the walking lateral view test of subject 5. Points A, B, C, D and E correspond to the peaks of GRF data.

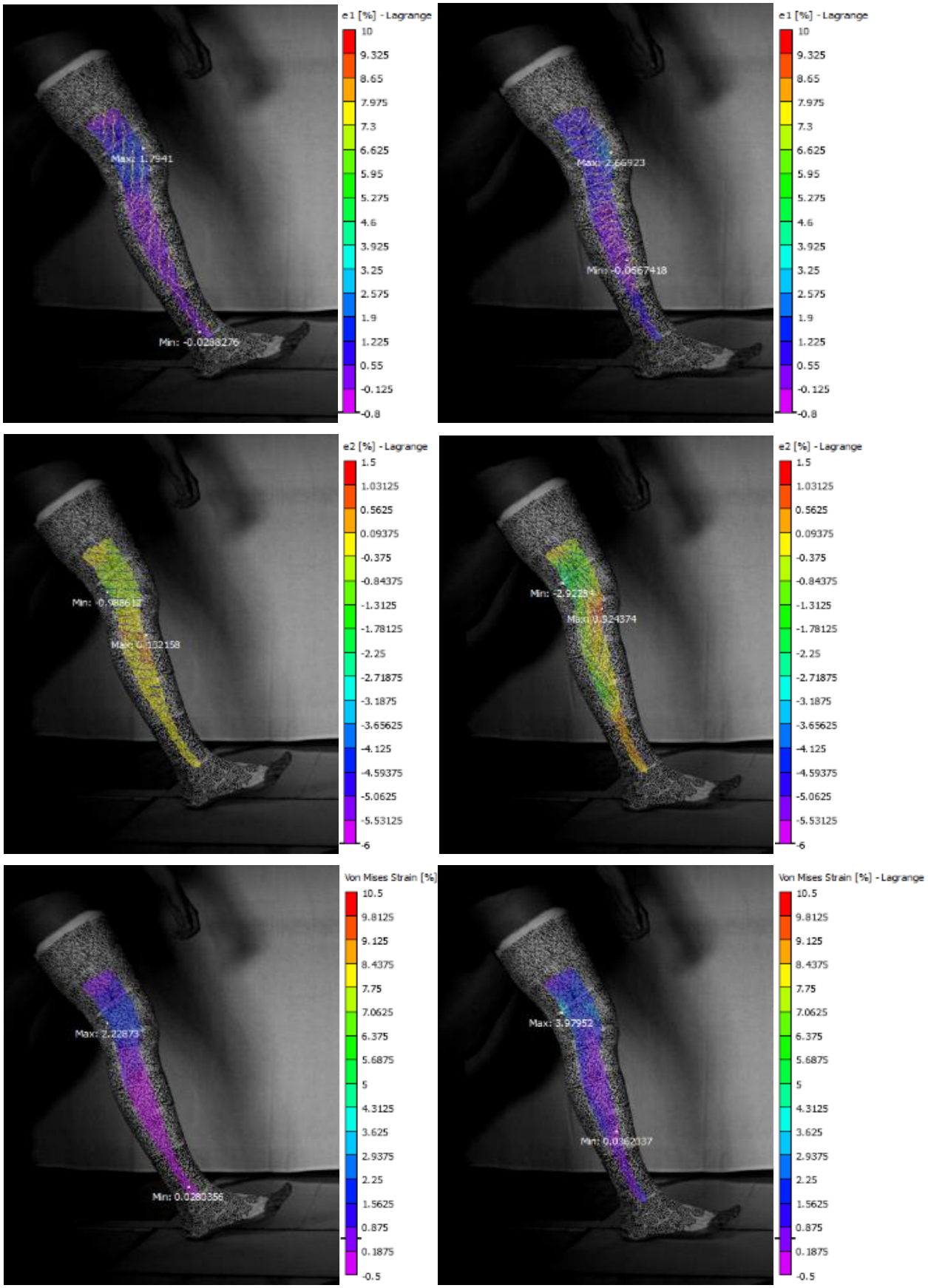

Figure 4.4 – Lateral view of *e1*, *e2* and *von Mises* strain of the leg in point A (left) and point B (right).

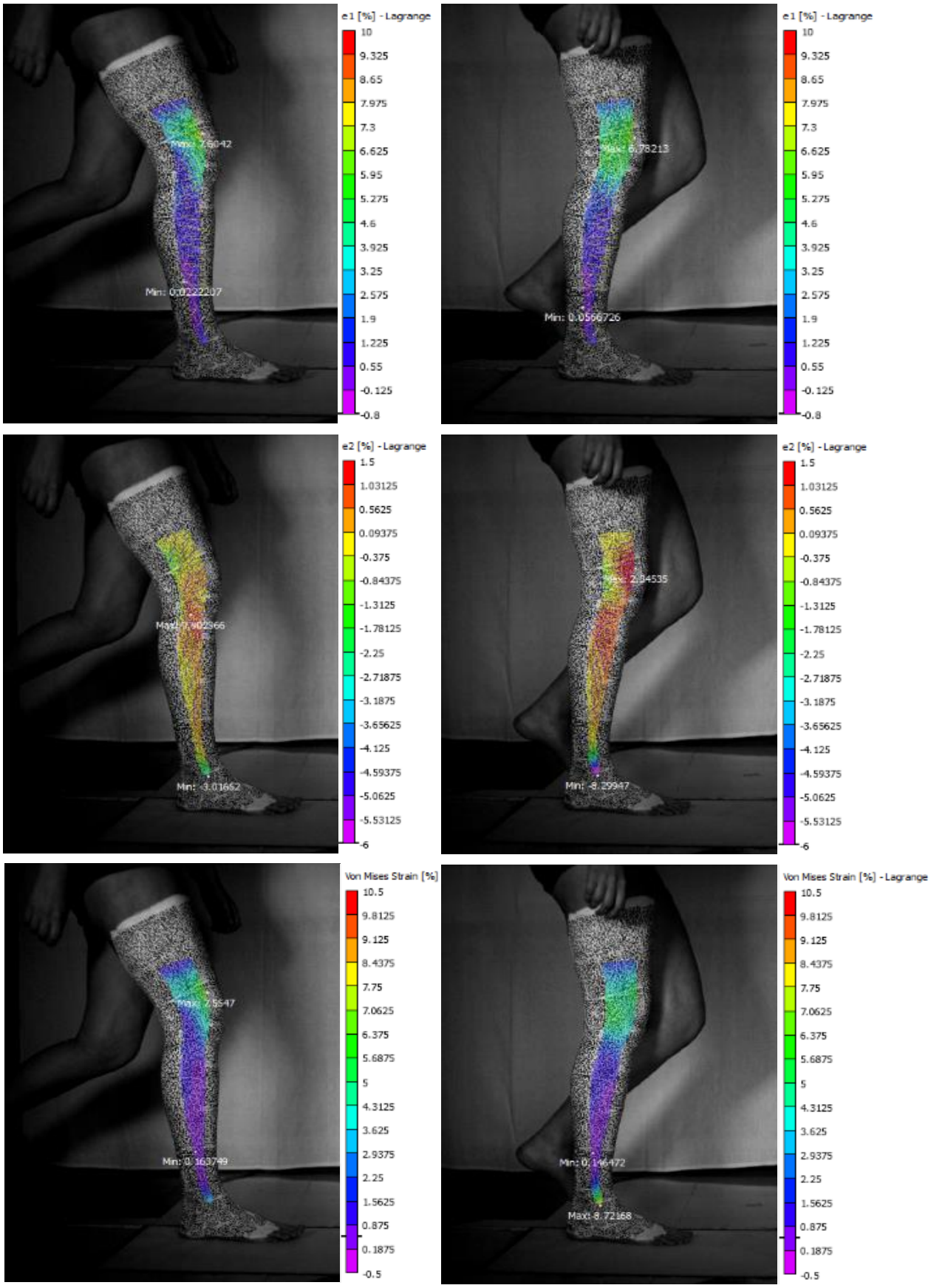

Figure 4.5 – Lateral view of *e1*, *e2* and *von Mises* strain of the leg in point C (left) and point D (right).

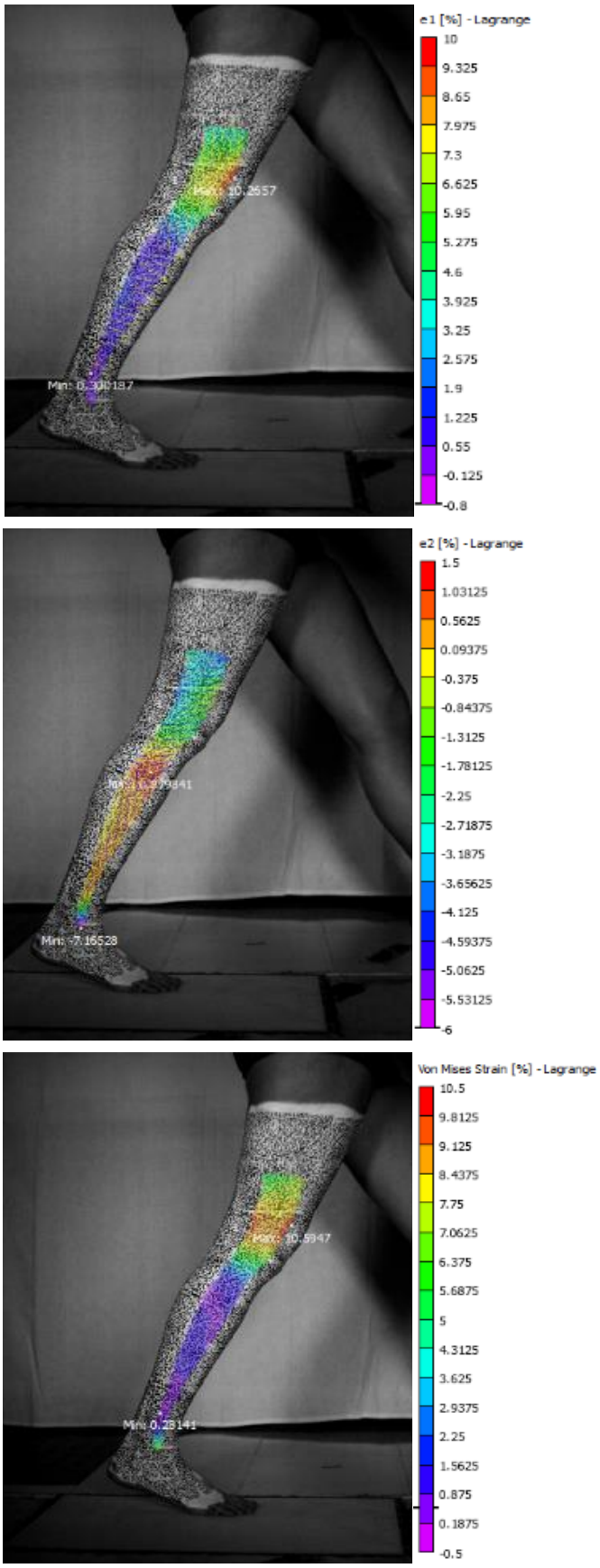

Figure 4.6 – Lateral view of *e1*, *e2* and *von Mises* strain of the leg in point E.

Focusing on the kinematics and skin strain of walking gait, the following description details their evolution throughout the same established points:

- **Point A** – The foot strikes the floor, with the leg fully stretched. Here strain values are very low since the frame is still very close to the reference frame, however a distinct rise in values start to appear in the knee region, with lower values predominating on the area below the knee. Major strain directions are mainly directed upwards whilst minor strain directions are directed towards the forward movement.
- **Point B** – The entire heel is in contact with the plate and the foot rotates downwards, transitioning the weight from heel to midfoot. Maximum values of strain still predominate in the knee region, with minimum values still present in the lower leg (*e2* image is the exception).
- **Point C** – The whole foot is in contact with the floor as the body goes trough midstance phase, flexing the knee and rotating over the ankle. Maximum strain values start to shift from the anterior to the posterior region whilst the minum values gather around the posterior region of the lower leg (*e1* and *von Mises* images). A distinct maximum region appears in the centre of the ROI in *e2* analysis.
- **Point D** – The subject finishes midstance, the leg is fully stretched. The higher deformation values are evenly distributed along the knee region and minimum values still predominate along the lower leg. In *von Mises* and *e2* images a peak of values appear in the ankle region, indicating its compression during this phase of stance. A clear peak in *e2* values also appears in the upper knee region.
- **Point E** – The leg stretches as the heel rises from the floor and the forefoot propels the body forward. A maximum is visible once again in the anterior region of the knee (reaching the highest strain values, around 10 % for *e1* and *von Mises* scales) and a minimum is found near the ankle (common in all variables). In *e2* frame, once again, maximum values of strain predominate at the center of the ROI.

4.3. Walking Gait – Anterior view

For the anterior view tests, a similar behaviour is observed in all data graphs, albeit with some minor changes:

GRF (Figure 4.7) presented its typical double peak and impact peak, once more characterized by five similar stages (points A to E). However, the second peak, point E, does not surpass the body weight limit, a direct result of the subject pushing off the plate with less intensity than the previous test. Another noticeable change is in the impact peak (point A): it is characterized by much more data points, and therefore distributed over a big time interval – this is due to a softer heel strike on the floor, where the GRF vector is distributed over a larger area of the heel, as proved by the CoP and VCoP graphs.

VCoP (Figure 4.8) differs mainly in the presentation of the initial triple peak, where the values between point A and C show higher, yet closer, values than the test before. Once again, this is related to the impact peak and the heel strike motion.

CoP (Figure 4.9 (b)) trajectory featured the same behaviour as before, with the only differences being the proximity of data points between points A and C (smoother transition of foot on the floor) and a slightly more rectilinear pattern from heelstrike to push off.

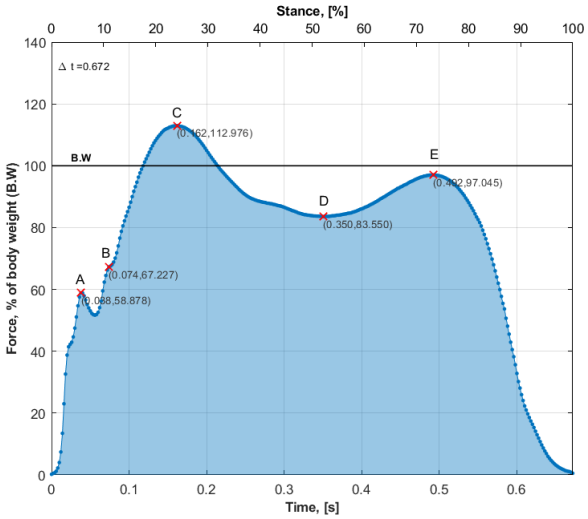

Figure 4.7 - GRF evolution of the walking anterior view test of subject 5. Points A, B, C, D and E correspond to the peaks of GRF data.

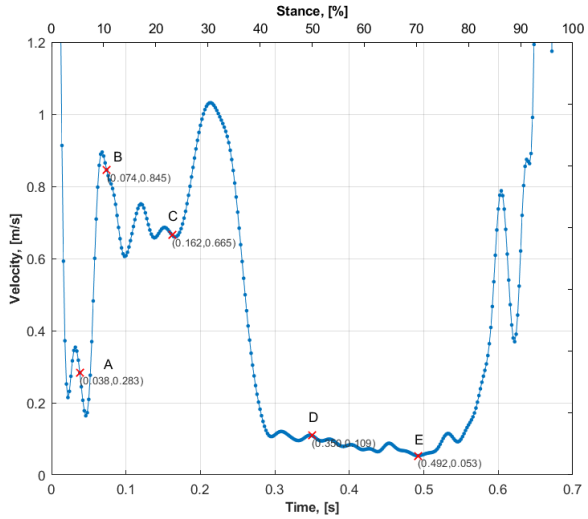

Figure 4.8 - VCoP evolution of the walking anterior view test of subject 5. Points A, B, C, D and E correspond to the peaks of GRF data.

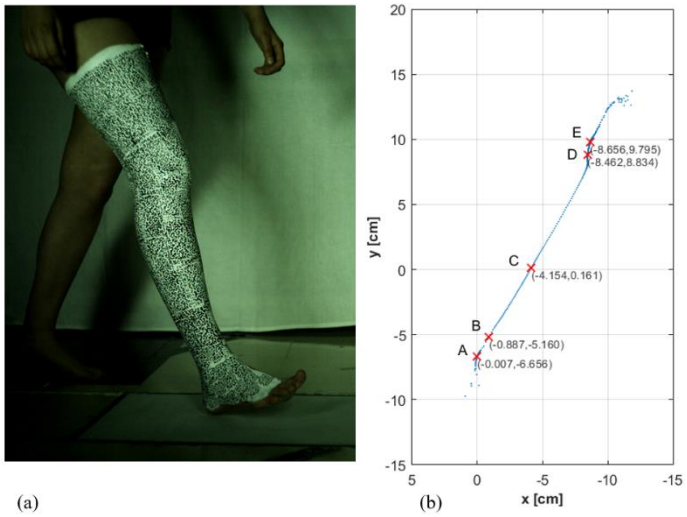

Figure 4.9 - Strain analysis reference frame (a) and CoP evolution (b) of the walking anterior view test of subject 5. Points A, B, C, D and E correspond to the peaks of GRF data.

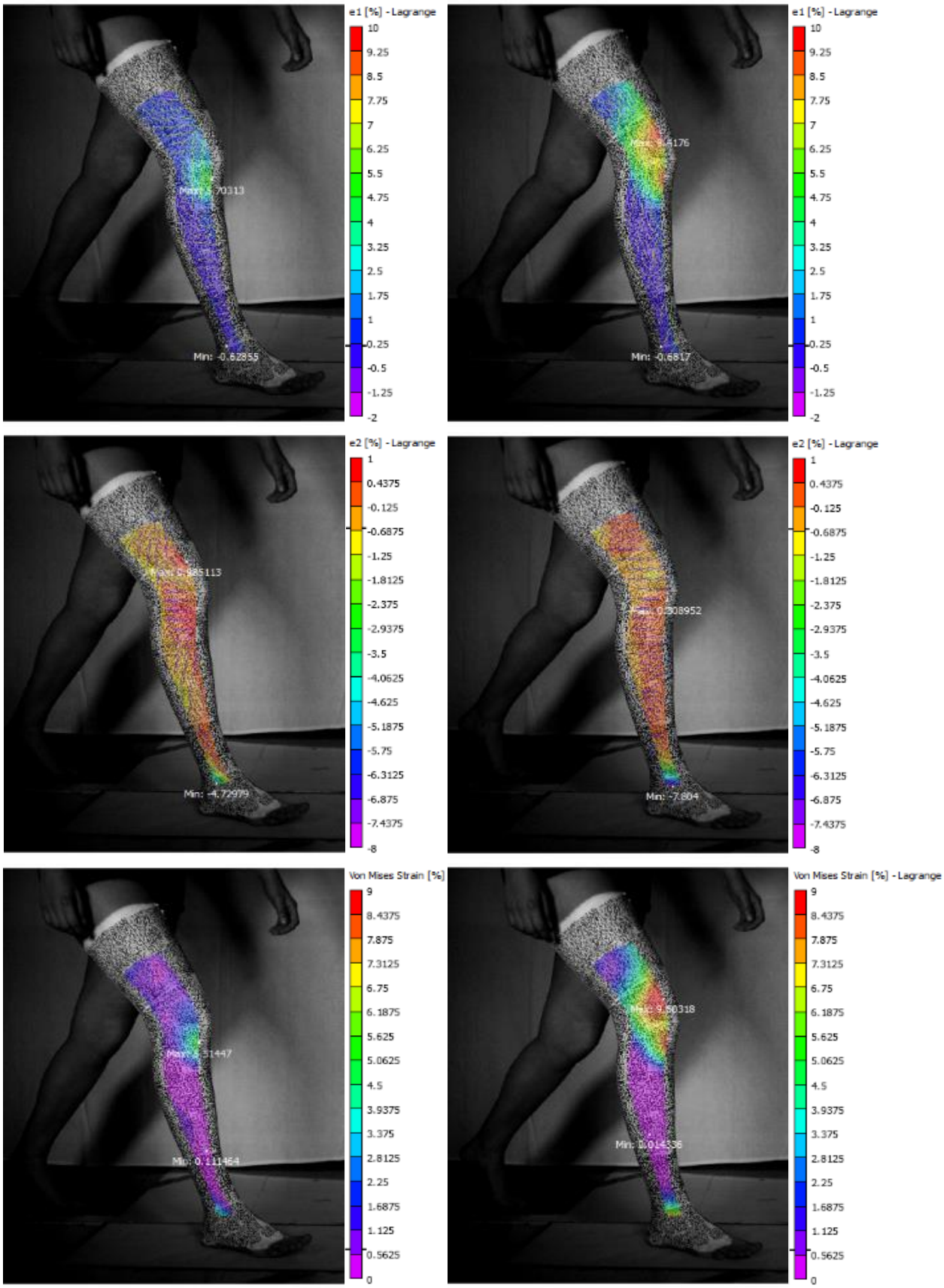

Figure 4.10 – Anterior view of *e1*, *e2* and *von Mises* strain of the leg in point A (left) and point B (right).

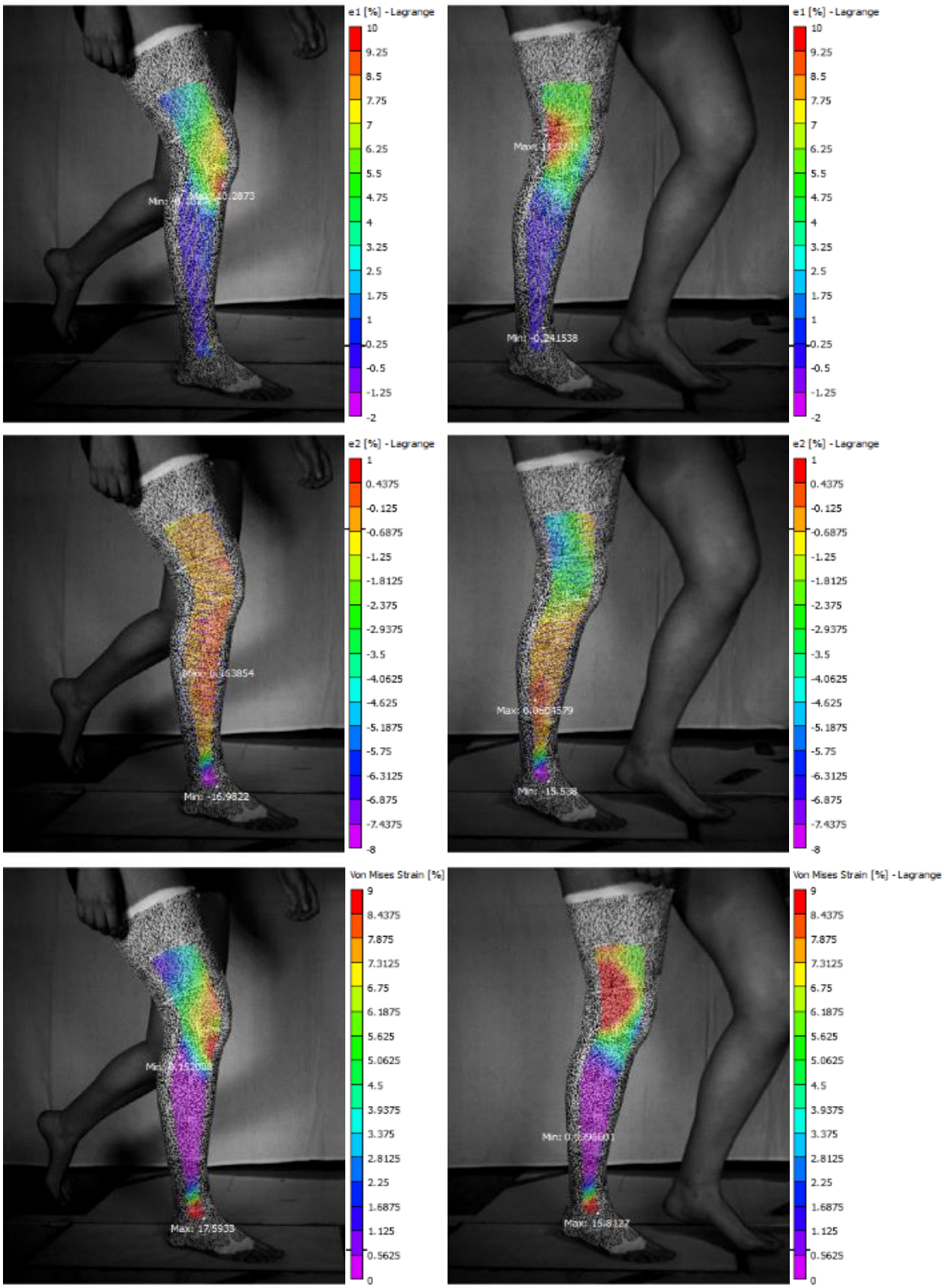

Figure 4.11 - Anterior view of *e1*, *e2* and *von Mises* strain of the leg in point C (left) and point D (right).

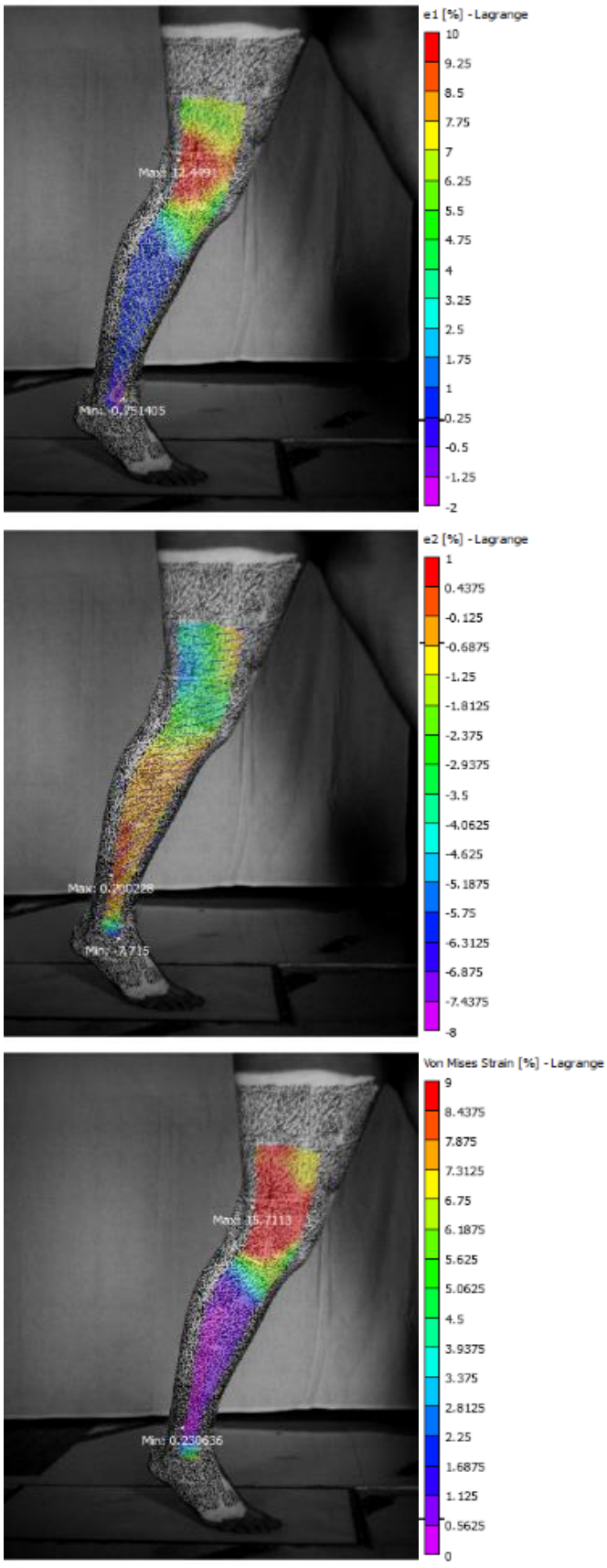

Figure 4.12 - Anterior view of *e1*, *e2* and *von Mises* strain of the leg in point E.

Figure 4.10, Figure 4.11 and Figure 4.12 demonstrate the strain maps of the synchronized frames:

- **Point A** – Notice the foot angle during the impact peak moment when compared to the lateral view test: the majority of the heel is already in contact with the plate, with the toes touching the plate within moments. Similar to the first analysis, higher values appear surrounding the anterior region of the knee (*e1* and *von Mises*), spreading throughout the entire leg in the *e2* frame.
- **Point B** – The foot is in full contact with the floor, with the knee flexing (as seen by higher strain values surrounding it in *e1* and *von Mises*). The same heterogeneous high strain pattern still persists throughout the leg in *e2* analysis, with a minimum area appearing in the ankle, indicating its compression.
- **Point C** – The subject initiates midstance, with a shift of the maximum values from the knee towards the lower leg (*e1* and *von Mises*). A clear minimum strain pattern is observable in the ankle in *e2*.
- **Point D** – Midstance finishes and the legs starts to stretch to propel the subject forward (high strain in the lateral-posterior area in *e1* and *von Mises*). In both *e2* and *von Mises* frames the ankle compression throughout gait is highlighted.
- **Point E** – Push off occurs. A large strain area is observed in the thigh as the extensor muscles extend the knee. As the ankle also extends, returning to its original state, strain values drop once more.

4.4. Walking Gait – Posterior view

The posterior view test results (Figure 4.13, Figure 4.14 and Figure 4.15) present an almost identical pattern the ones in front view, with the only noticeable changes being the chosen reference image (Figure 4.15 (a)) and point B in the GRF graph (Figure 4.13):

- The **reference image** chosen for strain calculation is taken midway through midstance, where the leg is stretched without being too far, nor too close to the camera. Since in the heelstrike frame the upper leg intersects the FOV, another frame had to be chosen, preferably showing the leg stretched, to easily understand skin behaviour during the flexion and extension of the joints;
- Through the **GRF** graph it is possible to observe a more noticeable bump in the increasing values between the impact peak and first peak, entirely due to transition of the GRF vector throughout the foot as it contacts the floor.

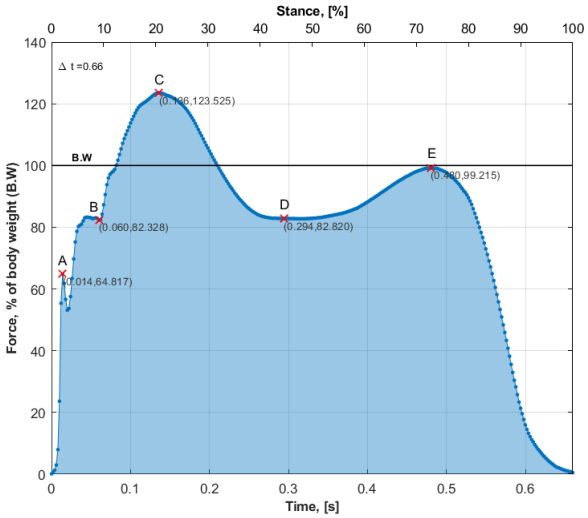

Figure 4.13 - GRF evolution of the walking posterior view test of subject 5. Points A, B, C, D and E correspond to the peaks of GRF data.

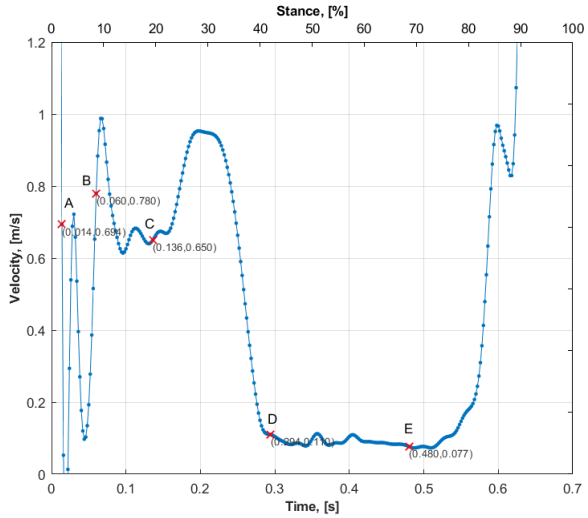

Figure 4.14 - VCoP evolution of the walking posterior view test of subject 5. Points A, B, C, D and E correspond to the peaks of GRF data.

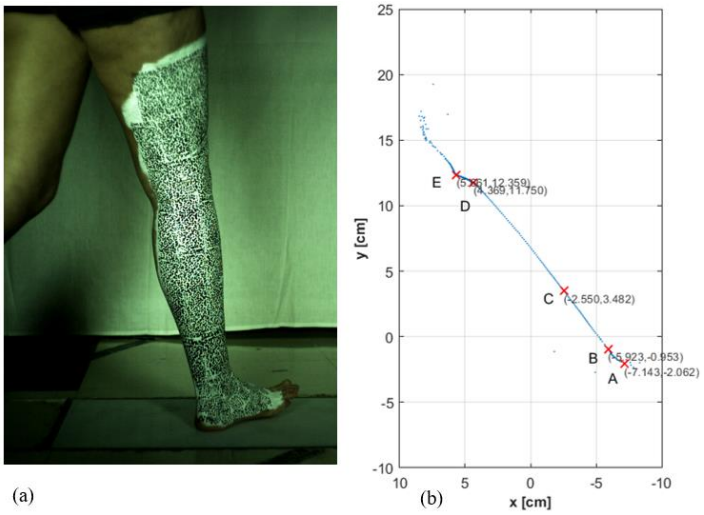

Figure 4.15 - Strain analysis reference frame (a) and CoP evolution (b) of the walking posterior view test of subject 5. Points A, B, C, D and E correspond to the peaks of GRF data.

Figure 4.16 – Correspondent frame to point A.

Figure 4.17 – Correspondent frame to point B.

As shown in Figure 4.16 and Figure 4.17, the blurring effect present in the upper leg produced by the open aperture/ high exposure to light prevented the correct analysis of the previous frames corresponding to the beginning of the stance phase. For this reason, *e1*, *e2* and *von Mises* strain maps for frames A and B are not presented.

- **Point A** – Heelstrike – the leg is fully stretched as the stance phase begins.
- **Point B** – The knee slightly flexes and the foot comes down towards the plate as gait progresses.

The remaining synchronized frames are presented in Figure 4.18 and Figure 4.19:

- **Point C** – The subject goes trough midstance, stretching the leg. A visible peak area appears in the anterior region of the ankle (*e2* and *von Mises*) with also high strain values in the posterior thigh, surrounding the hamstring muscles (*e1* and *von Mises*).
- **Point D** – The leg is fully stretched as midstance finishes and push off initiates. Maximum values surround the posterior upper leg (*e1*, *e2* and *von Mises*).
- **Point E** – The heel rises and CoP moves towards the forefoot. A U-shaped high strain appears (*e1* and *von Mises*), whilst in *e2* anterior and posterior regions share opposite peaks of strain values.

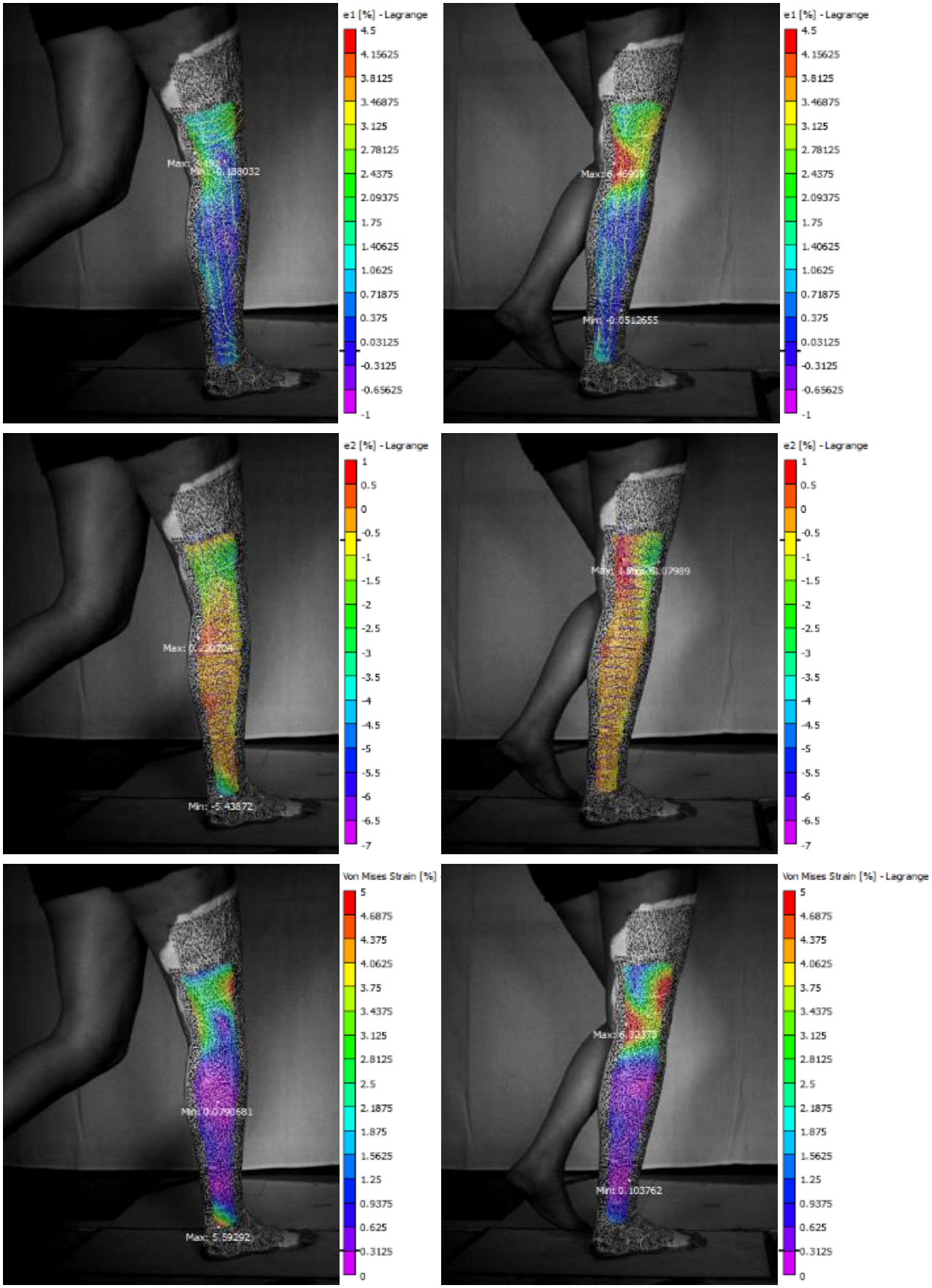

Figure 4.18 - Posterior view of *e1*, *e2* and *von Mises* strain of the leg in point C (left) and point D (right).

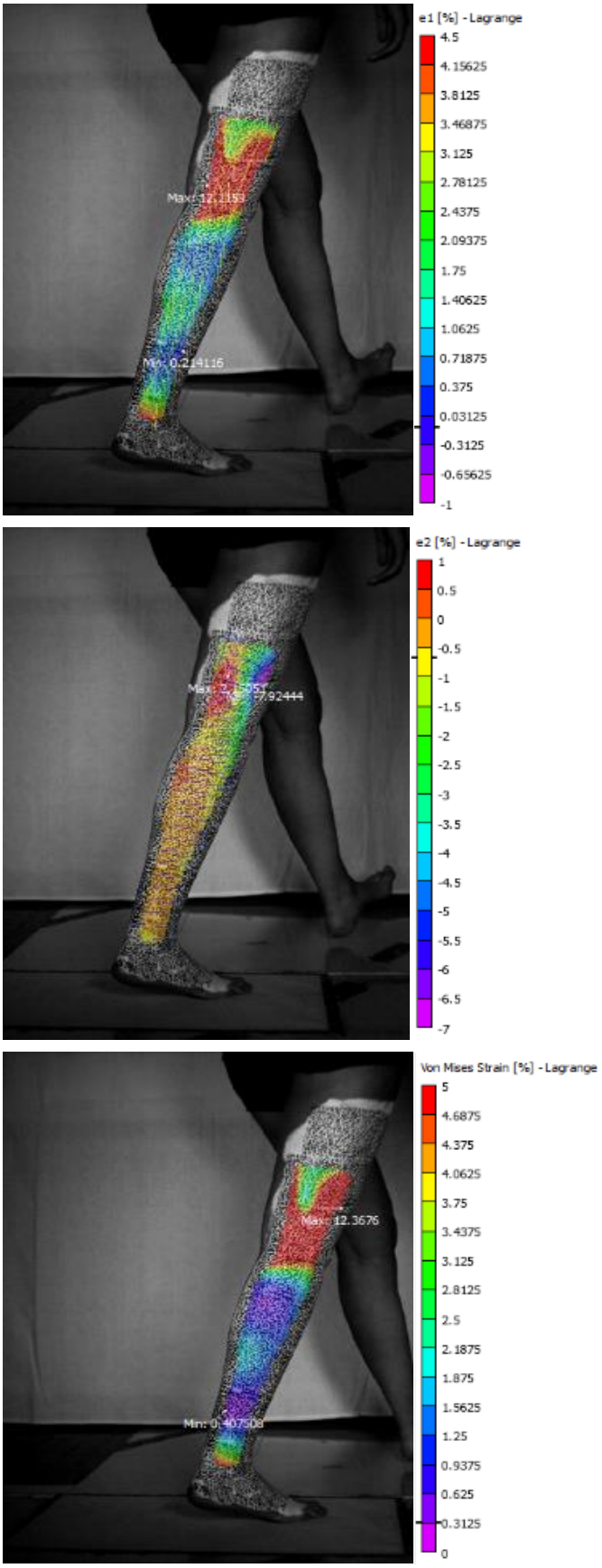

Figure 4.19 - Posterior view of *e1*, *e2* and *von Mises* strain of the leg in point E.

4.5. Walking – Multiple view data comparison

The following graphs (Figure 4.20) feature the same information previously presented for each view, condensed into two graphs, demonstrating the synchronized evolution of GRF, CoP and VCoP.

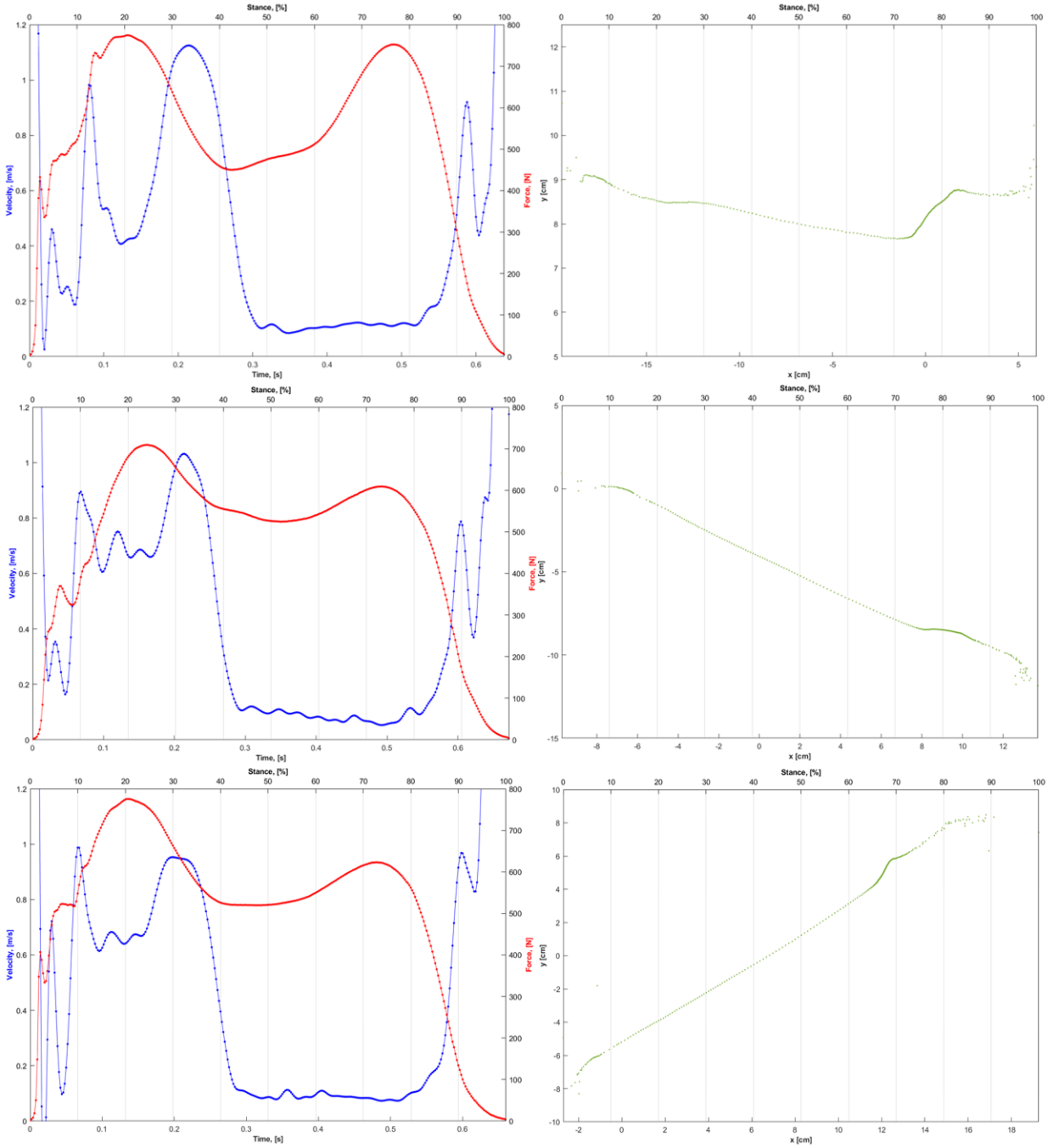

Figure 4.20 - Combined data analysis of lateral (top), anterior (middle) and posterior (bottom) views of subject 5. Features GRF (red), VCOP (blue) and COP (green) temporal progression.

4.6. Walking Gait – Subject comparison

The following graphs present the comparison of GRF, CoP and VCoP over 3 seconds of data recording of 4 different subjects, under the same conditions and tests (lateral, anterior and posterior).

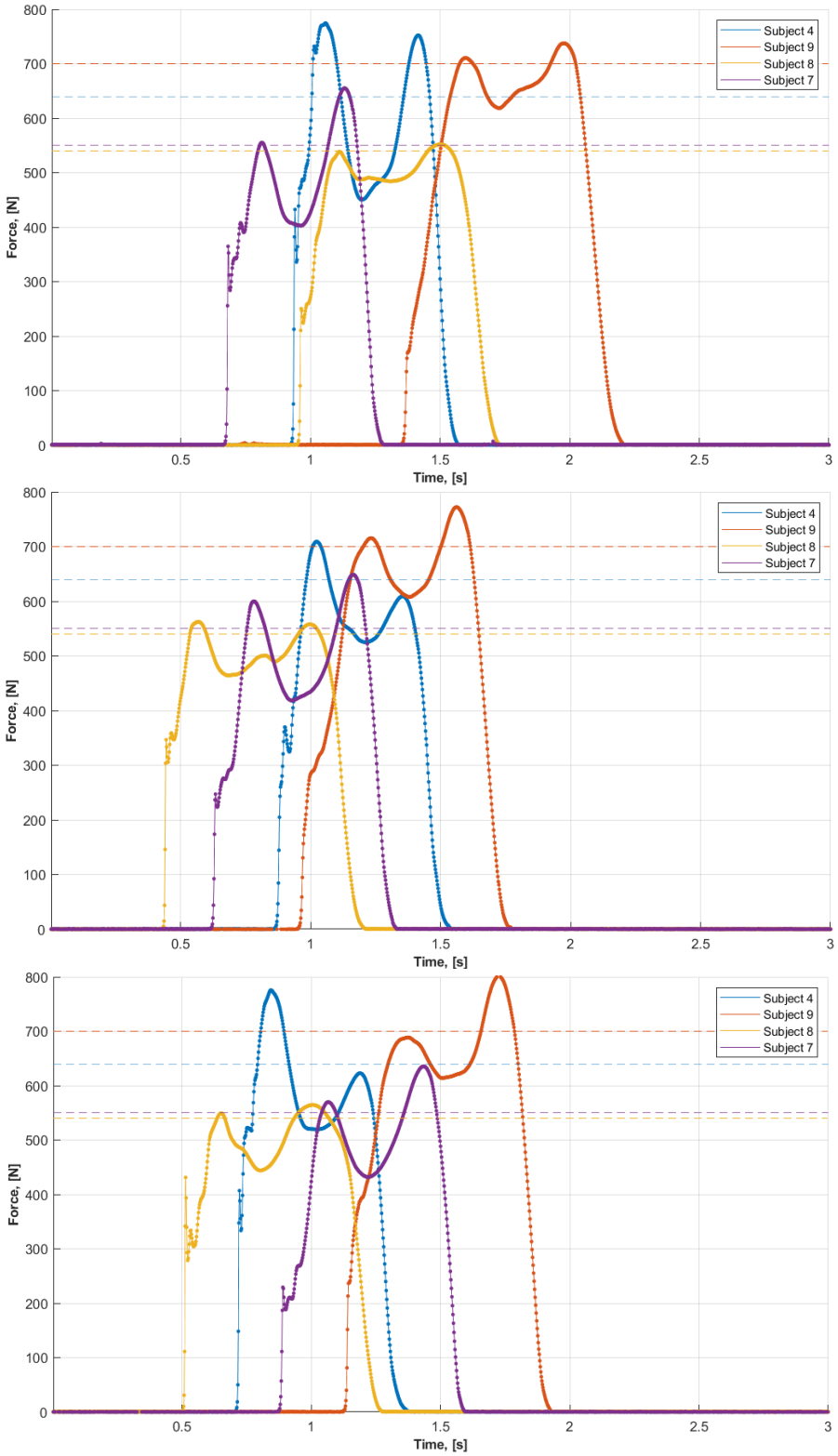

Figure 4.21 - Comparison between subjects' 4, 7, 8 and 9 GRF registered in lateral (top), anterior (middle) and posterior (bottom) views. Dashed lines represent each subject's weight.

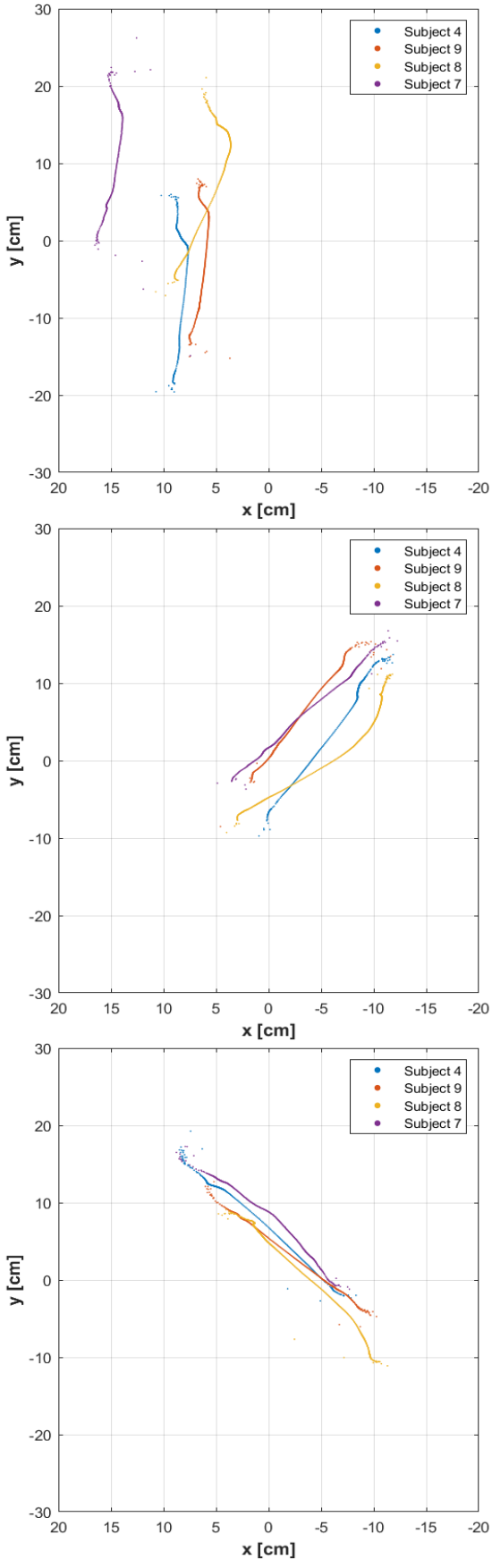

Figure 4.22 - Comparison between subjects' 4, 7, 8 and 9 CoP trajectory registered in lateral (top), anterior (middle) and posterior (bottom) views.

Overall, the M-shape (Figure 4.21) is still observable for each one of them, although a few discrepancies can be registered, especially among the heel transient intensity. Previously analysed, subject 4's impact peak is also observable in subject 7 in a similar fashion (sudden peak then drop of values, followed by a continuous increase, affected midway by a bump), and with much less intensity in subject 8 – shares approximately the same weight with subject 7, yet peak intensity is much lower, however, the opposite occurs in the walking posterior view tests. Subject 9 demonstrates the absence of an impact peak throughout all tests, demonstrating a much softer foot strike, perpetuated by a mid foot strike (landing on both forefoot and heel). Subject 8's double peaks featured near identical values throughout all tests, meanwhile subject 4's second peak (push-off) decreased in the anterior and posterior view tests.

Regarding CoP trajectory, the trajectory behaviour is similar between subjects: an initial deviation to the right after foot strike, followed by a steep deviation to the left when the subject pushes off the floor to propel himself forward, centred on the forefoot. A mainly vertical propagation is observed in all subjects, with subject 8 presenting a wider deviation than the others. This deviation is also observable in Figure 4.22 (middle), portraying the trajectory in the anterior view.

Since the initial starting position of the subjects in both anterior and posterior views was much closer to the plate than the lateral view tests, the CoP trajectories were much closer to the centre of the plate, resulting in data overlapping.

The more spread out, "left weighted" trajectories present in Figure 4.22 (top) are a direct result of the laboratory's layout – the force plate was placed in a strip of other untethered plates that, when stepped on, collided with the force plate, producing erratic readings and destabilizing the force reading channels. To avoid this, the subjects were told to keep the left foot on the floor and let the right foot strike the plate strip, thus minimizing force plate distortions. Regarding VCoP data, some subjects share similar displays of the evolution of CoP. All subjects share a distinct triple peak pattern, although at different stages of stance; once more, the reason for this differences are subject specific, due to their own unique gait characteristics.

In the walking lateral view tests (Figure 4.23), one can notice the similarity between subjects' 4 and 8 graphs, and subjects' 9 and 7: the first pair features a more distinct set of peaks predominating in the first half of stance (0-40%), each one increasing its values, whilst in the second pair the third peak is much more spread out towards the middle of the stance phase (20-70%). Since the third peak signals the change of CoP trajectory from midfoot to forefoot (Point C to D), the higher and shorter duration a peak is, the faster the CoP travels towards the forefoot. Also important is the behaviour of VCoP during the impact peak (Point A): subjects 4 and 7 presented the highest impact peak and consequently, the highest initial peak values, with subject 7 even presenting an initial extra peak. Subjects 8 and 9 featured lower values for their initial peaks, demonstrated by their little to non-existent impact peaks.

In the walking anterior and posterior view tests, the semblance between subjects 4 and 8 peaks diminishes, as the VCoP values of subject 8 slightly decrease, although still sharing the same temporal behaviour (Figure 4.24, Figure 4.25).

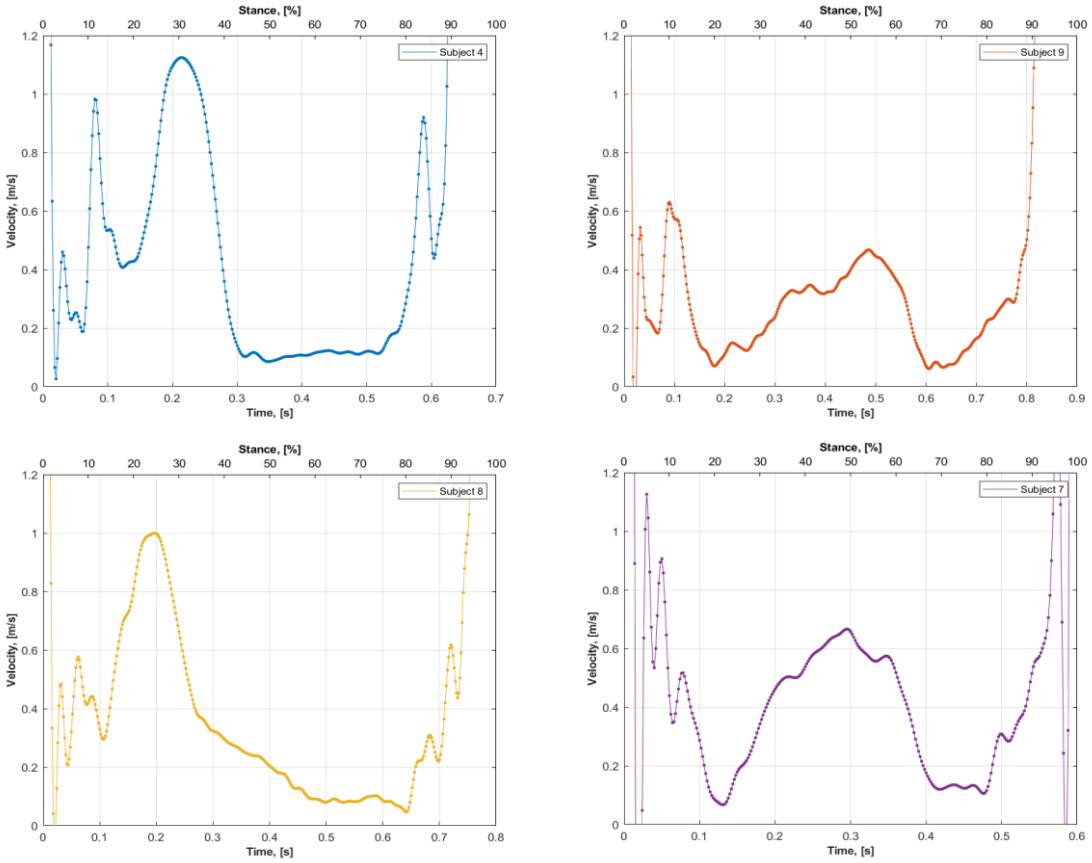

Figure 4.23 – VCoP for subjects 4, 7, 8 and 9 in walking gait lateral view test.

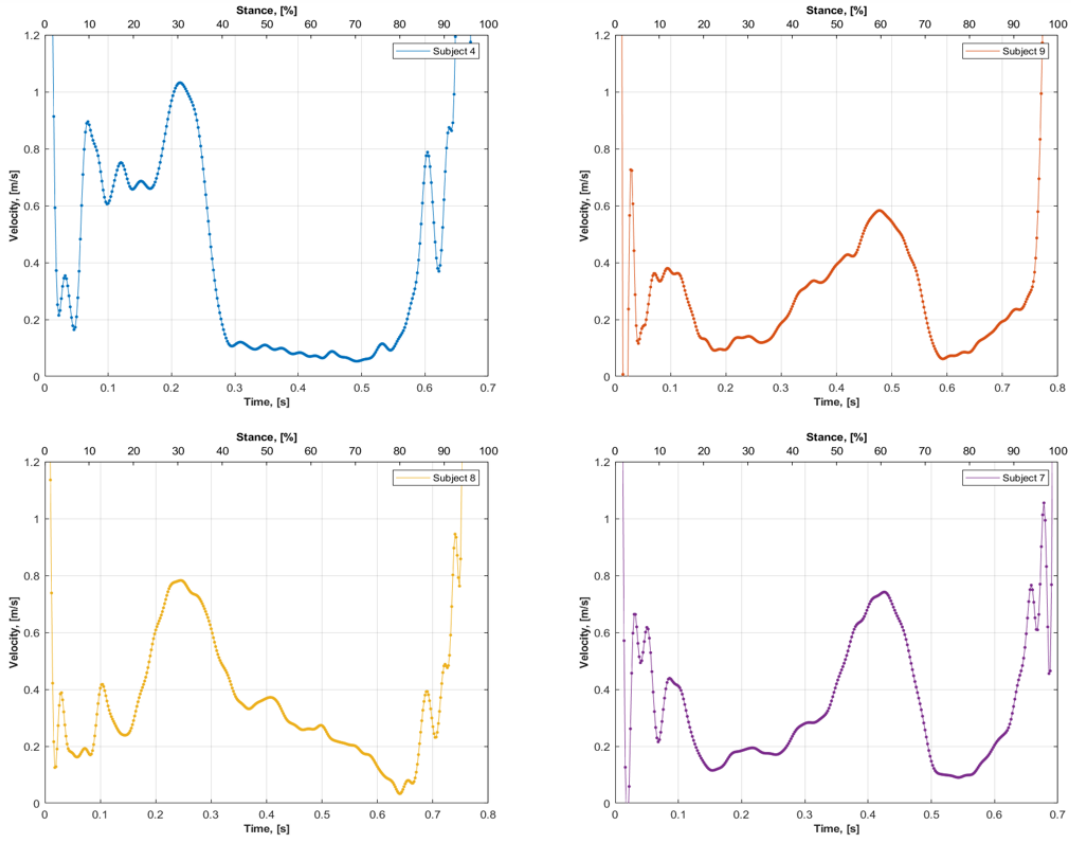

Figure 4.24 - VCoP for subjects 4, 7, 8 and 9 in walking gait anterior view test.

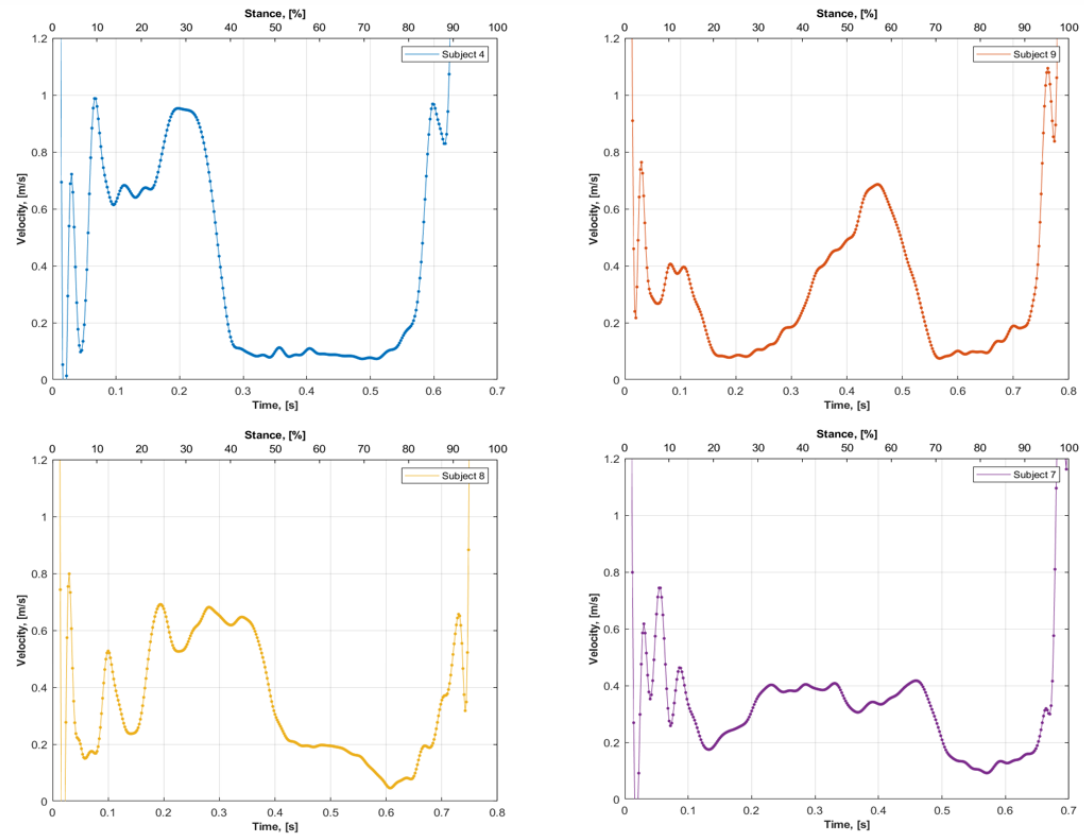

Figure 4.25 - VCoP for subjects 4, 7, 8 and 9 in walking gait posterior view test.

4.7. Running Gait – Lateral view

Running results also feature the same presentation scheme, with strain, GRF, CoP and VCoP data fully synchronized. Once again, the reference frame (Figure 4.28 (a)) portrays the beginning of the stance phase, demonstrating the subject's limb in forefoot strike. The chosen ROI covers an identical area of the leg and the same strain variables are analysed, however, due to the fast angular motion of the limb throughout gait execution the correlation proved to be far worse, with the majority of tests scoring a high correlation error (reason for subject 4 data absence).

Regarding GRF (Figure 4.26), the M-shape is now absent, replaced by a single peak. Also absent is the presence of an impact peak due to the correct footstrike – forefoot strike – performed by the subject, a comparison with other subjects will be made. To help explain the motion, three points were chosen: two of them were arbitrarily created since the created code only marked peaks in GRF. To help explain the flow of motion throughout stance phase, two datapoints whose GRF value where the nearest to the subject's bodyweight were chosen – points A and C.

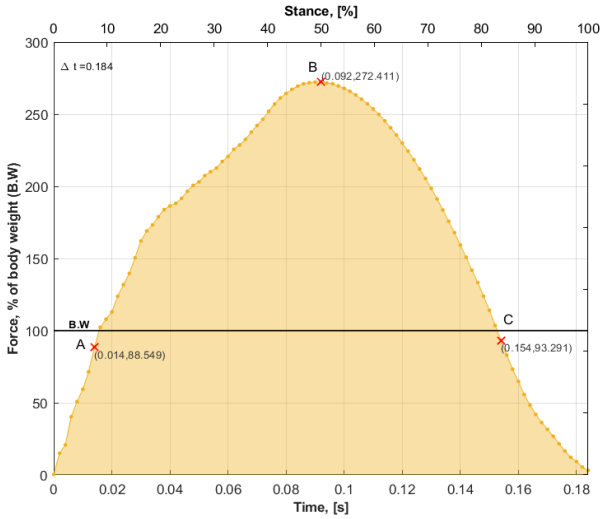

Figure 4.26 - GRF evolution of the running lateral view test of subject 8. Point B corresponds to the peak of GRF data, points A and C aid visual gait explanation.

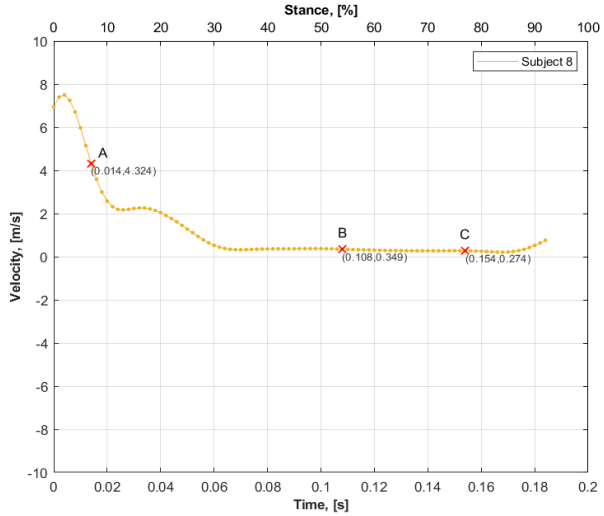

Figure 4.27 - VCoP evolution of the running lateral view test of subject 8. Point B corresponds to the peak of GRF data, points A and C aid visual gait explanation.

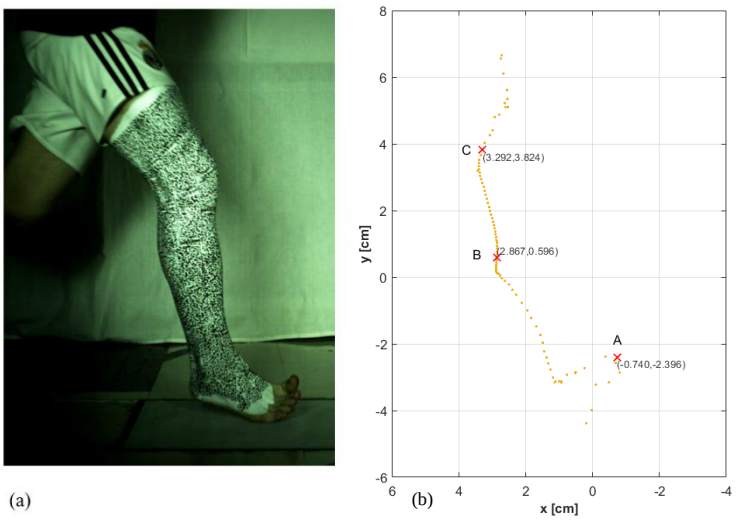

Figure 4.28 - Strain analysis reference frame (a) and CoP evolution (b) of the running lateral view test of subject 8. Point B corresponds to the peak of GRF data, points A and C aid visual gait explanation.

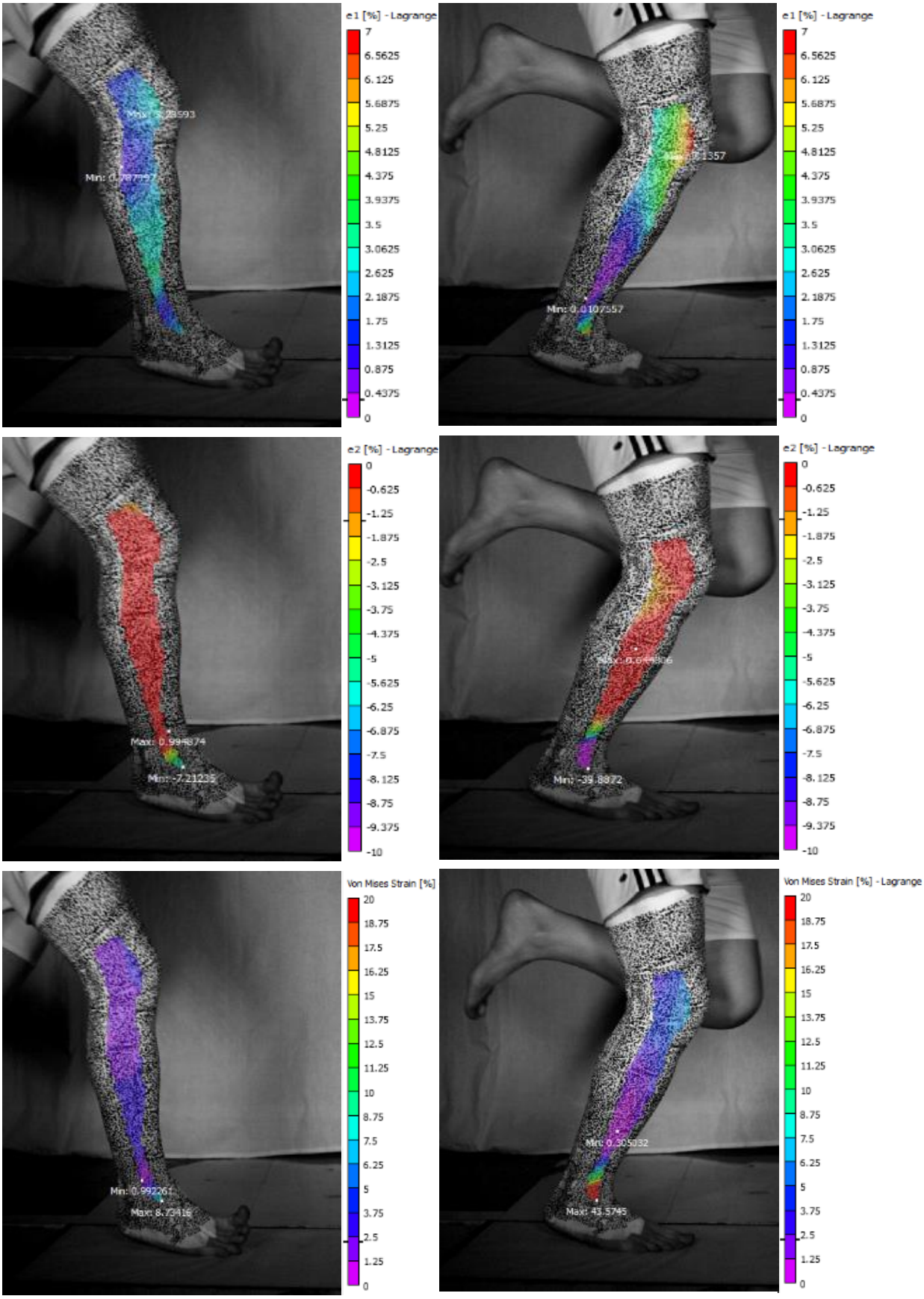

Figure 4.29 – Lateral view of *e1*, *e2* and *von Mises* strain of the leg in point A (left) and point B (right).

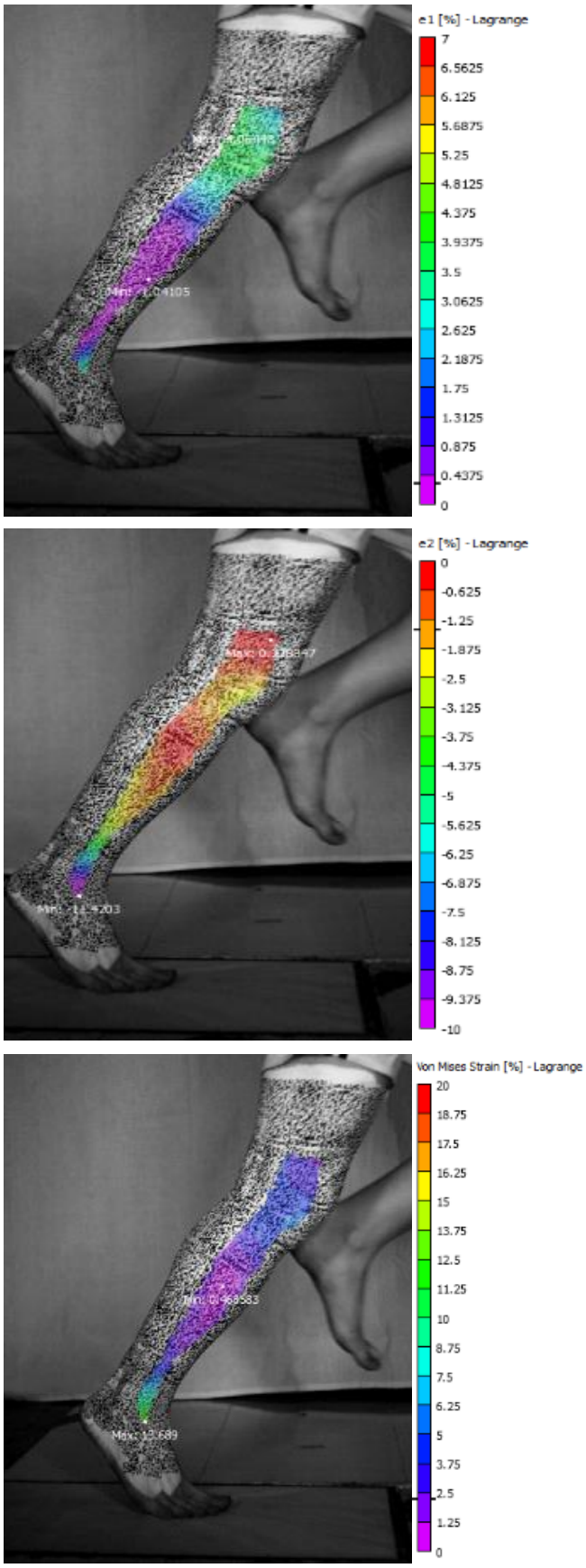

Figure 4.30 - Lateral view of *e1*, *e2* and *von Mises* strain of the leg in point C.

CoP trajectory (Figure 4.28 (b)) demonstrates the evolution of the GRF vector propagation on the forefoot (note the difference in scale of the x and y axis), featuring a quick change to the left and then forwards until toe-off. The rate at which the CoP datapoints change is also demonstrated in the VCoP graph (Figure 4.27), starting with a sudden drop of values that attenuate throughout the majority of the gait execution. This attenuation is due to the small changes in centre of pressure over a very short period of time, where the subject lands his entire weight on the floor and propels himself forward (point B). Once more, Figure 4.29 and Figure 4.30 present the synchronized, strain analysed frames:

- **Point A** – The subject lands on the right side of his forefoot. The knee is slightly flexed. Strain values are similar (although opposite) in *e2* and *von Mises*, with 2 distinct regions separating the majority of the leg and the ankle. The *e1* graph shows a maximum strain region in the anterior region of the leg.
- **Point B** – The ankle, previously fully compressed, starts to extend to push the subject off the plate and propel himself forward. The knee features the same transition from maximum compression to extension. Remains of this compression can be observed in the red region in *e1* graph, but the strain values near the ankle are far higher (*e2* and *von Mises*).
- **Point C** – Heel is completely of the floor, with the leg almost fully stretched. Knee strain intensity decreases, with higher strain values predominating on the plantarflexing ankle.

4.8. Running Gait – Subject comparison

Once more, observing and comparing different subjects' GRF data allows for the identification of different foot strikes (Figure 4.31). As such, a clear distinction can be made between both subjects 4 and 8 and subjects 5 and 7: the presence of an impact peak. Subjects 4 and 8 demonstrate a "clean" single peak, characteristic of a correct forefoot strike; the opposite occurs for subjects 5 and 7 that feature high intensity impact peaks, around 1000 N and 1300 N transmitted to the foot and subsequently the lower limb's joints. The difference between subjects' 8 and 7 foot strike can be seen in Figure 4.32: subject 8 (left) strikes the plate with the forefoot and with the knee flexed, while subject 7 (right) performs heel strike, with the leg almost stretched.

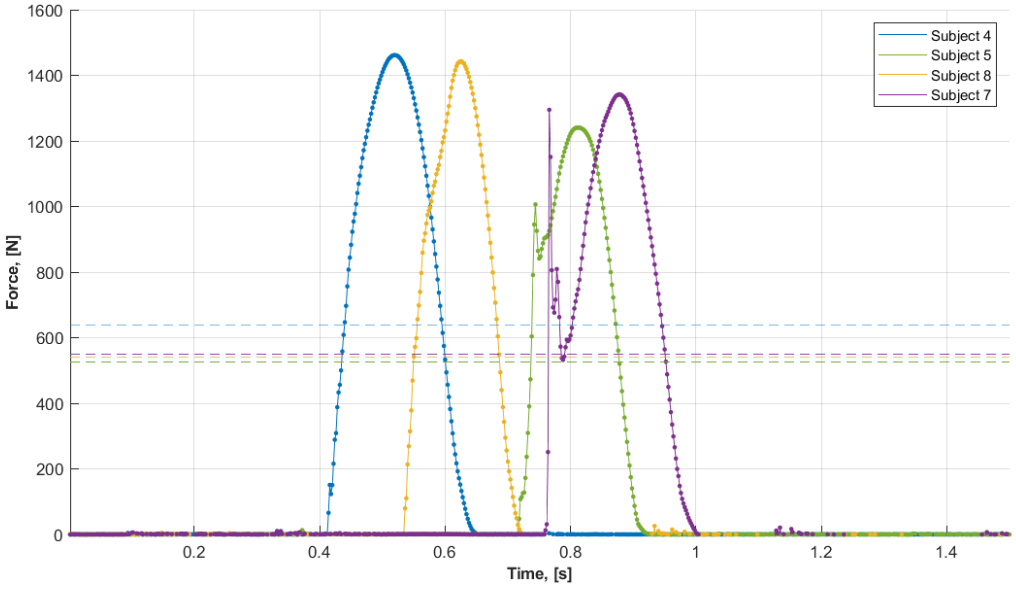

Figure 4.31 – Comparison between subjects' 4, 5, 7 and 8 GRF. Dashed lines represent each subject's weight.

Figure 4.32 - Visual difference between forefoot strike (left) and heelstrike (right) during running gait.

Analysing CoP data (Figure 4.33), the main differences (when comparing to walking CoP) are the shorter trajectories and their irregular propagation. Shorter trajectories were expected due to the faster nature of running gait, the propagation is due to each subjects floor striking technique, ranging from forefoot strikes to heel strikes; however, a repeating direction switch can be seen among the patterns, where after the foot strike, a sudden change towards the left occurs, once more indicating the progression of the trajectory towards the metatarsal heads due to a more pronounced eversion of the foot, as stance phase finishes.

VCoP data (Figure 4.34) highlights an identical pattern between all subjects even though subjects 5 and 7 featured an impact peak, non-present in subjects' 4 and 8 GRF data. All graphs feature an initial down trending peak – a direct result of CoP attenuation after foot contact (evidenced by the drastic dispersion of data points in Figure 4.33) – followed by a constant, near zero velocity values trend, with values rising during the toe-off phase.

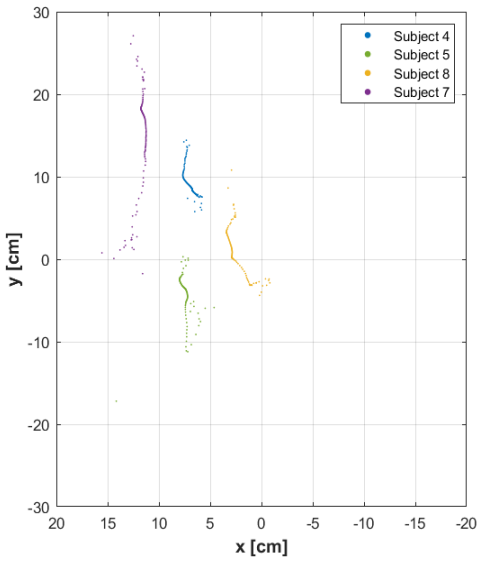

Figure 4.33 – Comparison between subjects' 4, 5, 7 and 8 CoP trajectory registered in lateral view.

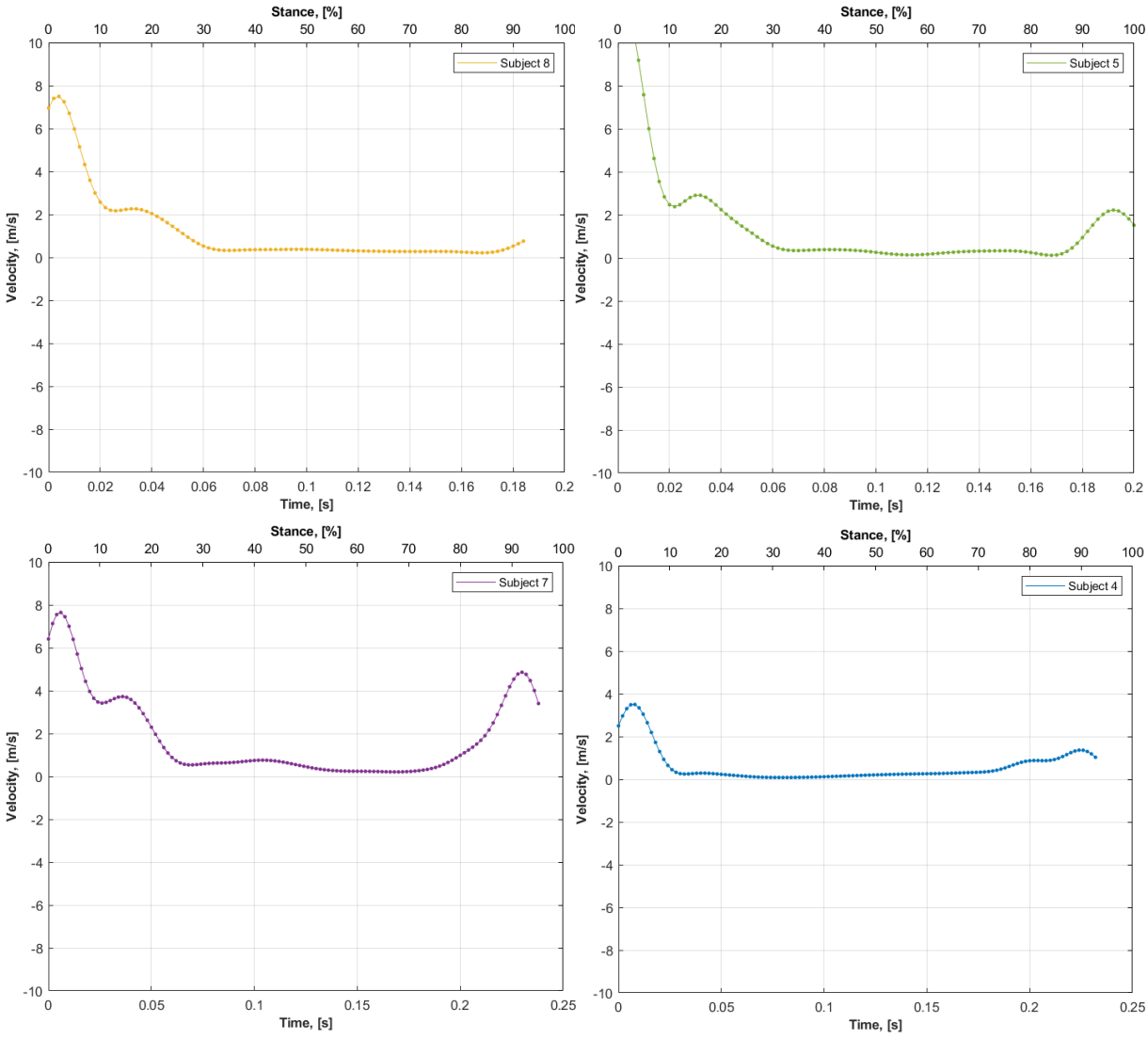

Figure 4.34 - VCoP for subjects 4, 5, 7 and 8 in running gait lateral view test.

4.9. Walking and Running Gait – Pull tests

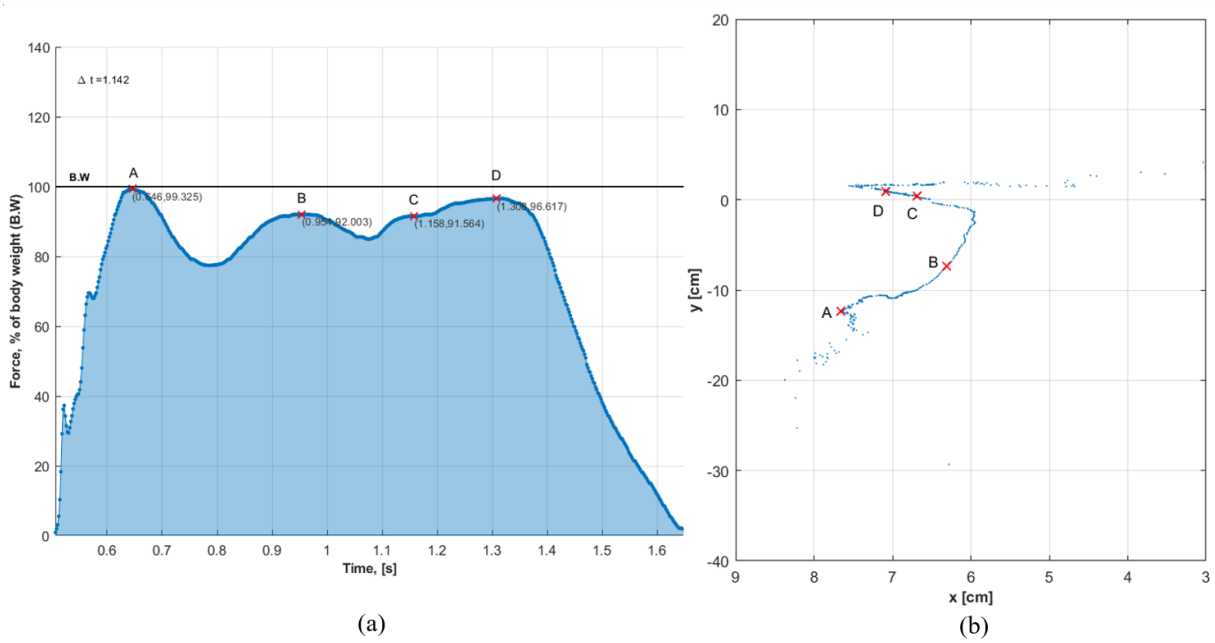

(a) (b)

Figure 4.35 - GRF (a) and CoP (b) data of subject 1 walking pull test.

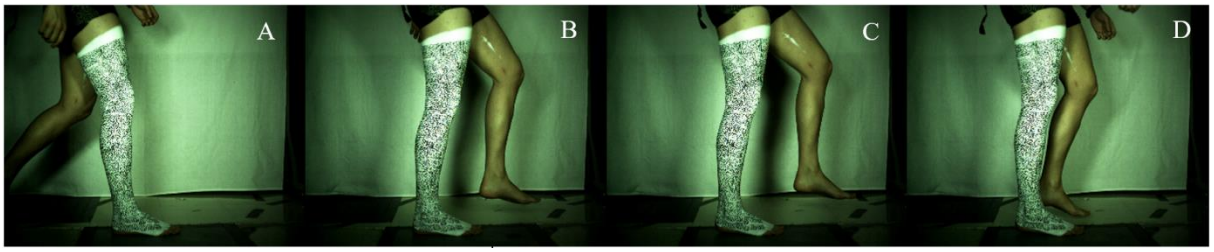

Figure 4.36 - Video footage of subject balance restoration during walking gait.

For the walking pull test, a similar GRF shape can be observed (Figure 4.35 (a)), although with some changes in peaks and duration. Since the attached cord was pulled when the subject was in midstance – leg stretched and opposite foot midswing – the initial behaviour is identical to previous tests: an impact peak and the first peak can be identified. However, after the cord was pulled (around 0.9 s of gait progression), an equilibrium response pattern (Figure 4.36) was visible in all subjects, consisting of:

- Straightening of the leg and rise of the opposite limb's knee, to balance the body forward in response to the backwards pull (point B);
- This behaviour reaches a peak where stability is achieved (point C) and the swinging limb starts to descend in order to have both feet on the floor (point D);

CoP data (Figure 4.35 (b)) features a drastic deviation to the right, followed by an adjustment to the left, demonstrating the response of the ankle in maintaining the subjects balance: after the cord is pulled (during midstance, therefore moments after point A), the swinging leg rises, tipping the balance to the left side; to counter this weight shift the subject applies most of his body weight on the right side

of the foot, on the metatarsal/cuboid. As the leg comes down to a resting position, CoP shifts once more the left (points C and D), maintaining the subjects equilibrium.

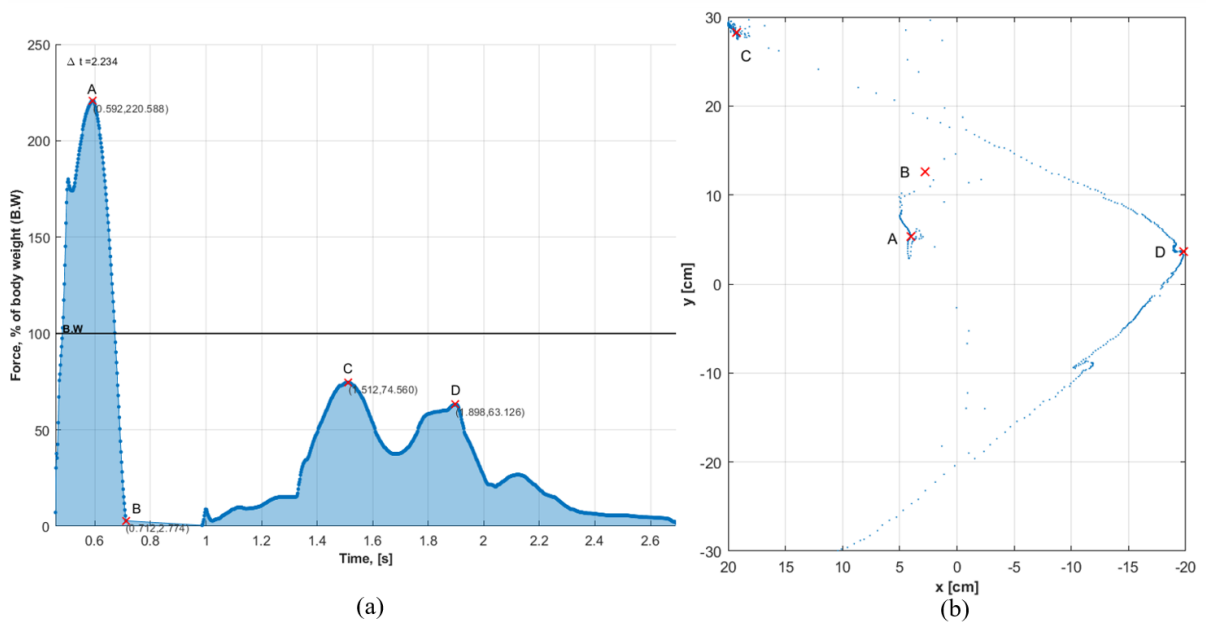

Figure 4.37 – GRF (a) and CoP (b) data of subject 1 running pull test.

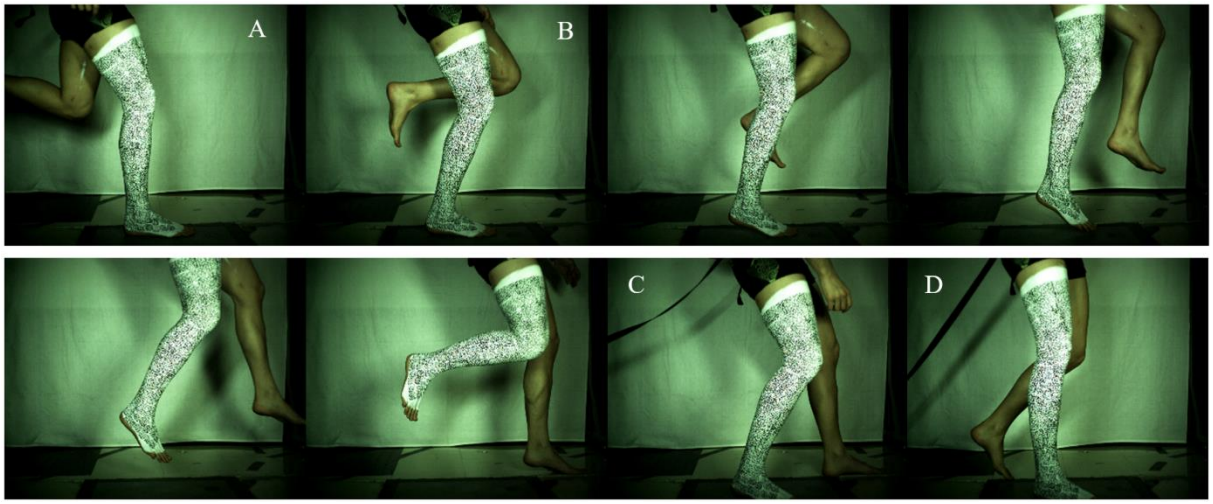

Figure 4.38 – Video footage of subject balance restoration during running gait.

Running pull tests also featured a similar response between subjects, cinematically speaking. The GRF data (Figure 4.35 (a)) shows that the cord was pulled moments after foot strike, after the peak in GRF values (between point A and B). The balance response (Figure 4.38) was once more common in all subjects, consisting of the following movements:

- The subject strikes the floor, performing gait as usual (point A);
- Moments after, the cord is pulled, pulling the subject in an opposite direction, removing his weight from the plate - notice the rising left knee (point B). Due to the higher speed of gait when running and the sudden opposite force, the subject lifts himself of the ground, propelling himself upwards. Whilst lifting , the opposite knee rises to a maximum and then

the entire leg descends to make contact with the floor, with the right leg accompanying the same movement with a slight delay (Frames between B and C).

- As soon as both feet are on the floor, the subject strives to regain a straight, balanced posture (points C and D).

CoP data (Figure 4.37 (b)) does not provide any specific behaviour due to rise of the stance foot of the plate. The first two points, A and B, are in similar trajectory as the ones presented in the running analysis whilst the remaining represent the trajectory shift after the landing of the left foot (point C) and shortly after the right one (point D).

4.10. Heel strike analysis – Rigid body motion

To complement previous work, aimed at identifying a relationship between rigid body motion of the ankle-foot complex and heel strike, the subjects' angular variation between fixed points of the lower leg and foot was analysed. Presented in Figure 4.39 is the beginning and end of the timeframe where the measured ankle angle "locked" throughout gait, maintaining its values. Small deviations of 1 degree are present through some frames, but these can be attributed to small tracking issues due to the non-optimal lighting and the irregular speckle pattern. This motion corresponds to a total of 33 frames (0.066 s), spanning between moments after heelstrike and ending in a small peak before the first GRF peak, most probably due the landing of the forefoot (foot flat). In the same timeframe, the knee flexes (decrease in angle values), accompanying the lower leg motion.

As evidenced in Figure 4.40, the ankle joint locks and maintains its values throughout the duration between heel strike (after the peak) and foot flat, where afterwards the angle diminishes due to the forward motion of the leg (midstance). GRF data increases over time, with VCoP data rising from minimum values to its second peak, consequence of the foot landing (rapid shift of CoP). Strain values are also somewhat constant near the ankle region, presenting minimal variation over time (Figure 4.41).

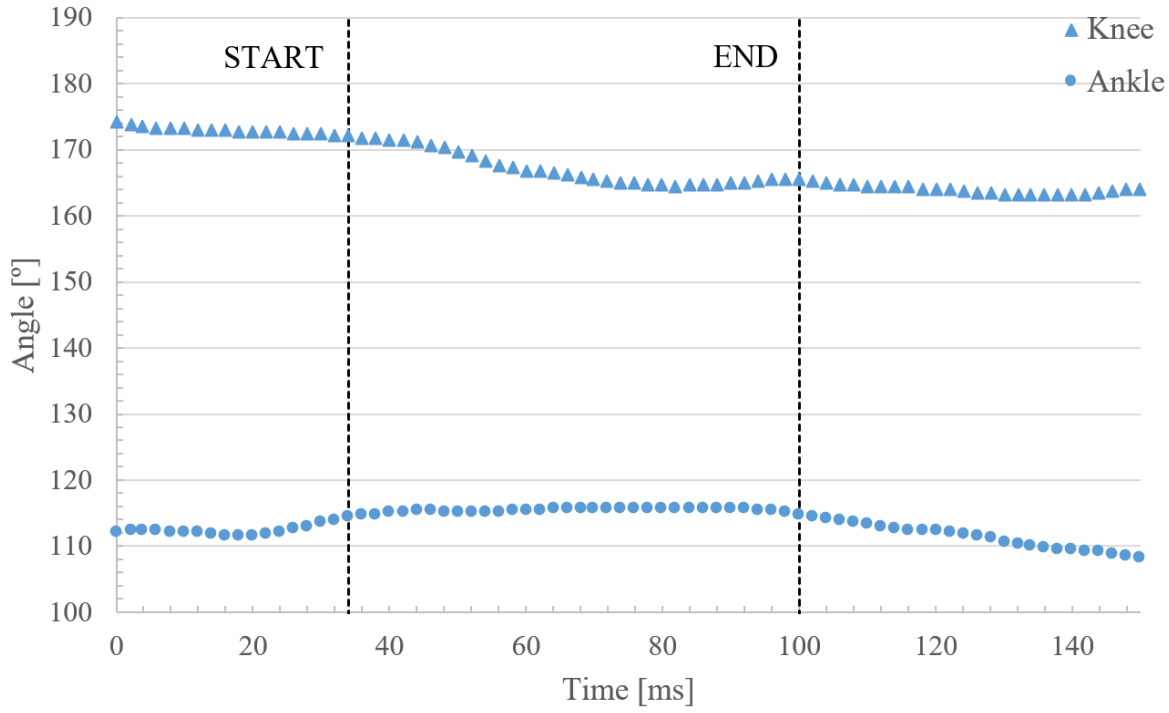

Figure 4.39 – Knee and ankle angle progression during gait. Dashed lines represent the start and end of the rigid body rotation phase.

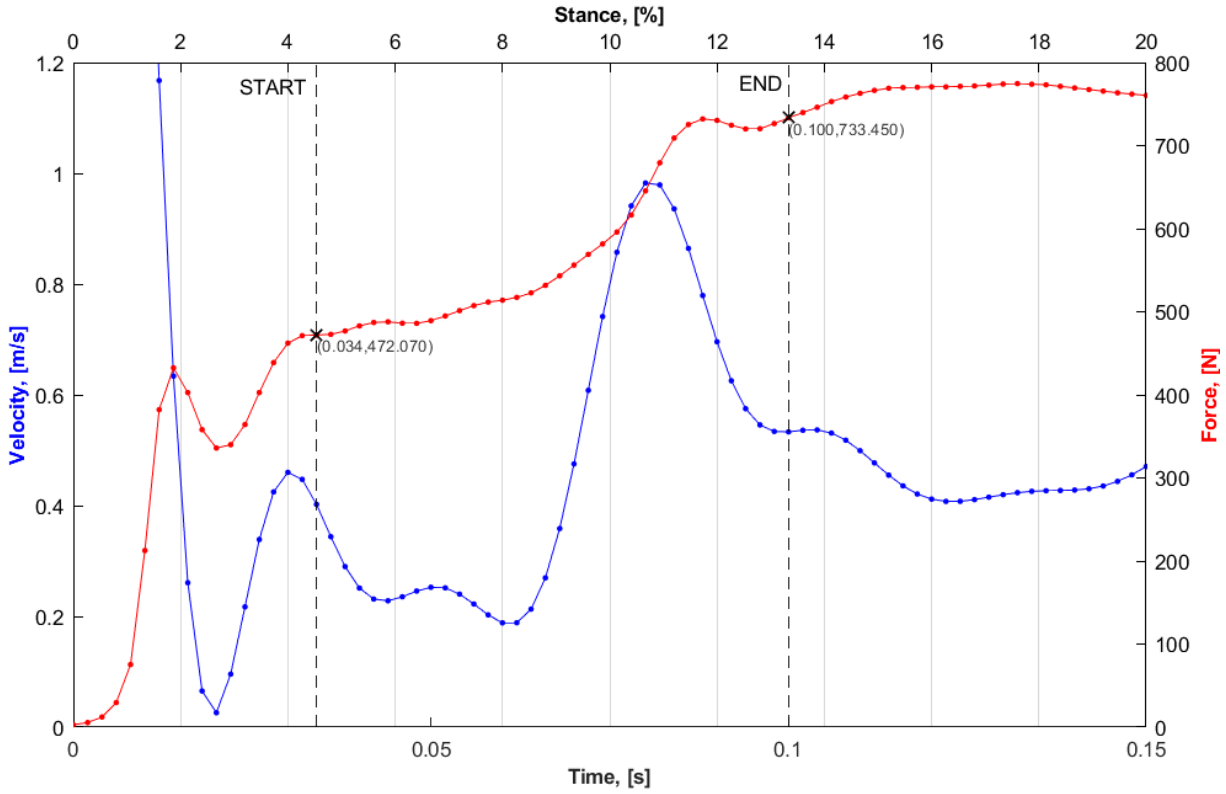

Figure 4.40 – GRF (red) and VCoP (blue) data progression during gait. Dashed lines represent the start and end of the rigid body rotation phase.

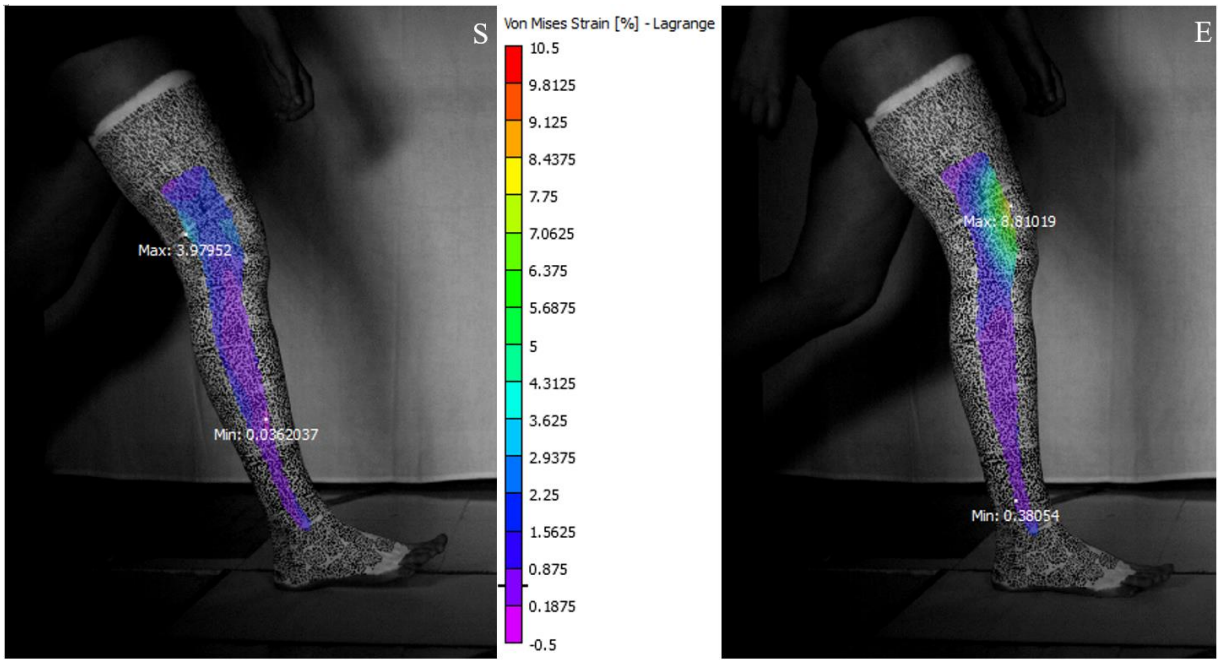

Figure 4.41 – Leg skin strain at the start (S) and end (E) of rigid body rotation.

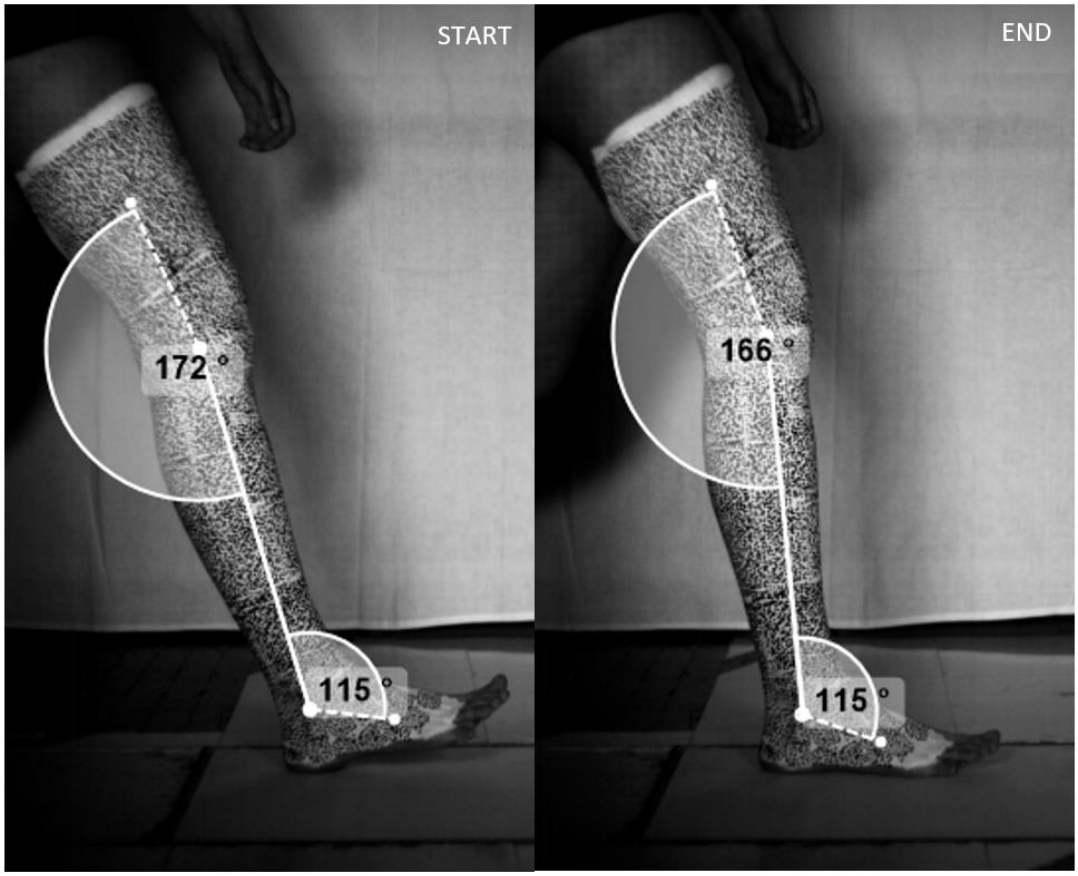

Figure 4.42 – Angles of knee and ankle joint at the start and end of the rigid body rotation phase.

CoP data (Figure 4.43) confirms the propagation of the event and the rise in VCoP values, starting in the rearfoot and transitioning to the midfoot as it ends, with visible gaps between the datapoints.

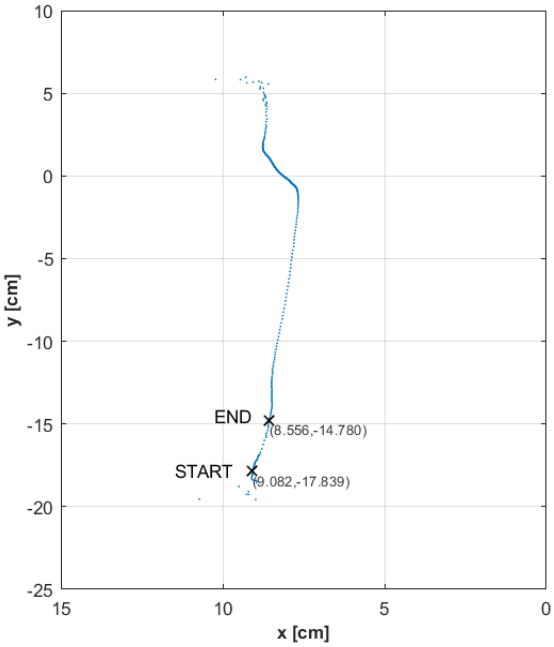

Figure 4.43 – CoP data progression during gait. Markers represent the start and end of the rigid body rotation phase.

A similar behaviour was found in other subjects, with a decreasing knee angle (Figure 4.44) and a stabilizing ankle angle (Figure 4.45) moments after heelstrike. The event lasted a nearly similar period of time, with 42 ms and 48 ms for subjects 7 and 9, respectively.

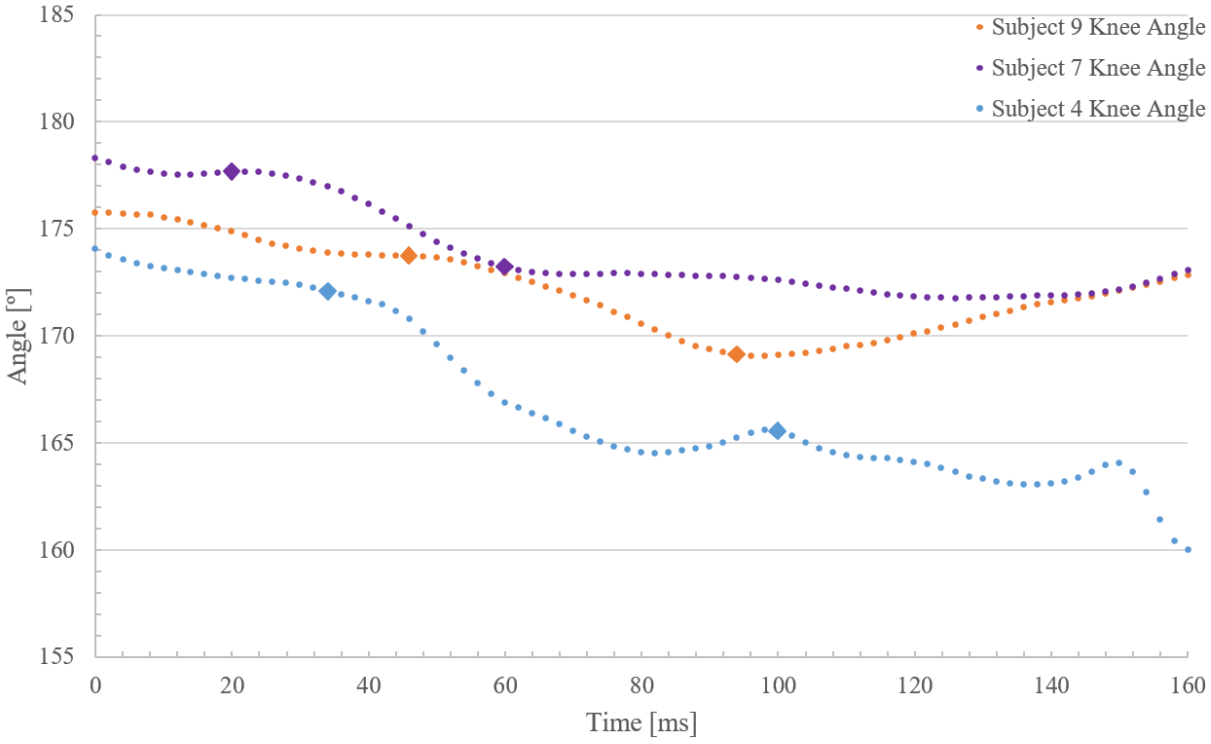

Figure 4.44 – Subject's 9, 7 and 4 knee angle evolution. The larger dots mark the beginning and end of the rigid body rotation event.

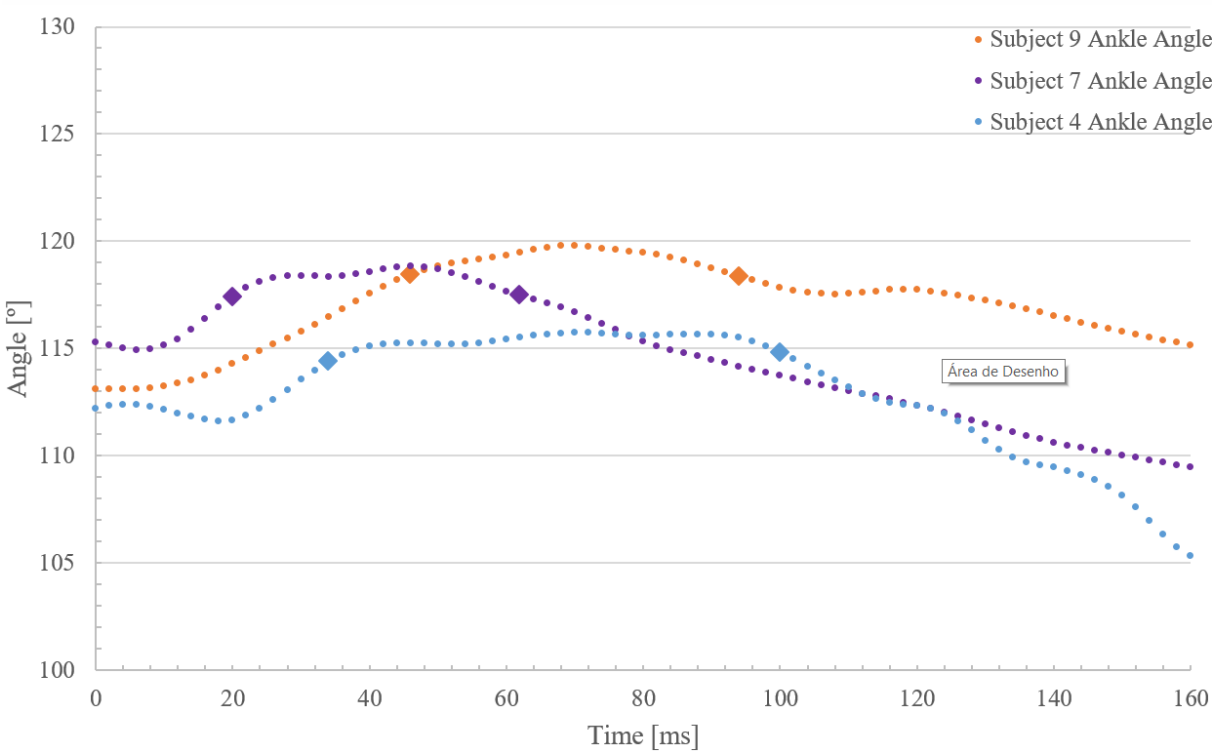

Figure 4.45 – Subject's 9, 7 and 4 ankle angle evolution. The larger dots mark the beginning and end of the rigid body rotation event.

This data then complements the usual gait description of the foot commonly present in literature, which instead of featuring a direct transition from heel strike to foot flat (via ankle rotation), adds a small description of events occurring in between (Figure 4.46):

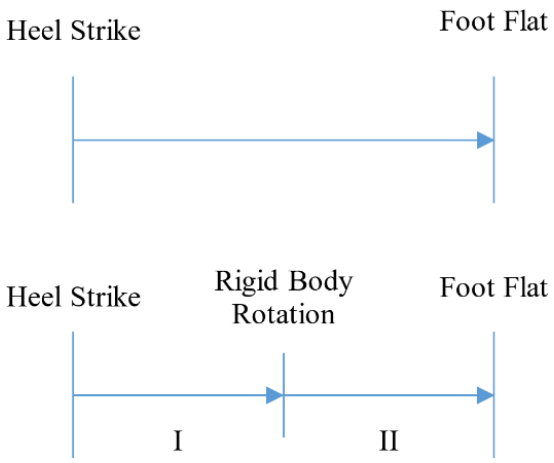

Figure 4.46 – Comparison between literature description (top) of stance phase events and newly proposed description (bottom).

where I is the stage right after heel strike, where the body weight is applied over the heel and rotation of the ankle "separates" an independent foot from the rest of the leg and II is where the foot, ankle and leg rotate as one (the leg accompanies the downwards movement of the foot) until there is full contact with the ground.

The lack of this rigid rotation stage in biomechanics literature may be due to the difficulty of its identification in lower frame rate footage, used in most kinematic research studies (around 100 frames per second, 1 frame every 0.010 s). Since the time frame between the beginning and end of this stage ranges between 0.040-0.060s (40-60 milliseconds), a 500 frames per second capture rate retrieves information every 0.002 seconds (2 milliseconds), providing plenty of footage capable of showing this phenomenon.

5. Conclusions

5.1. Achievements

A brief conclusion regarding the utilized methods and end results, the improvements over previous work, quality of results and future work possibilities.

Understanding the lower limb behaviour during walking and running gait is essential in the creation and development of medical treatments and devices related to the correction or support of gait. Utilizing a setup consisting of high frame rate cameras synchronized with a force plate, both acquiring data at a rate of 500 datapoints/s, and with both strain measurement tool VIC-3D and biomechanical analysis tool Kinovea, it was possible to synchronize skin strain behaviour, joint angles, ground reaction force, centre of pressure and velocity of centre of pressure data evolution during the stance phase.

This thesis improved on previous works performed at IST by Ricardo Ferreira and Joana Capacete, by expanding the strain analysed region from the ankle-foot complex to the entire leg, without severely compromising spatial resolution. A correlation between strain evolution and other kinematic/kinetic quantities featuring a higher number of subjects and views also improves the amount of data available, important for result validation.

Regarding strain analysis, VIC-3D proved an efficient and robust tool, providing accurate data even when subjected to non-ideal conditions such as large FOV with small ROI, high curvature of speckled target, large rotation over time of the ROI and glare issues present in calibration due to insufficient lighting. Although results in non-lateral views and running featured a higher correlation error, they still yielded rational results that were used in this thesis. The strain analysis provided by VIC-3D were in accordance with what was expected: the joints feature the regions where these values peak, changing "position" (i.e. from anterior to posterior) when flexing or extension occurs. Just above the knee and on the lower leg, the values did not change drastically throughout gait, varying mainly due to the leg rotation influence in the strain calculating algorithm (i.e. leg rotates away from reference image, algorithm interprets as deformation).

The lateral view tests provided the best results, featuring low correlation errors and the entire kinematic evolution of gait; the other views (front and back) led to a reduced number of frames, and therefore quality, due to their non-profile view: since the aperture of the lenses was fully opened in order to avoid the blurring of the faster movements, this reduced the depth of field severely, meaning that any frames beyond and after were not focused, damaging the quality of data. Running gait analysis offered the highest correlation error values of all the tests, with a majority of the results being inadequate for presentation.

Regarding GRF, CoP and VCoP data, a template code was created for each of these quantities, that only requires as input the .txt file of the test subject provided by the force plate software and outputs all of the graphs presented in this thesis. The majority of the data was in accordance to the literature, except minor discrepancies caused by the external factors (vibrations of the plate strip when performing gait) and subject conditioning factors (subjects commented on the unease of gait with the paint applied, that it was "grabbing" the leg, making it stiff, affecting the results). Also, the subjects inadvertently altered gait stride throughout the tests, leading to an increase in data collection time, an already lengthy process, with each subject taking up to 2 hours form start (leg painting) to finish (all gait tests executed).

Synchronization of all existing data was achieved, supplying the reader with strain, kinematic and kinetic information of the subjects' behaviour throughout the stance phase. Such information is useful for a clear understanding of all variables progression throughout gait, and the presence of common patterns in healthy subjects.

5.2. Future work

To improve on the present work, one can achieve this through multiple methods, either improving the skin deformation measurement method or changing the analysis views. As mentioned before, one of the main limitations in strain analysis was the lighting conditions and the nature of the experiment itself; a way to improve this would be to perform the tests in a white background room and feature more LED sets surrounding the force plate to create an homogeneous lighting environment, minimizing glare issues and allowing for a higher depth of field, since the aperture would not need to be fully opened. A positive consequence of the aperture closure would also be the rise in quality of anterior and posterior views, benefiting directly from a longer depth of field.

Another direct improvement over the different views would be an increase in cameras, since the same movement could be analysed in different views instead of multiple movements analysed in different views. This would offer a more consistent analysis, since the same amount of the data and the same gait would be present in all views, minimizing the number of tests and the amount of repeated information.

One of the next steps in future work would be the identification of LoNE's throughout the leg, throughout the entire stance phase, producing similar results to the ones presented by Ricardo Ferreira. Identification of LoNE's would facilitate the placement of actuator strands and planning the development of future biomedical devices.

Finally, one of the initial tasks outlined for this thesis was the use of Multi-DIC [41], a library of functions written in MATLAB syntax, which provide all DIC processes in simple and easy-to-use interfaces, simplifying object analysis. This tool stands out for its adaptation to the biomedical field (calibration method encompasses irregular surfaces such as those of the human body) and a more facilitated calibration of a setup with multiple cameras. Initial work was performed with this toolbox – calibration object and specific stamps were created – but the featured correlation algorithm, NCorr, was not robust enough to handle the deformation of a highly rotating target (i.e. rotation of the leg throughout gait). Future work could make use of this tool if the analysed area is reduced, if multiple cameras are used or even if the user divides the stance phase into multiple stages, reducing the overall target rotation.

Bibliography

[1] R. Ferreira, “Skin strain field analysis at the ankle-foot complex through digital image correlation Biomedical Engineering,” Masters Thesis, Instituto Superior Técnico, 2015.

[2] J. D. C. Capacete, “Analysis and interpretation of vertical ground reaction force, center of pressure trajectory and velocity , and dorsal skin deformation in Normal Gait,” Unpublished Manuscript, Instituto Superior Técnico, 2016.

[3] S. J. Hall, *Basic Biomechanics*, Seventh Ed. New York: McGraw-Hill Education, 2015.

[4] A. R. Domingues, S. Marreiros, J. Martins, M. T. Silva, and D. J. Newman, “Analysis of Ankle Skin Deformation for the Development of Soft Orthotics,” *J. Biomchanics*, vol. 45, no. 1, 2012.

[5] C. L. Vaughan, B. L. Davis, and J. C. O’Connor, *“Dynamics of Human Gait.”* Human Kinetics Publishers, 1992.

[6] J. Perry, *Gait Analysis - Normal and pathological function*. Thorofare: SLACK Incorporated, 1992.

[7] D. E. Lieberman *et al.*, “Foot strike patterns and collision forces in habitually barefoot versus shod runners,” *Nature*, vol. 463, no. 7280, pp. 531–535, 2010.

[8] A. Tongen and R. E. Wunderlich, “Biomechanics of Running and Walking,” pp. 1–12, 2010.

[9] D. Winter, *The Biomechanics and Motor Control of Human Gait: Normal, Elderly and Pathological*. New York: Wiley, 1991.

[10] C. Y. Hong, L. Y. Guo, R. Song, M. L. Nagurka, J. L. Sung, and C. W. Yen, “Assessing postural stability via the correlation patterns of vertical ground reaction force components,” *Biomed. Eng. Online*, pp. 1–18, 2016.

[11] M. W. Cornwall and T. Mcpoil, “Velocity of the center of pressure during walking,” *J. Am. Podiatr. Med. Assoc.*, no. 7, 2014.

[12] D. Tran *et al.*, “Strain rate and anisotropy effects on the tensile failure characteristics of human skin,” *J. Mech. Behav. Biomed. Mater.*, vol. 41, pp. 241–250, 2015.

[13] X. Liu *et al.*, “New Non-invasive Techniques to Quantify Skin Surface Strain and Sub-surface Layer Deformation of Finger-pad during Sliding,” *Biotribology*, 2017.

[14] H. Joodaki and M. B. Panzer, “Skin mechanical properties and modeling : A review,” 2018.

[15] K. Bethke, “The Second Skin Approach : Skin Strain Field Analysis and Mechanical Counter Pressure Prototyping for Advanced Spacesuit Design,” PhD Thesis, Massachusets Institute of Technology, 2005.

[16] D. G. Caldwell, N. G. Tsagarakis, S. Kousidou, N. Costa, and I. Sarakoglou, “‘Soft’ Exoskeletons for Upper and Lower Body Rehabilitation — Design, Control and Testing,” *Int. J. Humanoid Robot.*, vol. 04, no. 03, pp. 549–573, 2007.

[17] A. T. Asbeck, S. M. . De Rossi, I. Galiana, Y. Ding, and C. J. Walsh, “Stronger, Smarter, Softer: Next Generation Wearable Robots,” vol. 1, no. 11, pp. 22–33, 2011.

[18] D. J. Newman, M. Canina, and G. L. Trotti, “Revolutionary Design for Astronaut Exploration – Beyond the Bio-Suit System,” *AIP Conf. Proc.*, vol. 880, p. 975, 2007.

[19] A. Iberall, “The experimental design of a mobile pressure suit,” *J. Basic Eng.*, pp. 251–264, 1970.

[20] P. Kelly, “Mechanics Lecture Notes: An introduction to Solid Mechanics,” pp. 207–234.

[21] M. Frehner, “Notes on strain and deformation tensors,” no. September, 2006.

[22] Correlated Solutions, “Vic-3D - User Manual,” 2010.

[23] M. Sutton, J. Orteu, and H. Schreier, *Image Correlation for Shape, Motion and Deformation Measurements*. New York: Springer Science, 2009.

[24] M. Palanca, G. Tozzi, and L. Cristofolini, “The use of digital image correlation in the biomechanical area: A review,” *Int. Biomech.*, vol. 3, no. 1, pp. 1–21, 2016.

[25] F. Verdini, M. Marcucci, M. G. Benedetti, and T. Leo, “Identification and characterisation of heel strike transient,” *Gait Posture*, vol. 24, pp. 77–84, 2006.

[26] S. Fuchioka, A. Iwata, Y. Higuchi, M. Miyake, S. Kanda, and T. Nishiyama, “The Forward Velocity of the Center of Pressure in the Midfoot is a Major Predictor of Gait Speed in Older Adults *,” *Int. J. Gerontol.*, vol. 9, no. 2, pp. 119–122, 2015.

[27] S. P. Marreiros, “Skin Strain Field Analysis of the Human Ankle Joint,” PhD Thesis, Instituto Superior Técnico, 2010.

[28] A. T. Marecki, “Skin strain analysis software for the study of human skin deformation,” PhD Thesis, Massachussetts Institute of Technology, 2012.

[29] A. M. Wessendorf and D. J. Newman, “Dynamic Understanding of Human-Skin Movement and Strain-Field Analysis,” *IEEE Trans. Biomed. Eng.*, vol. 59, no. 12, pp. 3432–3438, 2012.

[30] E. W. Obropta and D. J. Newman, “A comparison of human skin strain fields of the elbow joint for mechanical counter pressure space suit development,” *2015 IEEE Aerosp. Conf.*, 2015.

[31] E. W. Obropta and D. J. Newman, “Skin strain fields at the shoulder joint for mechanical counter pressure space suit development,” *2016 IEEE Aerosp. Conf.*, pp. 1–9.

[32] R. Maiti *et al.*, “In vivo measurement of skin surface strain and sub-surface layer deformation induced by natural tissue stretching,” *J. Mech. Behav. Biomed. Mater.*, vol. 62, pp. 556–569, 2016.

[33] X. Hu *et al.*, “Skin surface and sub-surface strain and deformation imaging using Optical Coherence Tomography and Digital Image Correlation,” in *Proc. SPIE 9710, Optical Elastography and Tissue*, 2016, vol. 9710, pp. 1–7.

[34] L. Horton, “Vibration analysis of healthy skin : toward a noninvasive skin diagnosis methodology a noninvasive skin diagnosis methodology,” *J. Biomed. Opt.*, vol. 24, no. 1, 2019.

[35] N. Amirah *et al.*, “Measuring Ankle Angle and Analysis of Walking Gait using Kinovea,” *Int. Med. Device Technol. Conf.*, pp. 247–250, 2017.

[36] S. H. Elwardany, W. H. El-sayed, and M. F. Ali, “Reliability of Kinovea Computer Program in Measuring Cervical Range of Motion in Sagittal Plane,” *Open Access Libr. J.*, vol. 2, pp. 1–10, 2015.

[37] R. M. A. El-raheem, R. M. Kamel, and M. F. Ali, “Reliability of Using Kinovea Program in Measuring Dominant Wrist Joint Range of Motion,” *Trends Appl. Sci. Res.*, vol. 10, no. 4, pp. 224–230, 2015.

[38] C. Guzmán-Valdivia, A. Blanco-Ortega, M. Oliver-Salazar, and J. Escobedo, “Therapeutic Motion Analysis of Lower Limbs Using Kinovea,” *Int. J. Soft Comput. Eng.*, no. 2, pp. 359–365, 2013.

[39] A. Puig-diví, J. M. Padullés-riu, and A. Busquets-faciaben, “Validity and Reliability of the Kinovea Program in Obtaining Angular and Distance Dimensions,” *Preprints*, 2017.

[40] Correlated Solutions, “Vic-Gauge 3D Testing Guide - User Manual,” 2010. .

[41] D. Solav, K. M. Moerman, A. M. Jaeger, K. Genovese, and H. M. Herr, “MultiDIC: An open-source toolbox for multi-view 3D digital image correlation,” *IEEE Access*, vol. 6, pp. 30520–30535, 2018.